Using Ultra-Small Radiocarbon Dates to Obtain Reliable Ages on Shells Affected by Hard Water

A thesis

submitted in partial fulfilment

of the requirements for the degree

of

Master of Science (Research) in Chemistry

at

The University of Waikato

by

Catherine Milson

THE UNIVERSITY OF
WAIKATO
Te Whare Wānanga o Waikato

2022

Abstract

Radiocarbon dating is used across a wide range of scientific disciplines including archaeology, forensics, and geosciences. Interest in reducing the minimum sample size limit required for obtaining reliable radiocarbon dates has grown over the years as this would offer many new research opportunities. Contamination introduced by the radiocarbon dating process becomes more problematic for samples <0.10 mgC, and in order to reliably radiocarbon date ultra-small samples, contamination is one of the issues that needs to be resolved.

Reducing the amount of sample required for radiocarbon analysis has been specifically applied to an archaeological problem. The Mariana Islands, located in the Western North Pacific, are home to the archaeological site Bapot-1. While the exact date of human arrival is currently under debate, it is thought to have occurred between 3300 – 3500 years ago. Establishing a date of human arrival is important because it represents the longest ocean voyage of its time, more than 2000 km, and is necessary for modelling when Neolithic expansion in Island Southeast Asia occurred.

Obtaining reliable radiocarbon dates from Bapot-1 is difficult as short-lived terrestrial materials, such as charred twigs, are often degraded or scarce. While shell material is abundant, the presence of limestone bedrock hinders its use. As freshwater travels through limestone, it picks up bicarbonate ions depleted in ^{14}C. This ‘old’ water is discharged into the water at the shore where it is then incorporated into the shells of some, but not all, shell taxa that live close to the shore. This results in older radiocarbon ages for some shellfish. To overcome this problem, it is hypothesized that ^{13}C can be used to identify shellfish that have been affected by hard water. However, for shellfish that have a tolerance for both marine and estuarine environments, different $^{13}C/^{14}C$ values will be obtained depending on where sampling occurs on the shell. To accurately radiocarbon date a single shell that may have been influenced by old ^{14}C at different times, it is necessary to identify which shell growth bands have been deposited while influenced by the different water sources. This necessitates the ability to date very small samples of shell material.

To overcome contamination issues associated with radiocarbon dating ultra-small samples, a series of vacuum line and chemical modifications were selected and substituted into current Waikato Radiocarbon Dating Laboratory (WRDL) procedures. To assess the effect of each modification, three standards (of known age) that are used at the WRDL were radiocarbon dated. The radiocarbon dating results from the standards showed that the volume and chemical modifications did not have any significant impact on improving contamination issues for ultra-small samples. However, there were some noteworthy observations. The graphitisation reaction was significantly faster when a quartz tube with “slush” was used instead of magnesium perchlorate. This time reduction has the potential to minimise contamination. Furthermore, the use of a six-decimal point balance for weighing ultra-small samples resulted in more precise CO_2 yields compared to the four-decimal point balance routinely used at the WRDL.

Selected volume modifications were used to radiocarbon date three growth bands from a *Gafrarium* sp. shellfish from the Mariana Islands. Two results from the same *Gafrarium* sp. shellfish that were previously radiocarbon dated were incorporated into this thesis, resulting in a representation of three “marine” and two “estuarine” growth bands. Radiocarbon results provided preliminary evidence supporting the hypothesis of a relationship between ^{13}C, ^{14}C, and hard water exposure. Using Chi-square statistics, the five radiocarbon dates were calculated to be statistically distinguishable, a significant result considering the five radiocarbon dates were from the same shell. Furthermore, the pooled radiocarbon age of the “marine” growth bands was statistically distinguishable from one of the estuarine samples, where a difference of 304 ^{14}C years was observed. Conversely, when the pooled radiocarbon age of the “marine” growth bands was compared to the other estuarine sample, the two radiocarbon dates were statistically the same. The reason for this was hypothesised to be due to variability in old ^{14}C. The tide, along with wind and storms, results in variable concentrations of marine and fresh water held close to the shoreline by onshore currents, and so these variable conditions result in variability of the concentration of old ^{14}C in the water.

Acknowledgements

I would like to express my gratitude to everyone who facilitated the completion of this research project. I am very grateful for my amazing supervisor, Dr. Fiona Petchey, who guided and encouraged me, reading countless drafts that had obscure formatting, answering my many questions throughout the workday, and taking the time to explain new concepts to me. Fiona's support has resulted in a thesis that I am very proud of.

I would like to acknowledge my fellow work colleagues at the Waikato Radiocarbon Dating Laboratory: Kathleen Dabell, Katy Reekers, and Vanessa Jackson, who, in addition to offering me technical advice, acted as therapists for the many challenges I faced. You guys are awesome!

Thank you to Helen Turner who taught me how to use the Scanning Electron Microscope, your cheerfulness made the process even more enjoyable. Thank you to Clayton Pace from Pace Engineering and Steve Newcombe (School of Science, scientific glassblower); modifications to the vacuum line would not have been possible without your assistance.

Thank you to Simon Eminson and my husband Geoffrey; your efforts to proofread my thesis and the advice you offered are very much appreciated. Thank you also to Cheryl Ward for helping me format my thesis.

And finally, this thesis would not have been possible without the love and support from my family and friends. To my parents, thank you for always being there for me, and to my friends, you all played some part in this journey, whether it be sending me funny memes to keep my spirits high, or being a listening ear throughout this project. I am especially grateful to my husband Geoffrey, who spent many hours helping me tame the beasts that are Excel, Word, and Paint. His knowledge and humour made it possible for me to complete this thesis and keep my head above water.

Table of Contents

List of Figures

List of Tables

Glossary

‰ (per mill): Parts per thousand.

^{14}C: A radioactive isotope of carbon containing six protons, six electrons and eight neutrons. The nucleus is unstable, resulting in the emission of ionization radiation of particles. Used to determine the time since death of carbon-based materials

^{14}N: A stable isotope of nitrogen containing seven electrons, seven protons and seven neutrons. It is a product of ^{14}C decay.

Accelerator: Instrument that accelerates ions to high kinetic energies before mass analysis.

Acid hydrolysis: Reaction in which a protic acid is used to catalyse the cleavage of a chemical bond, forming two or more substances, one of which is water.

Atom: The smallest unit of matter that has the characteristic properties of a chemical element.

Background Standard: Samples of known age are routinely run alongside unknown age samples to ensure accuracy and precision in the obtained dates. A background standard is a standard that has no detectable levels of ^{14}C left and is used to assess modern contamination.

Background: Radiation that exists throughout the environment.

Bake-Out/Baking Out: Heating items to a very high temperature in order to remove contaminant gas from glassware.

Beta Decay: Type of radioactive decay where a neutron is transformed into a proton by the emission of an election.

Biominerals: A mineral produced by the activity of living things.

Bioturbation: The disturbance of soils and sediments by animals or plants.

bp: stands for “before present’ or ‘years before present’. Because the ‘present’ time changes, it is set at 1st January 1950. Lowercase ‘bp’ refers to an uncalibrated radiocarbon age.

BP: Same definition as above except uppercase BP refers to a calibrated radiocarbon age.

Calibration Curve: Used in radiocarbon dating to convert a conventional radiocarbon age into a calendar age. This is achieved by comparing the unknown to a set of standards of known age.

Catalyst: A substance that assists in the graphitisation reaction.

Cathode Target: A target into which the graphite is loaded and pressed.

Cold finger: A glass or metal component, usually tube-like, that freezes, or holds, gas molecules within a vacuum line

Combustion: Reaction in which carbon is converted to CO_2 via oxygen and heat.

Convective loss: Loss of heat.

Conventional Radiocarbon Age (CRA): A CRA is calculated from the measurement of isotopic ratios, along with these assumptions:

- 1950 is the base year, *i.e,* AD 1950 is the present
- Atmospheric level of ^{14}C is constant
- Half-life of ^{14}C is 5568 years
- Isotopic fractionation is normalized to $\delta^{13}C = -25‰$

Cosmic-Rays: High energy atomic nucleus or other particle travelling through space.

Cryogenically: Using low temperatures, to freeze water produced during graphitisation.

Dead ^{14}C: Beyond current ^{14}C detection limits.

Dead Space: Areas within a vacuum line where gas can become trapped.

Decay Rate: The rate, referred to as half-life, at which a radioactive isotope decays due to its unstable atomic nucleus. The half-life of ^{14}C is 5730 ± 40 years (Cambridge half-life).

Dendrochronology: Also referred to as tree ring dating. Many species of trees produce annual growth rings, which can be used to interpret when past events occurred, particularly paleoclimates and climatic trends.

Desiccant: Drying agent.

Dissolved Inorganic Carbon (DIC): Sum of the aqueous species of inorganic carbon available to a shell from the environment it lives in.

$F^{14}C$: Also called fraction modern. Refers to the deviation of a sample's radiocarbon content from a modern standard.

Flux: An effect that appears to pass or travel through a surface or substance.

Fractionation: When a material undergoes a chemical reaction or a physical process, the different isotopes of an element will take part in the reaction at different rates, which is dependent on their mass. Lighter isotopes will generally proceed at a faster rate than heavier ones. This observation is defined as fractionation and occurs naturally in the environment, for example, when carbon is incorporated into the marine reservoir.

Gaussian Standard Deviation: Normal probability distribution of a variable.

Glass Cracker: A glass component used at the Waikato Radiocarbon Dating Laboratory for cracking open combustion tubes, allowing the gas within the tube to be processed through a vacuum line.
Graphite Yield: Percentage of CO_2 that has been converted to graphite.
Graphite: Carbon product formed from graphitisation.
Graphitisation: Reaction in which CO_2 is exposed to high temperatures, usually between 550 - 600°C, for a prolonged period, along with H_2, to form graphite.
Half-life: The time it takes for the radioactivity of an isotope to fall to half its original value.
Hard Water Effect: Causes the radiocarbon ages of mollusc shells, or plants, to be older than their true age due to old carbon being synthesised.
Infrared: Waves of light that are part of the electromagnetic spectrum.
In-house Standard: A standard of known age used by the measuring laboratory.
Isotope: Another form of an element whereby it has the same number of protons, and hence, atomic number, but with a different number of neutrons, resulting in a different atomic mass.
Laminar Flow Box: Enclosed cabinet or bench designed to prevent contamination by applying airflow or through filters.
Marine Reservoir Effect (MRE): The observed difference in ^{14}C age between the atmosphere and surface ocean due to the slow CO_2 exchange rate between the atmosphere and the surface ocean.
mb (millibars): Standard unit of measurement of atmospheric pressure
Mesh Size: Number of openings in one square inch of a screen.
mgC (milligrams carbon): Measurement of the quantity of carbon in graphite.
Neutron: Stable subatomic particle occurring in atomic nuclei, which has no charge.
Nucleus: Positively charged centre of an atom.
Oxidised: Combine an element with oxygen to oxidise it.
Peltier Cell: Also called a Peltier device. A voltage is applied across two different conductors, which causes heating of one junction and cooling of the other.
pMC: “Percent modern carbon”. Refers to the deviation of a sample’s radiocarbon content from a modern standard, expressed as a percentage.
Polycrystalline: Solids that are composed of many crystals of varying size and orientation.
Pooled Radiocarbon Date: When several radiocarbon dates are known or suspected to be from the same object, or context, they can be combined, or “pooled” together to

form a single mean age and error. A T test can be applied to the pooled radiocarbon dates to assess if each sample has the same true mean.

Pressure Transducer: Converts pressure into an analog electrical signal.

Primary Standard: A standard that has an internationally recognised consensus value for its radiocarbon age. NBS Oxalic Acid I is a primary standard.

Proportional-Integral-Derivative Temperature Controller: An instrument used to regulate temperature.

Proton: Stable subatomic particle occurring in atomic nuclei, which has a positive charge.

psi (pounds per square inch): Measurement of pressure.

Reaction Efficiency: How fast graphitisation occurs.

Reduced: Loss of oxygen.

Slush: Dry ice with a solution of 50% isopropyl alcohol and 50% ethanol.

Spallation Reactions: Reaction where a target is bombarded by high-energy particles.

Standard Volume Glass Ampoule: An ampoule that holds a known quantity of gas.

Standards: Radiocarbon measurements are performed relative to a standard of known activity. Several standards are mentioned in this thesis. Definitions are given below:

- Oxalic Acid: This is the principal modern standard used in radiocarbon dating, and is also referred to as Ox-I. It is no longer commercially available, where Oxalic acid II is now used (Ox-II), prepared by the US National Bureau of Standards (NIST). It is defined as the radiocarbon activity measured in AD 1950 of a wood sample growing in the Northern Hemisphere.
- IAEA C-1 (Carrara Marble): A secondary standard containing 100% $CaCO_3$. It has a ^{14}C activity of 0.00 ± 0.02 pMC
- IAEA C-2 (Travertine): Form of terrestrial limestone, deposited around mineral springs. IAEA C-2 has a ^{14}C activity of 41.14 ± 0.03 pMC
- IAEA C-6 (Sucrose): A secondary standard, calibrated relative to Ox-I. It has a ^{14}C activity of 150.61 ± 0.11 pMC
- IAEA C-7, C-8: Standards prepared from industrial oxalic acids, with a ^{14}C activity of 15.03 ± 0.17 pMC

Thermal Conductivity: Measure of a materials' ability to conduct heat.

Ultra-Torr® vacuum fittings: Metal components used in radiocarbon vacuum line systems, which can have a variable number of ports for connecting to other components, such as glassware.
Upwelling: Mixing of deep waters with surface waters.
Ventral Margin: Edge/lip of a shell.
Viton™ O-Ring: A chemically resistant sealing device used on vacuum lines to close off sections of a vacuum line when necessary.
Water Trap: Component in a vacuum line used to trap water that is formed from combustion, or during graphitisation.
ΔR: The difference between the measured radiocarbon age of a marine sample from a particular region and the expected modelled age as determined by the global marine calibration curve.

Chapter 1
Introduction

The invention of radiocarbon dating is considered one of the most revolutionary scientific techniques in the field of archaeology. It enabled archaeologists and geologists to build and develop a more precise chronological timeline based on a sample's age instead of ordering events based on relative stratigraphy at individual sites, or by comparing them to other similar sites (Taylor & Bar-Yosef, 2014). Willard Libby, a chemistry professor at the University of Chicago, inferred that the radioactive isotope, ^{14}C, should be incorporated into all living matter. Furthermore, because ^{14}C is an unstable isotope, Libby realised that if he could determine the decay rate and the residual ^{14}C content of an object, an age since death could be calculated. Libby was awarded the Nobel Prize in Chemistry in 1960 for his discovery (ACS Chemistry for Life, 2016).

Commonly dated materials include wood, charcoal, bone, and shell, though other carbon-containing materials such as hair, skin, and pollen can also be radiocarbon dated (Taylor & Bar-Yosef, 2014). Radiocarbon dating is used across a wide range of scientific areas of study such as archaeology, forensics, paleoenvironmental studies, and geosciences (Currie, 2004). The value of the technique in many scientific fields has resulted in more than 100 ^{14}C laboratories worldwide (Radiocarbon, 2021). While radiocarbon dating has come a long way in the last 70 years, research continues to further develop and refine the technique (Taylor & Bar-Yosef, 2014).

1.1 Overview

1.1.1 ^{14}C Production and Dispersal

The production of ^{14}C occurs when neutrons, formed by spallation reactions (caused by cosmic rays), react with the nucleus of ^{14}N. These atoms are rapidly oxidised to ^{14}CO and then subsequently to $^{14}CO_2$, which then enter the earth's carbon exchange cycle and are dispersed throughout the various reservoirs; atmospheric, terrestrial, and marine (**Figure 1.1**) (Tornqvist, 2015). In the terrestrial reservoir, carbon becomes incorporated into plant biomass via photosynthesis, and subsequently the animals that

eat these plants take up ^{14}C. In the marine reservoir, ^{14}C is absorbed onto the ocean's surface (top 200 m) via CO_2 exchange and then incorporated into marine life by various chemical processes (Taylor & Bar-Yosef, 2014).

Carbon incorporated into these various carbon reservoirs consists of three main isotopes: stable ^{12}C and ^{13}C, and radioactive ^{14}C. The time it takes for a radioactive isotope to decay is called the half-life, and in the case of ^{14}C, this was calculated to be 5730 ± 40 years (Cambridge half-life). This means that after 5730 years, half of the original amount of ^{14}C will remain (Taylor & Bar-Yosef, 2014). While living, an organism continually replenishes ^{14}C, thereby maintaining an approximate equilibrium ^{14}C content with the atmosphere. Once an organism dies, this metabolic process will cease, and ^{14}C will start to decay back to ^{14}N, initiating the radiocarbon "clock" (Jull, 2013).

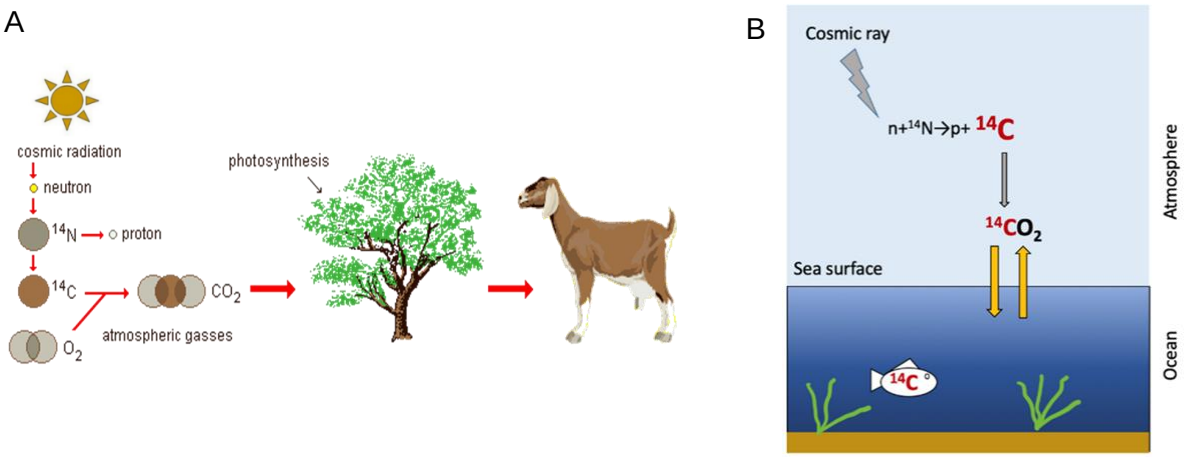

Figure 1.1 (A) Natural production of ^{14}C in the atmosphere and its incorporation into the terrestrial reservoir. Figure from O'Neil (1998). (B) Incorporation of CO_2 into the marine reservoir. Figure from Quarta *et al.* (2021).

1.1.2 Assumptions

When Libby first started to develop the concept of using radiocarbon as a dating tool, he made two major assumptions:

1) The concentration of ^{14}C in living organisms has remained constant over time.
2) Complete and rapid mixing of ^{14}C occurs between all reservoirs.

Neither of these assumptions holds. The production rate of ^{14}C has not remained constant over time because of changes in the cosmic-ray flux and solar magnetic field. Incomplete mixing also occurs between the atmospheric and terrestrial carbon reservoirs, and the atmosphere and surface waters (Alves *et al.*, 2019). Moreover, researchers identified offsets between calendar ages (determined via dendrochronology) and ^{14}C age determinations. These comparisons are the basis of calibration curves which are used to convert a 'conventional radiocarbon age' into a calendar age. On a worldwide scale, differences between the ^{14}C concentrations in tree rings of similar age from the Northern and Southern Hemispheres are apparent, with terrestrial material from the Southern Hemisphere appearing older than the Northern Hemisphere (Leavitt & Bannister, 2016, Taylor & Bar-Yosef, 2014).

The incomplete mixing between the atmospheric and surface ocean carbon reservoirs contributes to marine samples appearing, on average, 500 years older than contemporaneous terrestrial samples. This is known as the marine reservoir effect (MRE) or *R*. It is the result of the slow CO_2 exchange rate between the atmosphere and the surface ocean, and the upwelling of 'old' water from the deep ocean where it may have resided for thousands of years (Alves *et al.*, 2018, Taylor & Bar-Yosef, 2014). The global marine calibration curve is used to convert marine ^{14}C ages to calendar ages. However, regional corrections also need to be considered. These are termed Δ*R* and are defined as "the difference in age from the marine calibration curve, or *R*" (Heaton *et al.*, 2020).

1.1.3 Accelerator Mass Spectrometry

Initial radiocarbon dating methods relied on the measurement of ^{14}C beta decay events to calculate the unknown age of the sample; a technique termed radiometric dating. Beta decay, in relation to radiocarbon dating, is a process where a ^{14}C atom decays into a ^{14}N atom, "during which a neutron from a carbon atom becomes a proton" (Global Monitoring Laboratory, accessed 2/4/2022). Three radiometric techniques were initially developed: solid-carbon, gas proportional, and liquid scintillation. More recent

developments involve directly measuring the ^{14}C content relative to ^{12}C and ^{13}C[1] using a technique called accelerator mass spectrometry (AMS).

The main advantage of AMS is its ability to date smaller samples, where the amount of sample required is roughly three orders of magnitude less than needed for radiometric dating. This reduction in minimum sample size expanded the types of materials that could be radiocarbon dated (*e.g.,* individual seeds, pollen, and single amino acids). Smaller sample requirements enable pre-treatment protocols for AMS to be much more rigorous, both chemically and physically, without compromising the accuracy and precision of a ^{14}C measurement (Taylor & Bar-Yosef, 2014).

1.1.4 Upper Age Limit

After eight to ten half-lives, the concentration of ^{14}C is reduced below what can be effectively detected. This is a result of the measured concentration of ^{14}C being indistinguishable from background values. Consequently, depending on the measurement precision at each radiocarbon dating laboratory, the upper limit of ^{14}C dating is between 40,000 and 60,000 years ago. Because AMS uses a relatively small amount of sample, any extraneous carbon can significantly impact the final age (**Table 1.1**). This is especially true for older samples (samples ≥ 20,000 years) as trace amounts of modern contaminants become even more problematic. Contaminant carbon can be introduced in a variety of ways, from sample handling, pre-treatment, combustion, and conversion of CO_2 during the graphitisation process (Taylor & Bar-Yosef, 2014). These issues are discussed in more detail in section 1.1.5.

1.1.5 Contamination

Contamination of a sample refers to the incorporation of any carbon-containing compounds that are not part of the original sample matrix. Laboratory pre-treatment protocols are designed to eliminate common carbon compounds derived from the burial environment, while careful quality control protocols and measurement of replicate standards minimise the introduction of contamination from within the laboratory.

[1]Carbon has 15 isotopes, but only ^{12}C, ^{13}C, and ^{14}C are naturally occurring, making up 98.9%, 1.1%, and 10^{-10}% of all carbon, respectively.

High purity chemicals are used to minimise contamination. These include using Type 1 water, and analytical reagents with high purity (hydrochloric acid, sodium hydroxide, orthophosphoric acid). Glass consumables undergo rigorous cleaning protocols to reduce dust and cross-contamination which involves rinsing, sonicating and baking them out at 500ºC before use. Plastic or metal consumables are wiped down with methanol and air blasted to reduce cross-contamination. Memory effects (cross-contamination) are reduced by running young samples after old samples on the vacuum lines.

When contamination of a sample does occur, the extent to which it affects a sample depends on the age of the original sample, the radiocarbon activity of the contaminant, and the percentage age contribution of the contaminant.

Table 1.1 shows how modern contamination affects samples of different ages. For example, if a 50,000-year-old sample is contaminated with just 1% modern carbon (pre-bomb ^{14}C), the apparent age of the sample will be 35,000 years BP, and as the percentage of modern carbon increases, the difference between the true and apparent age becomes bigger. However, a sample that is 1000 years old is much less affected by the addition of modern carbon; 1% modern carbon will result in an apparent age of 990 years – only 10 years difference. In contrast, the effect of “dead carbon” contamination on modern age samples is much less severe. For example, the addition of 1% dead carbon to a modern age sample will result in the sample appearing around 80 years too old, and a 10% addition will result in an apparent age that is 850 years too old (Taylor & Bar-Yosef, 2014). While 850 years is still quite significant, it is less significant than the 31,000-year difference that is observed for 10% modern carbon contamination in a 50,000-year-old sample.

Table 1.1 Impact of contamination on radiocarbon age with varying percentages of modern carbon contamination. Table from Taylor & Bar-Yosef (2014).

Actual Age (BP) years	Approximate age with the addition of the following percentages of modern carbon		
	1%	**5%**	**10%**
1000	990	950	900
2000	1950	1890	1750
3000	2950	2800	2650
4000	3950	3750	3500
5000	4950	4650	4350
6000	5900	5550	5150
7000	6900	6450	5950
8000	7850	7350	6750
9000	8850	8200	7500
10000	9800	9050	8200
15000	14860	13250	11600
20000	19850	16950	14450
25000	23350	19100	15750
30000	27200	21000	1700
35000	30500	22300	17600
40000	32700	23100	18000
45000	34700	23500	18250
50000	35650	23800	18360

Resolving contamination issues is an ongoing area of research and development in AMS as it is critical to the ability to radiocarbon date small size samples. While contamination usually involves the addition of secondary carbon added to the sample post-deposition, the introduction of carbon in vivo from a secondary reservoir can have a similar impact on the apparent age of a sample. One example is the uptake of ancient bicarbonate ions derived from limestone by estuarine shellfish. This hard water effect is at the core of this research project and how it occurs, and the effect it has on samples are discussed in section 1.2.

1.2 Reservoir Effects

The skeletons of molluscan shells are polycrystalline biominerals, mainly composed of calcium carbonate ($CaCO_3$). Carbon is incorporated into molluscan shells from two different pools: dissolved inorganic carbon (DIC) from the ocean, and carbon from respiratory CO_2, mainly from food metabolism. Because the carbon that forms their

exoskeletons originates in various carbon pools, the interpretation of radiocarbon age is complicated (Douka, Higham, & Hedges, 2010).

Radiocarbon dating of shellfish requires consideration of:

- The global marine reservoir and temporal variations (Marine reservoir effect).
- The incorporation of CO_2 from the atmosphere takes much longer to distribute throughout the ocean water column, resulting in a gradient of ^{14}C age, *i.e*, shells at 100 m and 1000 m depth will have different ^{14}C ages.
- Temperature affects the solubility of CO_2 in seawater, where colder temperatures contribute to a faster exchange rate of CO_2 (Alves *et al.*, 2018).
- Regional reservoir effects (Alves *et al.*, 2019).
- Hard water effect (Petchey & Clark, 2011).

1.2.1 The Marine Reservoir Effect

As discussed previously, radiocarbon dates for marine shellfish appear older than terrestrial samples, a result of the slow CO_2 exchange rate between the atmosphere and the surface ocean (**Figure 1.2**).

Figure 1.3 illustrates the global marine ^{14}C calibration curve, Marine20 (Heaton *et al.*, 2020), which represents a global modelled average of the ^{14}C activity of the surface ocean and is thought to account for changes over time. On average, the offset (*R*) between the global marine (Marine20) and terrestrial (IntCal20) calibration curves is approximately 500 years (Butler *et al.*, 2009, Heaton *et al.*, 2020).

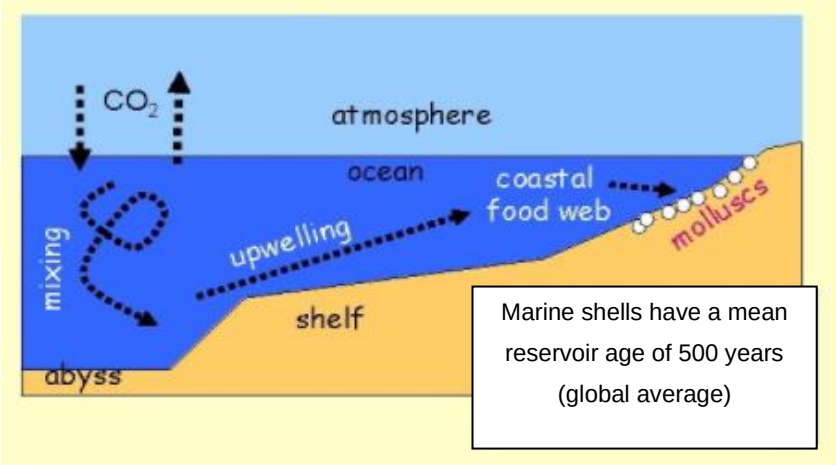

Figure 1.2 Diagram demonstrating the marine reservoir effect. Figure from Lonsberry (2022).

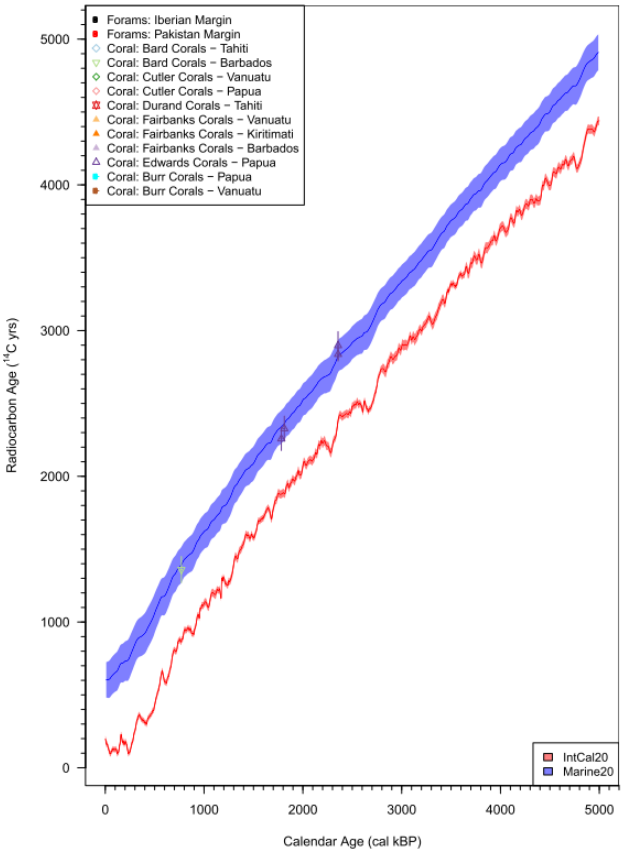

Figure 1.3 ^{14}C concentration over the last 5,000 years in the terrestrial atmosphere (red) and the ocean (blue). The marine curve represents the modelled global average. Figure from Heaton *et al.* (2020).

1.2.2 Local Reservoir Offset

While the global marine calibration curve allows for a correction due to the observed difference between the ^{14}C activity of the marine and terrestrial reservoirs, it does not account for local variations (Petchey *et al.*, 2012). A local reservoir offset is referred to as ΔR and is the difference between the modelled ^{14}C age of surface water and the actual ^{14}C age of surface water in that area (Keaveney & Reimer, 2012). ΔR values are location specific and can vary over time because of oceanic circulation, terrestrial runoff, changes in current systems, sea level or tidal range, freshwater discharge, and varying levels of upwelling (Gómez *et al.*, 2016, Petchey & Schmid, 2020, Philippsen, 2013). Upwelling can lead to age differences of up to 1,200 years due to water from deeper parts of the ocean, which can reside there for centuries, being brought to the surface (**Figure 1.2**) (Butler *et al.*, 2009, Gómez *et al.*, 2016, Taylor & Bar-Yosef, 2014, Quarta *et al.*, 2021).

Regional differences can be quite large; $\Delta R = 697 \pm 50$ ^{14}C years, Signy Island, Antarctica (Peck & Brey, 1996), but also relatively small; $\Delta R = 45 \pm 19$ ^{14}C years, Solomon and Coral Seas (Petchey, Phelan, & White, 2016).

Regional ΔR values are measured by:

1) ^{14}C dating paired terrestrial and marine samples of the same age.
2) ^{14}C dating marine samples of known age collected before AD 1955.

1.2.3 Hard Water Effect

The hard water effect occurs in areas where there is limestone. As water travels through limestone, it picks up bicarbonate ions depleted in ^{14}C. This ‘old’ water is incorporated into the shells of molluscan shellfish, making them appear older. In estuarine environments, limestone or ancient carbonate sources can cause the local radiocarbon reservoir age to be older by hundreds of years (Bezerra, Vita-Finzi, & Lima Filho, 2000, Douka, Higham, & Hedges, 2010). In contrast, incorporating terrestrial organic material can result in lower reservoir ages (appearing younger) (Alves *et al.*, 2018, Philippsen, 2015). Shellfish that live in locations with restricted water circulation and areas close to

the shore are more likely to be affected. Therefore, it is essential to investigate habitat preferences and local geological and hydrological information (Philippsen, 2013). Dye (1994) and Anderson, Higham, & Wallace (2001) found a difference of up to 600 ^{14}C years for herbivores (*Nerita atramentosa* and *N. picea*) and omnivores (*Cypraea caputerpentis* and *C. exarate*) living in limestone environments around Hawai'i and Norfolk Island.

1.3 The Mariana Islands

1.3.1 Archaeological Context

The Mariana Islands are an archipelago located in the northwest Pacific. One of the oldest archaeological sites, Bapot-1, is located at the south end of the Island of Saipan, on the edge of Laulau Bay (**Figure 1.4**). The site was investigated in the 1920s, and radiocarbon dates from excavations were first carried out in 1977 (Petchey *et al.*, 2018). While the exact date of human arrival is currently under debate (Carson, 2014), it is thought the site was first occupied around 3300 years ago (Petchey & Clark, 2021). This timing is significant because it represents the longest ocean voyage of its time, more than 2000 km. Therefore, establishing a date of human arrival is necessary for modelling the timeframe of Neolithic expansion in Island Southeast Asia and the subsequent spread of humans into the Pacific (Petchey *et al.*, 2017).

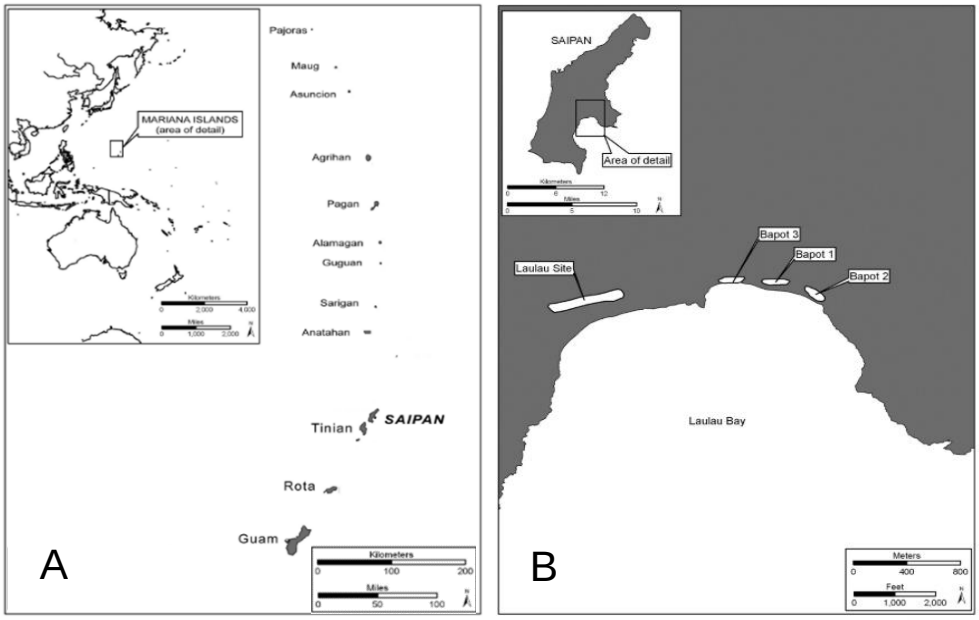

Figure 1.4 (A) Location of the Mariana Islands, (B) Saipan and Bapot-1 location at Laulau Bay. Figure from Clark *et al.* (2010).

1.3.2 Difficulty in Obtaining Reliable Radiocarbon Dates

Colonisation of the Pacific is an important chapter in the history of human dispersal. Obtaining reliable radiocarbon dates from Bapot-1, however, has been difficult. Short-lived terrestrial materials such as charred twigs are either highly degraded or scarce, and although shell material is abundant, uncertainty over what local reservoir correction to use hinders its use. The difficulty of radiocarbon dating shells from Saipan is caused by limestone dominating the local bedrock (Petchey & Clark, 2021). As freshwater seeps through the calcareous strata into the aquifer lens, it takes up bicarbonate ions which contain "dead" ^{14}C. This ^{14}C old water is then discharged at Laulau Bay, affecting some, but not all, shell taxa that live close to the shore (Petchey & Clark, 2021). In the bay, the tide, along with wind and storms, results in variable concentrations of marine and freshwater held close to the shoreline by onshore currents (Petchey *et al.*, 2017). The lack of information surrounding what ΔR value to apply to radiocarbon dates from Bapot-1 means that is it difficult to establish an accurate date of human arrival in the Mariana Islands (Petchey *et al.*, 2017). However, Petchey *et al.* (2016), and Petchey *et al.* (2017) noted that variation to stable isotope values could be used to separate shells that were

affected by terrestrial carbon input, effectively enabling the selection of shells unaffected by hard water.

1.3.3 Stable Isotopes

^{13}C isotopes offer key information about the environmental conditions that mollusc shells were living in at the time of shell formation because shellfish precipitate their shells in equilibrium with the local environment. ^{13}C is an indicator of water source and overall marine productivity, and any input of freshwater will result in the depletion of ^{13}C (Petchey *et al.*, 2012). In theory, marine bivalves should have a $\delta^{13}C$ value that is on average, 2‰ higher than the average ocean DIC (Tanaka, Monaghan, & Rye, 1986), which for the Mariana Islands is 1.3 - 1.7‰ (Tagliabue & Bopp, 2008). If the ^{13}C signal of a shellfish is more negative than the average DIC (*i.e*., <1.3‰) there is an increased risk that non-marine ^{13}C and ^{14}C was introduced into the shell and it may have been affected by hard water. While $\delta^{13}C$ values can be used to reveal the environment in which ^{14}C was deposited, they cannot directly offer information as to whether a shell has been impacted by hard water. This is where establishing a correlation between ^{13}C, ^{14}C and hard water exposure comes into play.

1.3.4 Stable Isotopes, ^{14}C, and Hard Water

By observing the correlation between shell stable isotopes and radiocarbon results, Petchey *et al.* (2017) and Petchey *et al.* (2018) made the following conclusions about shellfish from the site of Bapot-1:

1) Petchey *et al.* (2017) observed that *Tegillarca granosa* and *Gafrarium* sp. shellfish from the Mariana Islands exhibited $\delta^{13}C$ values that were much lower than expected for shellfish living in a marine environment.
2) When radiocarbon dated, samples that had $\delta^{13}C$ more positive than the average ocean DIC were much younger in comparison to those that had more negative $\delta^{13}C$.
3) Petchey *et al.* (2018) calculated that filter-feeding bivalves that were identified as “marine” based on $\delta^{13}C$ values had a ΔR offset of -55 ± 27 ^{14}C years (*i.e*, 55

years too young). In contrast, the average ΔR offset for those identified as "estuarine" was 197 ± 43 ^{14}C years (*i.e*, 197 years too old) (**Figure 1.5**).

The hypothesis put forward by Petchey is that shells displaying a $\delta^{13}C > 1.7‰$ indicate a marine environment whereas shells with a $\delta^{13}C < 1.3‰$ indicate an estuarine environment and are therefore most likely to be affected by hard water. Shellfish displaying a $\delta^{13}C$ signal between these two values could be influenced by hard water.

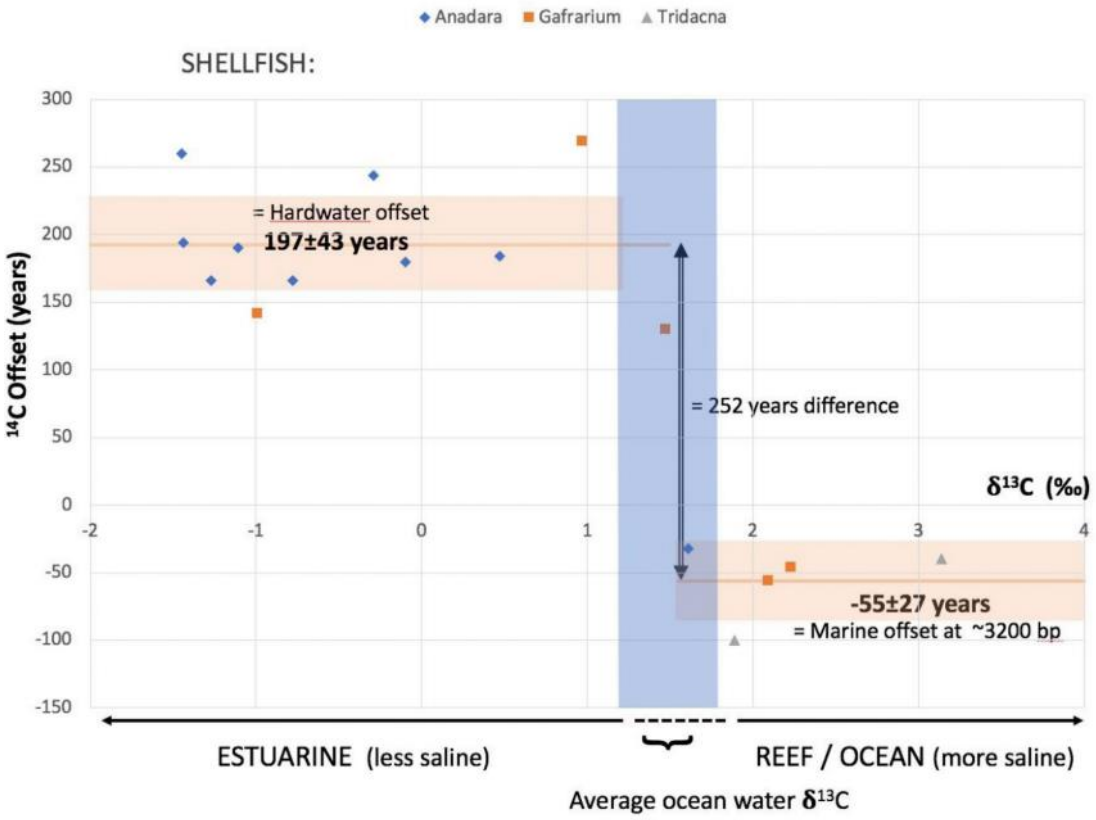

Figure 1.5 Graph demonstrating the isotopic separation ($\delta^{13}C$ and ΔR) between estuarine and marine shellfish from Bapot-1. Figure from Petchey & Clark (2021). Note: the name *Anadara* has changed to *Tegillarca granosa.*

1.3.5 Shell Growth Bands

While shellfish typically display annual or seasonal patterns of growth increments, recognised as bands that alternate with thinner bands or rings (**Figure 1.6**), microscopic daily growth bands also form in response to daily tidal cycles (Jones, 1989). Additional 'disturbance' bands may also be deposited due to changes in metabolic processes

caused by environmental extremes, such as water temperature, physical trauma, or sporadic weather events (Chute, Wainright, & Hart, 2012).

As discussed in Section 1.3.3, the shells of shellfish are composed of calcium carbonate, obtained from the water they live in. Therefore, ^{13}C and ^{18}O isotopes will reflect the environment during deposition. Because *Tegillarca granosa* and *Gafrarium* sp. can tolerate both marine and estuarine environments, ^{13}C signals can change over time as the environment changes. Therefore, to accurately radiocarbon date a single shell variously influenced by hard water and open ocean environments, it is necessary to sample seasonal growth bands, and even smaller subsections if possible. The challenges associated with this are discussed in Chapter 2.

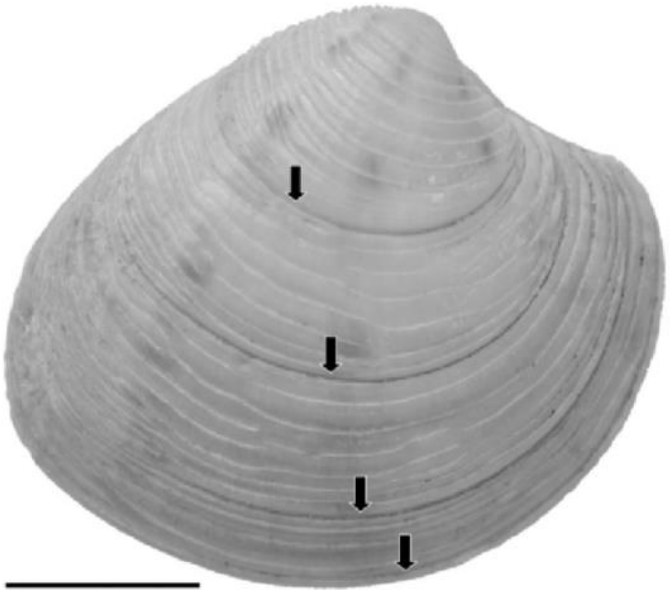

Figure 1.6 Growth rings (black arrows) visible on the surface of *Chamelea gallina*. Scale bar (black horizontal line) = 1 cm. Figure from Gaspar (2004).

1.4 Research Aims

My research project investigates the radiocarbon dating of shellfish seasonal growth bands that have been affected by hard water, as identified by $\delta^{13}C$. To prove the working hypothesis put forward by Petchey *et al.* (2018) of a ΔR change with changes in

$\delta^{13}C$, significant technical issues need to be overcome. Specifically, it is vital that laboratory-induced contamination issues be minimised when dating ultra-small samples. Therefore, the objectives of this research project are:

1) Improve the precision of ultra-small radiocarbon dating by experimenting with a selection of volume and chemical modifications to Waikato Radiocarbon AMS protocols.
2) Using these new ultra-small methodologies, radiocarbon date growth bands deposited at different times, as indicated by $\delta^{13}C$, from a *Gafrarium* sp. shellfish, to investigate the relationship between $\delta^{13}C$, ^{14}C, and hard water exposure.

The following chapters outline previous research into AMS dating of ultra-small samples, the methodologies used in this research project, radiocarbon results of standards using selected modifications, and the radiocarbon results from radiocarbon dating seasonal rings from a *Gafrarium* sp. shellfish from the archaeological site Bapot-1, dated to ~3000 cal BP.

The chapters are organised as follows:

- Chapter 2 discusses the various methods and findings used by other laboratories to improve ultra-small sample precision.
- Chapter 3 describes volume modifications that have been implemented to procedures currently used at the Waikato Radiocarbon Dating Laboratory.
- Chapter 4 describes three chemical modifications implemented to the AMS procedures currently used at the Waikato Radiocarbon Dating Laboratory.
- Chapter 5 discusses the radiocarbon results using the new methodologies as indicated from the replicate measurement of laboratory standards.
- Chapter 6 discusses previous research using ^{13}C to identify growth bands affected by hard water, the methods used for subsampling a *Gafrarium* sp. shellfish for this thesis, and the ^{13}C and ^{14}C results for five growth bands from the *Gafrarium* sp. shellfish from the Mariana Islands.
- Chapter 7 provides a summary for each chapter, recommendations for further research, and conclusions from this study.

Chapter 2

Radiocarbon Dating Ultra-Small Samples

2.1 Introduction

Radiocarbon dating has seen many developments since its invention in 1945, however further improvements are required to enable samples that are defined here as ultra-small (<0.10 mgC) to be reliably radiocarbon dated. Interest in this area of research has grown over the years for several reasons: in scenarios where a sample has cultural or religious significance (Fedi *et al.*, 2020), subsampling the smallest amount possible for radiocarbon analysis is ideal; small samples that generate a low carbon yield (Hua *et al.*, 2004) require the ability to radiocarbon date ultra-small samples. Specific cases that exemplify the latter include radiocarbon dating single foraminiferal shells to enhance the interpretation of the bioturbation effect (Missiaen *et al.*, 2020), or measuring the ^{14}C content of CO_2 air bubbles in Antarctic ice (Hua *et al.*, 2004). Typically, these new applications aim to date samples as small as 0.01 mgC.

Currently, the Waikato Radiocarbon Dating Laboratory (WRDL) routinely dates shell samples that are >0.30 mgC. This usually involves sampling approximately five mm back from the ventral margin of the shell, over an area of approximately one cm. Several growth bands are included in these sample sizes, and the sampling is specifically designed to minimise seasonal variation. However, as discussed in Chapter 1, this sampling strategy reflects the average ^{14}C age of all the incorporated growth bands and, therefore, could incorporate marine and estuarine signals in shells tolerant to both environments. To overcome this issue and to radiocarbon date shell growth bands that display only a marine signal, samples <0.10 mgC are required.

The WRDL classifies sample sizes as follows:

- Routine: >0.30 mgC
- Small: 0.30 mgC – 0.10 mgC
- Ultra-small: <0.10 mgC

2.2 Issues with Radiocarbon Dating Ultra-Small Samples

Contamination introduced by the radiocarbon dating process becomes more problematic once sample size decreases below 0.10 mgC. **Table 2.1** lists the steps for how contamination can be introduced when shell samples are processed for radiocarbon dating. Aspects associated with the running of an accelerator mass spectrometer are not included in this discussion as this process is not run at the WRDL.

Table 2.1 Sources of contamination associated with processing shell samples

Sources of contamination			
Pre-treatment	CO_2 evolution	Graphitisation	Sample pressing
Poor handling of samples in the laboratory, or in the field during sample collection, *e.g.,* not wearing gloves during sample handling, resulting in the introduction of contaminants such as hair. Consumables, such as test tubes or watch glasses, insufficiently cleaned. Contaminants can be introduced through chemicals, such as hydrochloric acid or water.	Glass vials (which contain shell samples) insufficiently cleaned. Faulty vacuum at any stage of acid hydrolysis, including the addition of orthophosphoric acid. Contaminants can be introduced through orthophosphoric acid, which is used to dissolve shell samples.	Atmospheric CO_2 is absorbed onto the walls of glass units. Glassware from vacuum lines not cleaned properly. Leaks in the vacuum line. Contaminants from chemicals such as iron (Fe) powder, magnesium perchlorate ($Mg[ClO_4]_2$), and hydrogen (H_2).	Cathode targets and the pin used for graphite pressing insufficiently cleaned. Atmospheric CO_2 absorption by the graphite target can occur if stored for too long. This is mitigated by using a 0.1 M reservoir of NaOH to absorb ambient CO_2, and also by minimising the time between sample pressing and analysis.

As sample size decreases, modern and dead carbon (^{14}C depleted) contamination becomes more prevalent (Santos *et al.*, 2007b). Modern contamination can be introduced during sample preparation and handling whereas dead carbon contamination can arise from the catalyst. Potentially, between 0.001 mgC and 0.005 mgC of contaminant carbon is introduced during pre-treatment and purification of the sample (Walter *et al.*, 2016). **Figure 2.1** illustrates the impact of modern carbon contamination on coal, and dead carbon contamination on the Ox-I (Oxalic Acid) standard, as contamination becomes more prevalent as sample size decreases.

Fractionation is also a concern for ultra-small samples (Santos *et al.*, 2007a, Walter *et al.*, 2016). Correcting for fractionation is an important factor in calculating radiocarbon ages as the radiocarbon process involves several chemical processes (combustion, transferal of CO_2 through a vacuum line, graphitisation) which alter the ratio of ^{14}C to ^{13}C and ^{12}C. While fractionation is accounted for, additional fractionation effects, which can occur during processing of ultra-small samples (Santos *et al.*, 2007b, Walter *et al.*, 2016), may result in incorrect ^{14}C to ^{13}C and ^{12}C ratios, leading to inaccurate ^{14}C measurements.

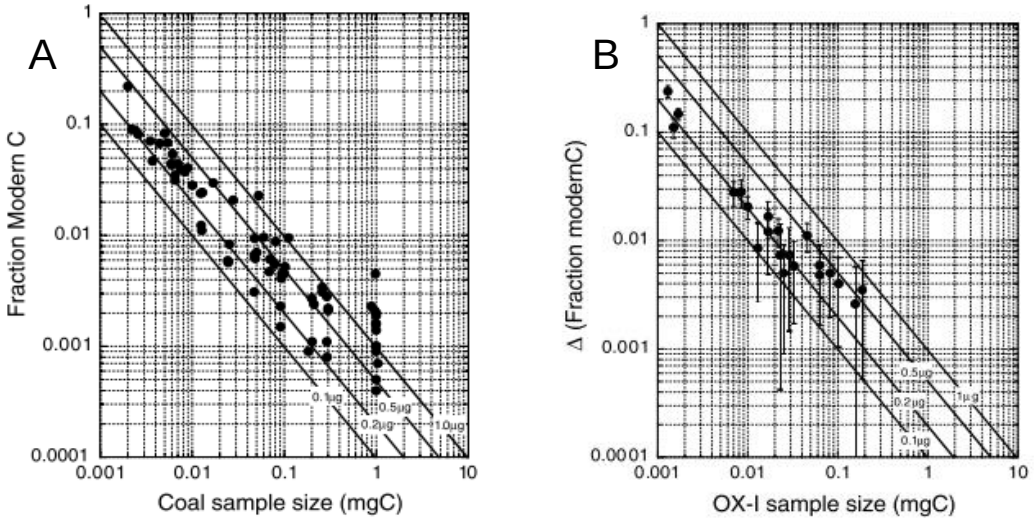

Figure 2.1 (A) $F^{14}C$ values for coal samples between 0.002 – 1 mgC. The solid lines represent fixed amounts of modern carbon contamination. (B) $\Delta F^{14}C$ modern values for Ox-I samples between 0.001 – 1 mgC. $\Delta F^{14}C$ represents the deviation of measured $F^{14}C$ carbon for small Ox-I samples from those of large normalising standards of 1 mgC. The solid lines represent the effects of fixed amounts of dead carbon contamination. Error bars represent propagated errors. Note that "Fraction Modern C", as listed in this figure, and in subsequent figures, is the same as $F^{14}C$. Figure from Santos *et al.* (2007b).

2.3 Improving Ultra-Small Radiocarbon Dating

A range of techniques have been used to improve radiocarbon dating ultra-small samples. These include: reducing the graphitisation time to reduce contamination via leaks and increase reaction efficiency (Fedi *et al.*, 2020); reducing sample loss which can occur during CO_2 transfer and graphite pressing (Fedi *et al.*, 2020); reducing the volume of components associated with CO_2 processing to reduce contamination (Delqué-Koli Caffy *et al.*, 2013); and choosing the correct catalyst for graphitisation (Smith *et al.*, 2010).

Table 2.2 outlines the modifications/methods used by key laboratories to improve several aspects associated with radiocarbon dating ultra-small samples. Broadly speaking, these methods aim to reduce contamination, sample loss, and fractionation, and improve graphite yield. Each method/modification is discussed in further detail in subsequent sections of this chapter, where an explanation of each technique is given along with example case studies.

Table 2.2 Modifications/methods to improve radiocarbon dating ultra-small samples, with specific descriptions where applicable.

Laboratory	Modifications/methods used for improving radiocarbon dating of ultra-small samples							
	Reactor volume reduction [Section 2.3.1]	Reaction temperature [Section 2.3.2]	Water removal [Section 2.3.3]	Oxygen [Section 2.3.4]	Fe catalyst [Section 2.3.5]	Graphite pressing [Section 2.3.6]	Reducing sample loss [Section 2.3.7]	Lower pressure range transducer [various case studies]
National Institute for Nuclear Physics, Florence. (Fedi *et al.*, 2020)	✓	-	-	-	-	Used a laminar flow box to reduce contamination	Use of copper insets	-
University of Tokyo (Yokoyama *et al.*, 2016)	✓	-	-	-	-	-	-	-
National Ocean Sciences Accelerator Mass Spectrometry Facility (Walter *et al.*, 2016)	✓	-	-	-	-	-	-	✓
Keck Carbon Cycle AMS Facility (Santos *et al.*, 2007b)	✓	Reduced reaction temperature	-	-	-	-	-	✓
Australian Nuclear Science and Technology (Smith *et al.*, 2010)	✓	Infrared laser beam instead of a furnace used to heat Fe powder	Combination of two-stage Peltier cells and dry ice/ethanol slush	Additional O_2 bake-out before graphitisation	Assessed several aspects of four Fe catalysts	-	-	-
Laboratoire De Mesure Du Carbone 14, Saclay, France (Delqué-Koli, Caffy *et al.*, 2013)	✓	Reduced reaction temperature during graphitisation	Exchanged liquid nitrogen for $Mg(ClO_4)_2$	-	-	-	-	✓

2.3.1 Volume Reduction

Reducing the volume of the vacuum line (where CO_2 is processed) and graphite reactors (where CO_2 is graphitised) is thought to aid in reducing contamination of ultra-small samples, as a reduced volume results in reduced surface area, and therefore, reduces the likelihood of contamination (Delqué-Koli Caffy *et al.*, 2013). Additionally, depending on the configuration of the vacuum line, a reduction in volume can lead to a reduction of dead space, which refers to areas within the vacuum line where gas can become stuck, which can lead to laboratory-induced fractionation (Walter *et al.*, 2016).

Reducing the graphite reactor volume can also aid in improving reaction speed, thereby increasing graphite yield (Yokoyama *et al.*, 2016).

2.3.1.1 Vacuum Line

The design of a vacuum line can contribute to dead space, leading to isotopic fractionation and gas becoming trapped. **Figure 3.3** in Chapter 3 illustrates how the curved nature of the vacuum lines at the WRDL could result in dead space.

2.3.1.2 Graphite Reactors

At the WRDL, a graphite reactor consists of an Ultra-Torr®-Union-Cross connecting to catalyst and water removal tubes, and a pressure sensor (**Figure 3.14**) Several researchers (Delqué-Koli Caffy *et al.*, 2013, Walter *et al.*, 2016) have identified that minimising the volume of the graphite reactors results in an increase in pressure, affecting three aspects: reaction speed, conversion efficiency (CO_2 to graphite), and more accurate pressure readings. However, depending on the limits of the pressure transducer being used, unreliable pressure readings may occur as sample size decreases. Reducing the volume of the graphite reactors means that previously low-pressure values may increase into a range that is accurately measurable.

2.3.1.3 Case Studies

Several case studies are presented below, demonstrating the application of reducing the volume of components that make up the vacuum line system. Differences between each case study's method of graphitisation, compared to the WRDL, are stated where necessary.

National Institute for Nuclear Physics, Florence

The National Institute for Nuclear Physics in Florence is home to the Laboratorio di tecniche nucleari per l'Ambiente e i Beni Culturali (LABEC laboratory). While they use a graphitisation method similar to the WRDL, specific parameters are not mentioned. Fedi *et al.* (2020) designed a small graphitisation reactor (**Figure 2.2**) with a volume of 1.5 cm^3, approximately a quarter of the volume of their regular reactors. In addition to the volume reduction, the Swagelok® Ultra-Torr® fitting was directly integrated into the valve that isolates it from the vacuum line during graphitisation, and a silver bar with a small canal, in conjunction with a cooling device, was used to trap water produced during graphitisation. The use of the silver bar was undertaken to further minimise the internal volume.

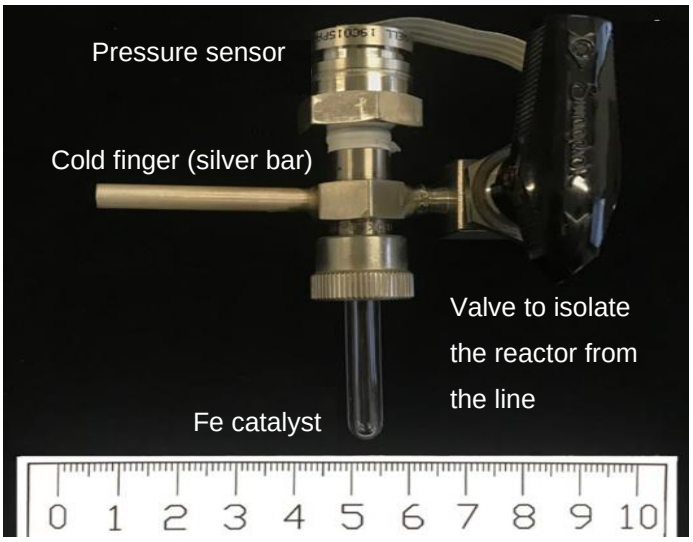

Figure 2.2 Ultra-small graphite reactor for 0.05 mgC samples. Figure from Fedi *et al.* (2020).

Fedi *et al.* (2020) ran a preliminary experiment to assess the newly designed reactors. Measurements collected on 0.05 mgC Oxalic Acid (IAEA C-7), and Travertine (IAEA C-2) showed good agreement with expected values (**Table 2.3**), but insufficient to fully evaluate the success of the new reactor. Additionally, because more than one variable was changed, a complete assessment of the success of each change is difficult.

Table 2.3 Radiocarbon results for standards graphitised using ultra-small graphite reactors at the LABEC laboratory. Figure from Fedi *et al.* (2020).

Lab code	Material	^{14}C conc. (pMC)	Certified ^{14}C conc. (pMC)
Fi3881	IAEA C7	49.40 ± 0.96	49.53 ± 0.12
Fi4083		49.37 ± 0.49	
Fi4092		48.43 ± 0.35	
Fi4152	IAEA C2	40.7 ± 1.1	41.14 ± 0.03

Note: Radiocarbon dates have been expressed as percent modern carbon (pMC).

The effect of smaller reactors on graphite yield was also investigated. The original graphite reactors were graphitising 0.70 mgC, whereas the ultra-small reactors have been designed to graphitise ~0.05 mgC. Fedi *et al.* (2020) found that graphite yield decreased from 85% efficiency to 50% efficiency for the smaller reactors, where this observation was noted by Fedi *et al.* (2020) as possibly being due to the use of an elemental analyser to combust solid samples into CO_2. This additional variable prevents evaluation of this technique further.

University of Tokyo

Yokoyama *et al.* (2016) designed a new metal vacuum line where the volume of the graphite reactor was reduced from 8 mL to 4.5 mL, equating to ~45% volume reduction (**Figure 2.3**). A graphitisation method similar to the WRDL was employed, except that a variable weight of Fe powder was used depending on sample size, and samples were graphitised at 630ºC for 6 – 10 hours. It was stated that reducing the volume of the reactor led to an improvement in the efficiency of the reaction for samples 0.01 – 0.10 mgC. However, two other variables outside the scope of this research project were also tested at the same time and, therefore, it is difficult to assess the contribution of the reduced reactor volume on the observed improvements.

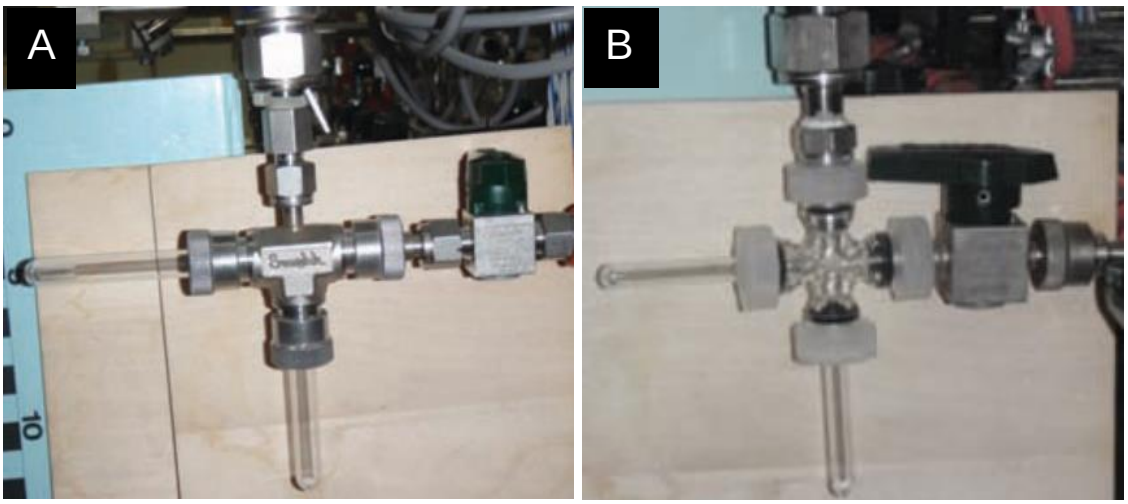

Figure 2.3 (A) 8 mL and (B) 4.5 mL graphite reactors. Figure from Yokoyama *et al.* (2016).

National Ocean Sciences Accelerator Mass Spectrometry (NOSAMS) Facility

The NOSAMS facility routinely produced graphite of 0.1 – 4.0 mgC and 0.025 – 1.5 mgC (11 mL and 3.5 mL graphite reactors). They use a graphitisation method similar to the WRDL, except for water removal, a Pyrex® tube immersed in a slurry of dry ice and isopropanol is used. To reduce sample size requirements (0.006 – 0.1 mgC) and minimise isotopic fractionation, Walter *et al.* (2016) reduced the volume of the graphite reactors to approximately 0.8 mL (77% reduction in volume). Modifications are listed below and illustrated in **Figure 2.4**.

- Smaller graphite reactors were assembled from $^{1}/_{8}$-inch Ultra-Torr®-Union-Tee fittings. To connect them to the vacuum line, a $^{1}/_{8}$-inch Swagelok® tube adapter was silver-soldered to make a cross, allowing a $^{1}/_{8}$-inch Swagelok® plug valve to be fitted.
- Quartz and Pyrex® tubes were reduced to 3.2 mm OD (outer diameter) x 2.5 mm ID (inner diameter), and 3.2 mm OD x 2.0 mm ID, respectively.
- An Omega PX139 pressure transducer was modified to be compatible with the $^{1}/_{8}$-inch Ultra-Torr®-Union-tee.

These modifications resulted in graphitisation going to completion within 30 minutes for samples 0.025 mgC or less, and produced graphite yields above 90%. It was noted however that for samples 0.01 mgC or less, the recorded pressures were close to the uncertainty limits of the transducers (*e.g.*, -0.2 ± 0.15 psi). Due to satisfactory graphite yield results, the overall conclusion was the ultra-small graphitisation reactors successfully graphitised 0.006 – 0.1 mgC samples.

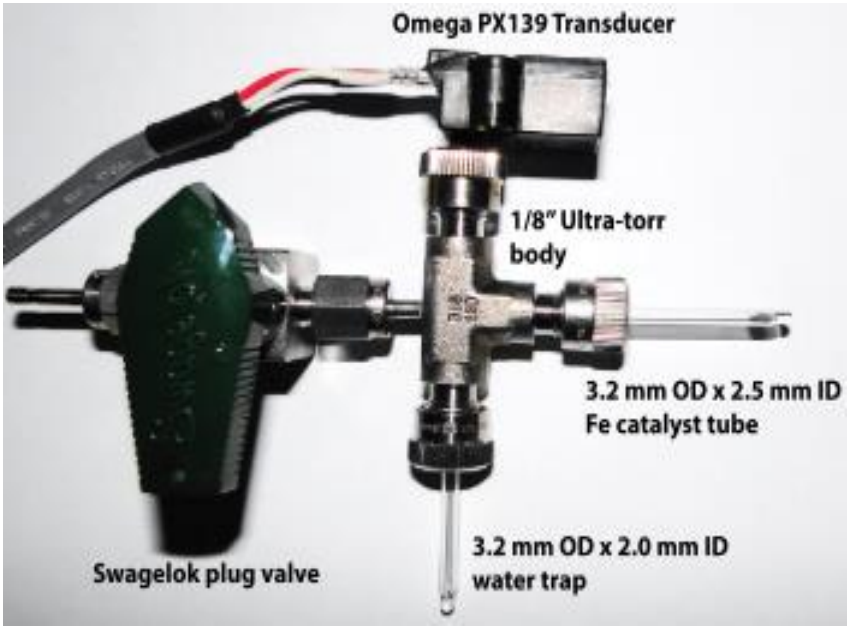

Figure 2.4 Ultra-small graphite reactor designed at the NOSAMS facility. Figure from Walter *et al.* (2016).

The addition of contaminant carbon (modern and dead) from the ultra-small reactors was also investigated using modern and ^{14}C depleted (also referred to as "blank") standards. Standards were prepared in large batches and split into small aliquots on the vacuum line to minimise contamination from preparative procedures. A consistent amount of "process blank" (dead carbon contamination) was identified, representing cumulative contamination from all preparation steps. **Figure 2.5** illustrates this for ^{14}C depleted standards IAEA C-1 and acetanilide. The solid horizontal line represents the expected $F^{14}C$ result, however, because the addition of process blank is constant, smaller samples are affected the most. **Figure 2.6** demonstrates that the Ox-1 modern standard is conversely affected by dead carbon contamination, as smaller samples deviate more from the expected consensus value compared to larger samples.

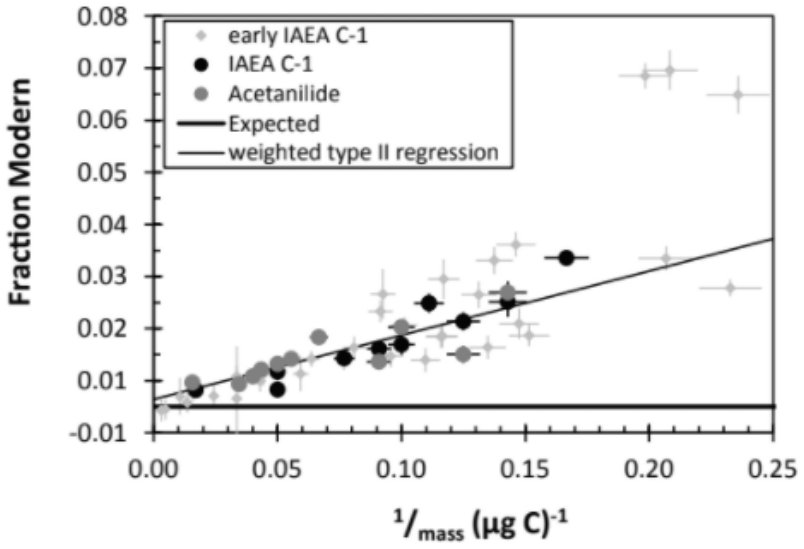

Figure 2.5 $F^{14}C$ values for ultra-small "dead" standards: IAEA C-1 (Carrara Marble, $F^{14}C = 0.0002 \pm 0.002$) and acetanilide (routine internal standard used at NOSAMS with a $F^{14}C$ value that is indistinguishable from other "dead" secondary standards) are plotted against inverse mass, along their uncertainty weighted regression line. The thick horizontal line represents the expected $F^{14}C$ value of 0.0. The light grey diamonds represent values from four previous wheels where graphite targets were produced under varying graphitisation conditions. Figure from Walter *et al.* (2016).

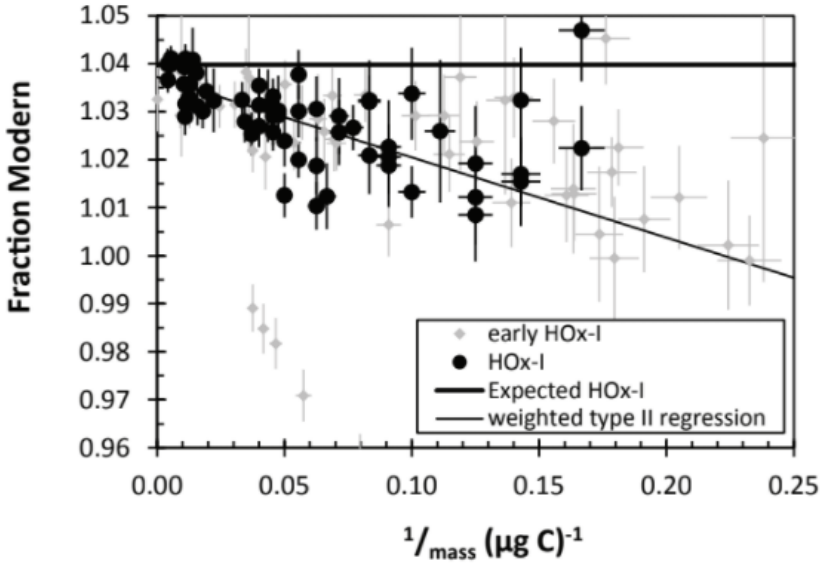

Figure 2.6 $F^{14}C$ values for ultra-small Ox-I targets, normalised to 1 mgC. $F^{14}C$ values from previous wheels are also plotted as small, light grey diamonds. Note HOx-1 and Ox-1 refer to the same standard. Figure from Walter *et al.* (2016).

Walter *et al.* (2016) calculated that modern and dead carbon contamination from the use of the ultra-small reactors were 0.12 ± 0.01 µgC and 0.20 ± 0.10 µgC, respectively, with a "combined graphitisation blank" of 0.30 ± 0.10 µgC. Walter *et al.* (2016) used this correction on samples <0.10 mgC, however samples less than 0.01 mg still deviated when this correction was applied.

The magnitude of isotopic fractionation caused by using the ultra-small reactors was also investigated. Four standards (Ox-1, IAEA C-1, IAEA C-2 and IAEA C-6) spanning a range of ^{13}C values were graphitised and then subsequently converted back to CO_2 by combustion in an elemental analyser. The ^{13}C values indicated that isotopic fractionation was mass dependent with the smallest samples being affected the most (**Figure 2.7**). Walter *et al.* (2016) concluded that the reaction is not going to completion, even though the pressure transducers indicate >90% yield. It was suspected that this was caused by samples <0.001 mgC generating pressures too low for the pressure transducers to accurately measure. The problem with incomplete graphitisation is that it will result in incorrect blank corrections, with the smallest samples being most affected. A comparison between the isotopic fractionation values for regular reactors and the newly designed smaller reactors was not given.

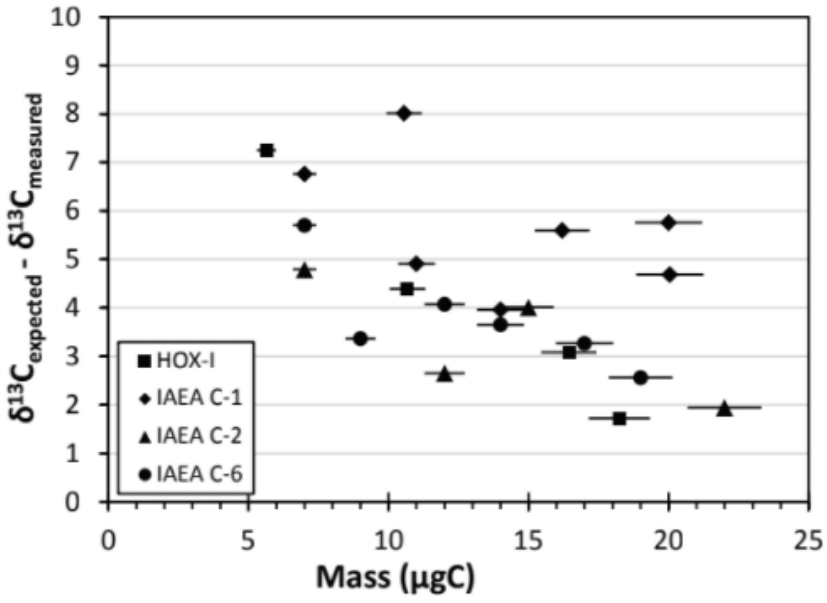

Figure 2.7 Isotopic fractionation observed from Ox-1 and IAEA C-1, IAEA C-2, and IAEA C-6. The difference between the measured and expected $\delta^{13}C$ values have been plotted against sample mass. Figure from Walter *et al.* (2016).

Keck Carbon Cycle AMS (KCCAMS) facility

During initial experiments using their regular graphite reactors, the KCCAMS facility found that samples below 0.025 mgC were not being fully graphitised, which was first evident by monitoring the pressure decrease during graphitisation and later confirmed by measuring carbon content and isotopic composition (graphite combustion is not possible at the WRDL). While lowering the temperature from 550°C to 450°C resulted in the successful graphitisation of samples as low as 0.006 mgC (discussed further in 2.3.2), a set of small-volume reactors were constructed to graphitise samples as low as 0.002 mgC (up to a maximum of 0.01 mgC) (Santos *et al.*, 2007b). **Figure 2.8** and **Table 2.4** illustrate and outline these modifications.

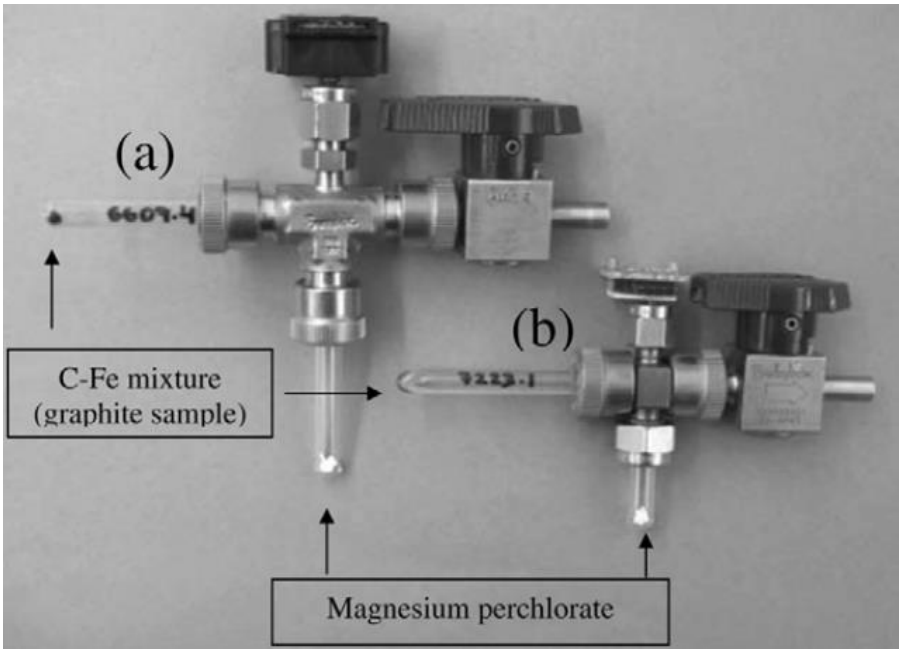

Figure 2.8 (a) Regular and (b) newly developed ultra-small graphite reactors at the KCCAMS facility. Figure from Santos *et al.* (2007b).

Table 2.4 Comparison between regular and small volume graphite reactors at the KCCAMS facility (Santos *et al.*, 2007b).

Reactor type:	Volume	Reactor core	Pressure Transducer	Fe tube dimensions	$Mg(ClO_4)_2$ tube dimensions
Regular	3.1 cm^3	Modified ¼" Ultra-Torr® tee	Omega PX139, 0-30 psi	4.5 mm x 6 mm x 50 mm	4.5 mm x 6 mm x 5 0mm
Small volume	1.6 cm^3	Modified ¼" Ultra-Torr® Union	Silicon Microstructures SM5812, 0-5 psi	4.5 mm x 6 mm x 30 mm	2.7 mm x 6 mm x 30 mm

Santos *et al.* (2007b) found that isotopic fractionation was an issue when using their regular reactors to graphitise samples below 0.025 mgC, which becomes more problematic for samples smaller than 0.01 mgC. Analyses of the carbon content and isotopic composition (using elemental analyser isotopic ratio mass spectrometry [EA-IRMS]) indicated that samples graphitised using the small reactors were less fractionated. **Figure 2.9** illustrates this with measurement values from the small reactors closer to the consensus values for Ox-1 and IAEA C-6 (19‰ and -10.8 ± 0.5‰).

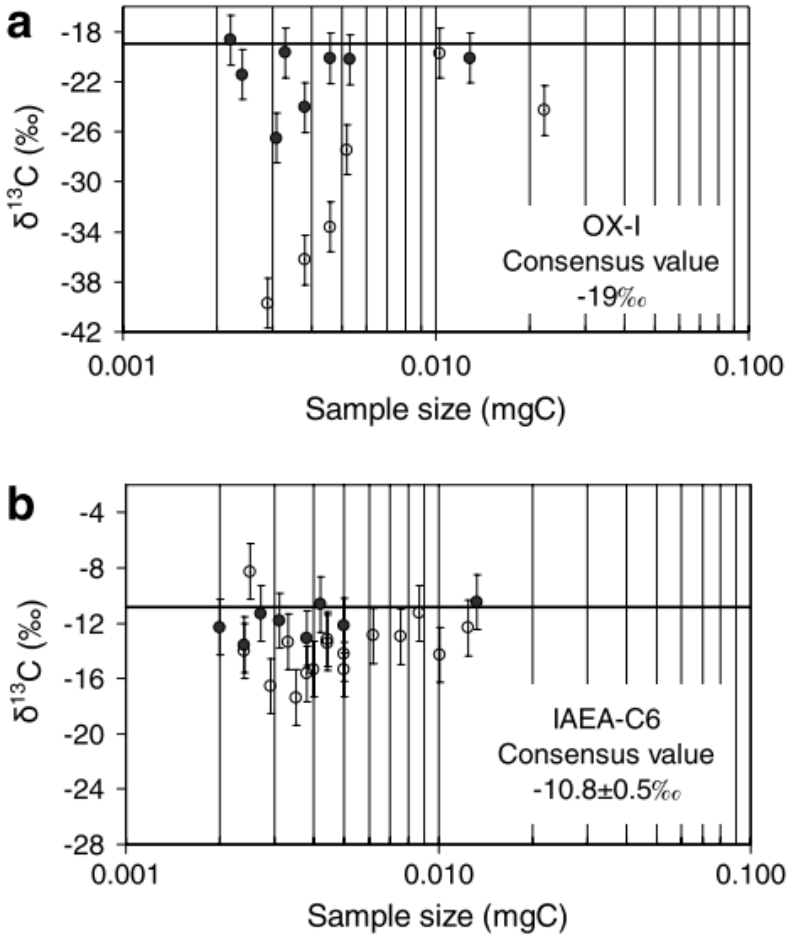

Figure 2.9 EA-IRMS measurements from graphite samples run at 450ºC. (A) Ox-I and (B) IAEA C-6, ranging from 0.002 to >0.02 mgC. The solid and white circles represent small volume and regular volume reactors, respectively. Figure from Santos *et al.* (2007b).

Australian Nuclear Science and Technology (ANSTO), Australia

Regular graphite reactors at ANSTO, designed for samples >0.10 mgC, are comprised of modified Swagelok® Ultra-Torr® fittings that have an internal volume of 2.5 mL. A graphitisation method similar to the WRDL is employed though the temperature during graphitisation is run at 600°C, 1 – 2 mg Fe powder is used, and

for water removal, a Peltier cell cools a cold finger to -40ºC. Smith *et al.* (2010) created a "microfurnace" (**Figure 2.10**) to maximise sample pressure while minimising the addition of extraneous carbon, enabling samples as low as 0.05 mgC to be radiocarbon dated. The microfurnace has several key features:

- A stainless-steel cold finger is welded to the furnace body, eliminating the need for an O-ring and removing a source of possible leaks.
- Fe powder is no longer contained within a quartz tube but instead sits in a quartz crucible where a quartz window enables infrared radiation to directly heat the sample.
- An integrated valve isolates the furnace once CO_2 and H_2 have been admitted.
- A stainless steel Entran EPB-C1 pressure sensor monitors the reaction.

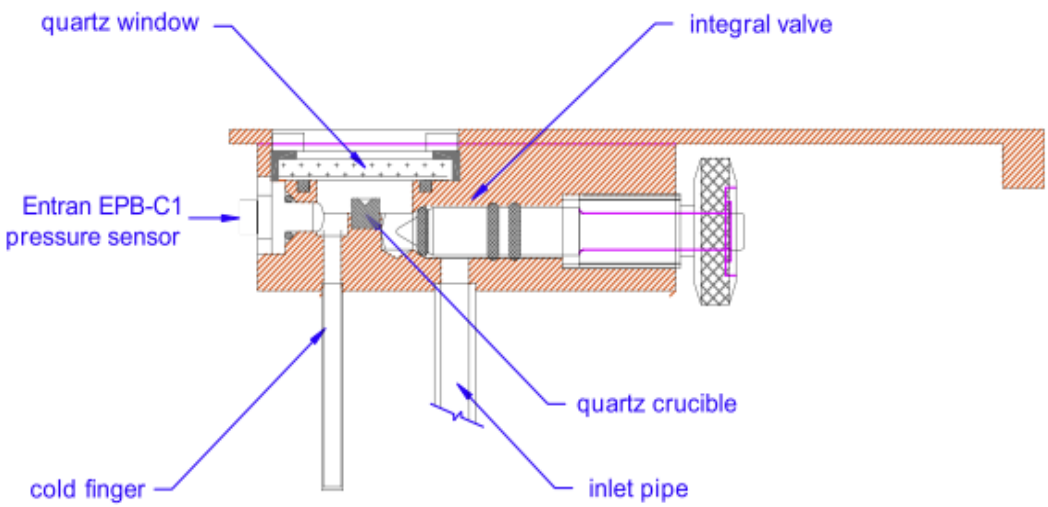

Figure 2.10 Microfurnace diagram. Figure from Smith *et al.* (2010).

To assess the potential improvements, Smith *et al.* (2010) compared near background CO_2 measurements using their regular furnaces with the prototype microfurnace. Results showed a linear relationship between sample mass and modern contamination, where the addition of extraneous carbon was thought to be due to insufficient cleaning protocols in-between running modern and ^{14}C depleted samples and, therefore, it was suggested that different microfurnaces should be used for modern and ^{14}C depleted samples. At the time that this research paper was published, development of a second-generation microfurnace had already commenced, with a design that facilitated easier cleaning and operation.

Laboratoire De Mesure Du Carbone 14 (LMC14) In Saclay, France

The LMC14 laboratory noted that 15% of samples below 0.10 mg have decreased graphitisation yields (<70%) and exhibit large fractionation effects. A graphitisation method similar to the WRDL is employed though the graphitisation temperature is run at 600ºC, and water removal occurs via a cold finger being immersed in liquid nitrogen with heating coils set at -70°C. To help combat large fractionation effects, graphite reactors were reduced in volume to 5 mL, equating to a reduction of more than 50%. The design of the smaller reactor is the same as regular reactors, however the diameter is narrower and a smaller pressure transducer (Omega PX72 – 015AV) with a lower pressure range is used (0 – 350 mb). Delqué-Koli Caffy *et al.* (2013) assessed the success of the small graphite reactors by monitoring reaction time and modern and dead carbon contamination. Graphitisation times are listed in **Table 2.5**. Results showed the smaller reactor resulted in shorter reaction times. For example, a 45 µg sample in a regular reactor took 195 minutes to graphitise whereas a 47 µg sample in the smaller reactor took 150 minutes.

Modern contamination was measured between 0.1 – 1.0 µg, falling into the same range that would be expected for regular reactors. Dead carbon contamination was measured between 0.5 – 1.0 µg, falling into the upper range that would be expected for regular reactors. Delqué-Koli Caffy *et al.* (2013) stated that while the Fe powder could be responsible for this, a machine-induced effect from the accelerator was thought to be more likely because all samples were measured in the same batch.

Table 2.5 Graphitisation time results for IAEA C-6 samples when large and small volume reactors were used (Delqué-Koli Caffy *et al.*, 2013).

Graphitisation reactor	Mass of carbon (µg)	Graphitisation time (minutes)
Large volume reactor	353	240
	61	180
	45	195
	29	180
	17	110
	13	150
Small volume reactor	239	150
	177	190
	56	140
	53	90
	47	150
	40	120
	30	90
	12	60
	12	90
	11	50
	11	60

2.3.2 Reaction Temperature

For CO_2 to be converted to graphite, heat must be applied for the duration of the graphitisation reaction. Different heating methods and reaction temperatures have been found to affect graphitisation time, graphite yield and fractionation.

2.3.2.1 Case Studies

Three case studies relating to research into reaction temperature and the method of heating are presented below.

Keck Carbon Cycle AMS (KCCAMS) facility

Santos *et al.* (2007b) investigated the impact of reaction temperature on graphite yield and ^{14}C measurements. At the KCCAMS facility, samples are typically graphitised at 550°C, however preliminary results showed that samples <0.025 mgC

were affected by isotopic fractionation. It was observed that lowering the temperature to 450°C reduced isotopic fractionation for samples >0.006 mgC, which was identified as the minimal size for fractionation to become significant (**Figure 2.11**).

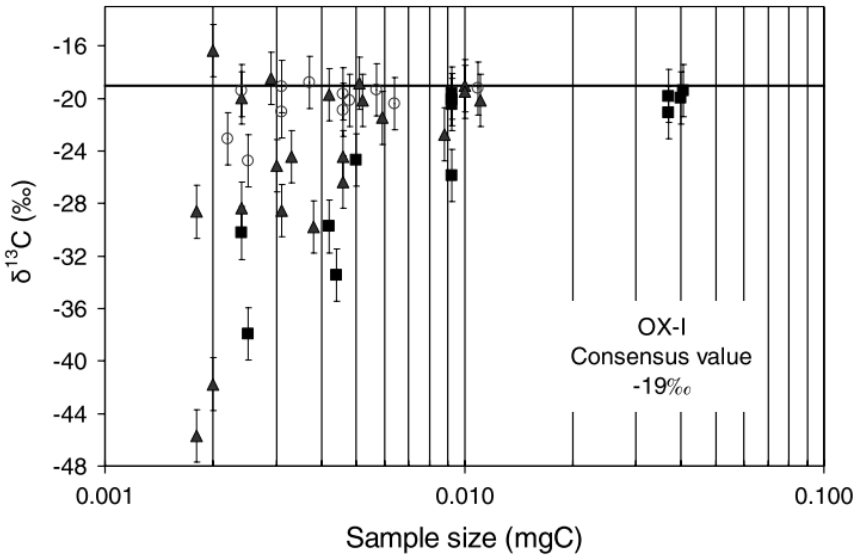

Figure 2.11 EA-IRMS measurements for graphite samples (produced in regular reactors) from Ox-I samples ranging from <0.002 – 0.1 mgC. The effect that temperature has on graphite isotopic fractionation was assessed by graphitising samples at 450ºC (white circles), 500ºC (black triangles) and 550ºC (black squares). The solid line represents the consensus value for Ox-I. Figure from Santos *et al.* (2007b).

ANSTO

Smith *et al.* (2010) used an infrared laser beam to directly heat the Fe catalyst, where an infrared thermometer measured the catalyst temperature during graphitisation. As the reaction proceeded, the catalyst temperature increased as pressure decreased, which was thought to be a consequence of diminishing convective losses as H_2, which has a high thermal conductivity, was consumed. To combat this, the applied laser power was decreased by the LabVIEW™ system during the reaction to maintain a constant temperature of 600ºC. **Figure 2.12** demonstrates this, evident that as laser power decreases, the catalyst temperature, overall, remains constant.

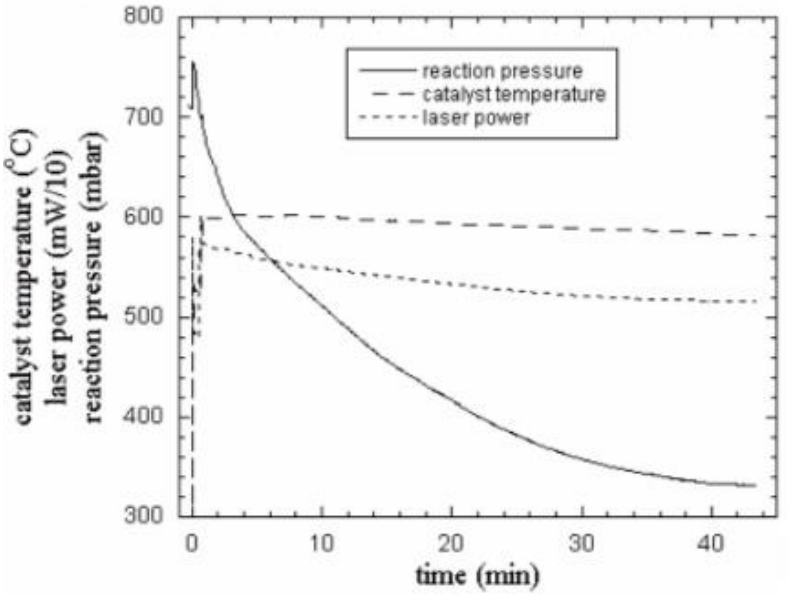

Figure 2.12 Reaction temperature, catalyst temperature and laser power during graphitisation of a 0.05 mgC sample. Figure from Santos *et al.* (2007b).

Laboratoire De Mesure Du Carbone-14 In Saclay, France

Delqué-Koli Caffy *et al.* (2013), following the observations of Santos *et al.* (2007b), adjusted the graphitisation temperature of four samples, close to or below 10 µg, from 550°C to 500°C after the reaction appeared to have gone to competition. Delqué-Koli Caffy *et al.* (2013) stated that the lower reaction temperature enabled the reaction to start up again and **Figure 2.13** illustrates this, showing a graphitisation curve for a sample where the reaction temperature is lowered at the point where the pressure plateaus. Four samples however are insufficient to be able to state that this lower temperature is favourable, and there is also not enough data to compare this method to normal procedures. It was stated that the observation of graphitisation starting up again could not be explained and that further experimentation at lower temperatures of 500ºC and 450ºC was recommended.

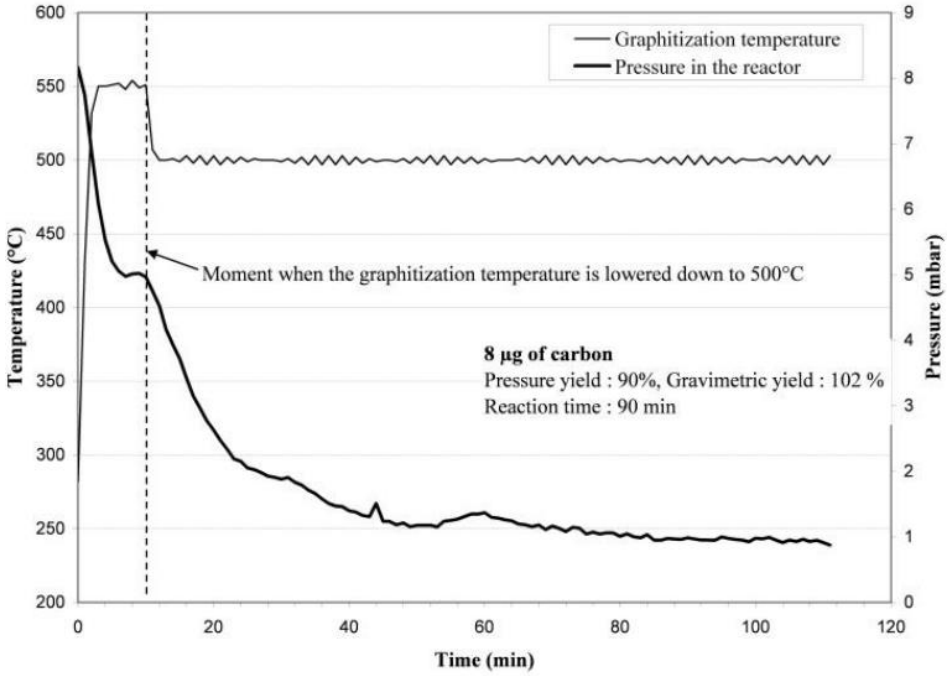

Figure 2.13 Graphitisation curve for an 8 µg sample graphitised in a small volume reactor using $Mg(ClO_4)_2$. Figure from Delqué-Koli Caffy *et al.* (2013).

2.3.3 Water Removal

Water is produced during graphitisation, as illustrated in **Figure 2.14**. Smith *et al.* (2010), found that efficient trapping of water was crucial for the reaction efficiency of microsamples (samples containing tens of µg of carbon) as it can lead to reducing the likelihood of leaks within the graphite reactor. Water removal can be achieved by the use of a desiccant, such as $Mg(ClO_4)_2$ (Santos *et al.*, 2016a), or by cryogenically trapping water using a cold finger (Yang, Smith, & Hua, 2013).

$$CO_{2(g)} + 2H_{2(g)} \xrightarrow[\text{Catalyst (Fe)}]{550^{\circ}C} C(s) + 2H_2O(aq)$$

Figure 2.14 Graphitisation reaction (Beta Analytic, accessed 30/4/22)

2.3.3.1 Case Studies

Two case studies relating to the method of water removal during graphitisation are presented below.

ANSTO

Yang, Smith, & Hua (2013) reported using either two-stage Peltier cells, or a dry ice/ethanol slush to trap water in a cold finger. Each method comes with its own set of advantages and drawbacks. The use of Peltier cells enables the temperature to be maintained with no input from an operator, but the water vapour pressure is too high to be able to prepare microsamples. And while the dry ice/ethanol slurry method results in a much lower water vapour pressure, it requires constant top-ups and therefore has high operator input. Yang, Smith, & Hua (2013) suggested a new approach for water removal for microsamples that combines the positive aspects of each method while also being compatible with conventional graphitisation lines and a laser-heated microfurnace. A cross-section diagram of the newly designed cooling system is shown in **Figure 2.15**.

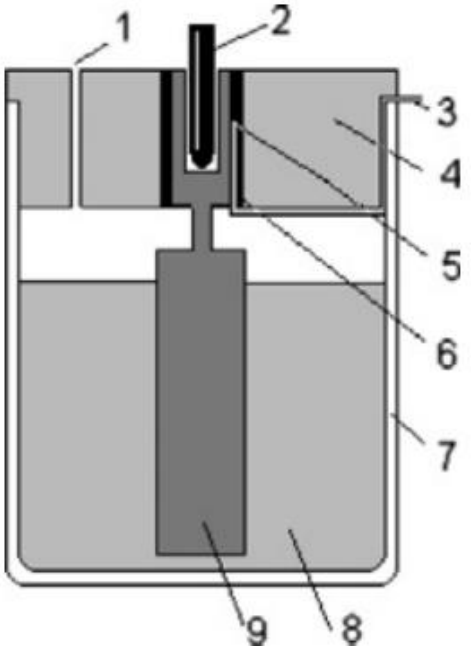

Figure 2.15 Schematic diagram of the cooler. (1) Vent hole. (2) Cold finger. (3) Cable for heater and thermocouple. (4) Cap for thermal isolation. (5) T type thermocouple. (6) Electrical heater. (7) Dewar. (8) Liquid nitrogen. (9) Machined aluminium rod. Figure from Yang, Smith, & Hua (2013).

The new design works by using liquid nitrogen in combination with a Proportional-Integral-Derivative temperature controller and aluminium rod to maintain the cold finger at -80 ± 1°C for three hours. Liquid nitrogen replaced the dry ice/ethanol slurry and the design results in less consumption of liquid nitrogen and rapid temperature changes (40°C/min). Yang, Smith, & Hua (2013) noted that the reaction time for 0.005 – 0.02 mgC samples was reduced significantly using this method. Previously, a sample containing 37 µg of carbon took 1 – 2 hours to graphitise using two-stage Peltier chillers, but in this instance, samples containing 20 µg and 50 µg of carbon took 15 and 30 minutes to graphitise, a significant reduction in time. While conversion efficiency (graphite yield) for samples containing 5 – 20 µg of carbon averaged 80 – 100% when the new water removal method was used (**Figure 2.16**), several samples returned efficiencies greater than 100%, which Yang, Smith, & Hua (2013) stated is possibly due to the formation of CH_4, as this would contribute to an over estimation in conversion efficiency calculations.

In addition to the development of this new cooling method, Yang, Smith, & Hua (2013) investigated a two-step cooling cycle, following the method outlined by Liebl *et al.* (2010). The temperature was initially set to -80ºC for 8 minutes (when CO_2 is converted to CO) and subsequently reduced to -160ºC for the remainder of the reaction. This two-step cooling cycle resulted in an improved graphite yield of 95%, compared to 80% for the single cold finger temperature.

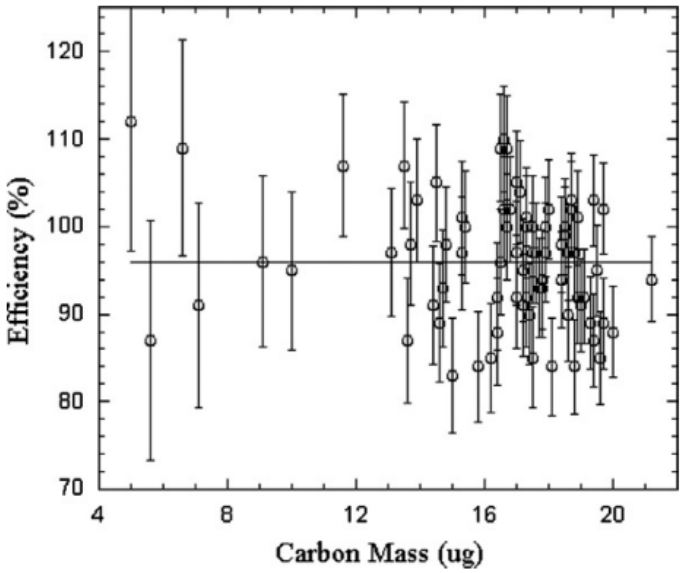

Figure 2.16 Graphite efficiency vs mass for small samples prepared using a new method for water removal; liquid nitrogen in combination with a PID temperature controller. Figure from Yang, Smith, & Hua (2013).

Laboratoire De Mesure Du Carbone 14 In Saclay, France

Delqué-Koli Caffy *et al.* (2013) experimented with $Mg(Cl_4O)_2$ as an alternative to their routine use of liquid nitrogen to remove water produced during graphitisation. While there was no difference in reaction times between the two methods, improved graphite yields were observed (**Table 2.6**).

Table 2.6 Graphite yield results, as a function of pressure, for IAEA C-6 samples when two methods of water removal were tested (Delqué-Koli Caffy *et al.*, 2013).

Water removal method	Mass of carbon (µg)	Pressure yield (%)
Cold finger with heating coil and liquid nitrogen (-70ºC)	239	67
	177	66
	56	77
	53	99
	47	73
	40	116
	30	75
	12	57
	12	21
	11	71
	11	24
$Mg(ClO_4)_2$	36	106
	32	71
	29	91
	14	87
	13	50
	10	87
	8	90
	6	93

2.3.4 Oxygen

Before a sample is graphitised, the Fe catalyst is reduced, which, depending on the laboratory, involves the sample being subjected to a certain pressure of H_2 for 30 – 60 minutes at a high temperature (usually between 450 – 600°C) while under vacuum. This process is often referred to as a H_2 bake-out, where the Fe powder is reduced, thereby removing any surface contaminants that may be present (Beverly *et al.*, 2016). Hua *et al.* (2004) refers to this process as the Fe being “activated”.

2.3.4.1 Case Study

One case study is presented below, demonstrating the use of O_2 as an additional bake-out method.

ANSTO

Hua *et al.* (2004) ran an experiment to test whether oxidising Fe powder before reducing it with H_2 would improve reaction rate and graphite yield for small samples. Three methods were investigated:

1) 750 mb H_2 at 600°C for one hour.
2) 750 mb H_2 at 600°C for 24 hours.
3) 500 mb O_2 at 450°C for 0.5 hour followed by 750 mb H_2 at 600°C for one hour.

Method one is commonly employed at AMS laboratories, method two was included to assess whether a longer bake-out would have any affect, and method three was chosen based on a method outlined by Nadeau *et al.* (1997), where the Fe powder is oxidised and then the iron oxide is reduced. Nadeau *et al.* (1997) observed that this method resulted in a reduction in graphitisation time, where “mg” sized samples took 5 – 6 hours. A description of what “mg” sized samples refers to was not given, however it has been assumed that it refers to samples ≤0.20 mgC, based on the sample sizes that were run by Hua *et al.* (2004) (0.009 – 0.16 mgC).

Figure 2.17 illustrates graphitisation times for each of the three methods. Compared to method one, methods two and three resulted in the fastest graphitisation times for all sample masses. A rapid decrease in pressure within two hours for method three was observed, for all sample masses. Method three also resulted in the minimum pressure being reached for samples >0.1 mgC within four hours. No significant differences between the graphitisation yields for each method was observed for samples >0.1 mgC, however for samples <0.1 mgC, graphite yield results were higher for methods two and three compared to one. The yield was very similar for methods two and three, 54% and 58%, however, method three had a much shorter “activation time” (bake-out time), requiring only 1.5 hour in comparison to 24 hours (method two). Hua *et al.* (2004) concluded that method three produced the best graphitisation yield results. It should be noted that no radiocarbon dates were reported from the use of each method.

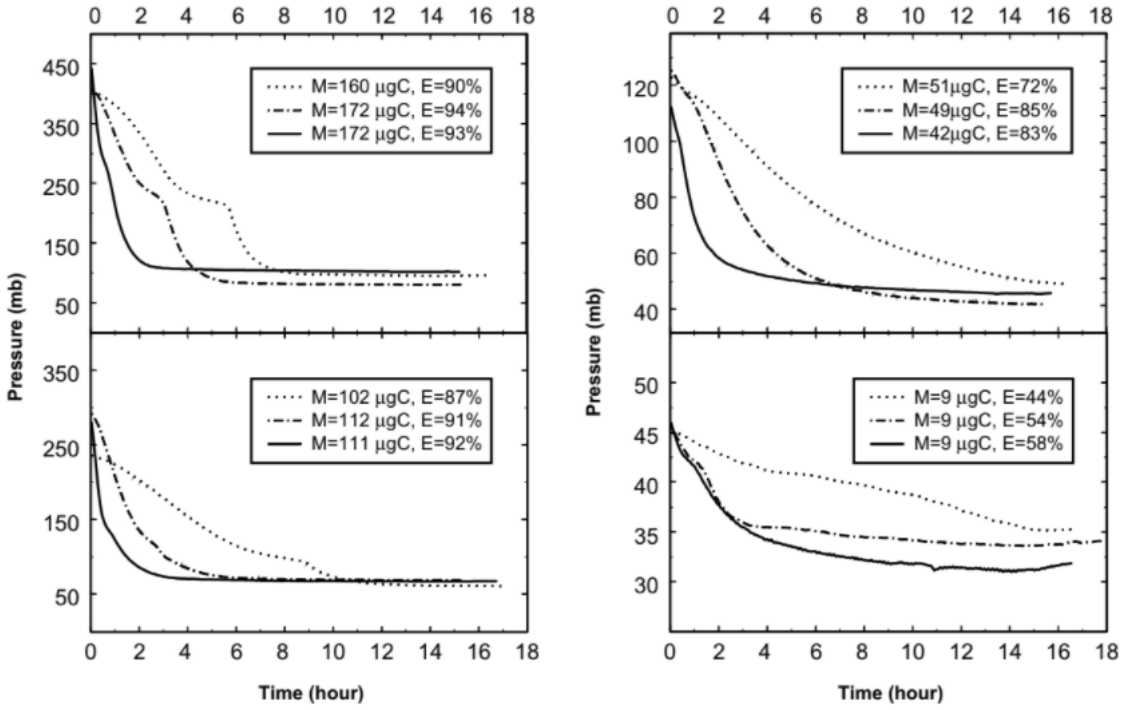

Figure 2.17 Recorded graphitisation reaction rates for 0.009 – 0.172 mgC samples (reported in this figure as µgC, represented by "M") using three Fe activation methods. The three lines; short-dotted, long-dotted, and solid represent methods one, two and three, respectively. E represents graphite yield. Figure from Hua *et al.* (2004).

The effect each method had on Fe morphology was examined using scanning electron microscopy (SEM) (**Figure 2.18**). Hua *et al.* (2004) found that untreated catalyst is much lighter in colour than treated catalyst, regardless of the method used. A note-worthy observation was that method three produced graphite that had a sponge-like appearance and a higher surface area. Hua *et al.* (2004) suggested that the high surface area may explain why method three had the fastest reaction rate.

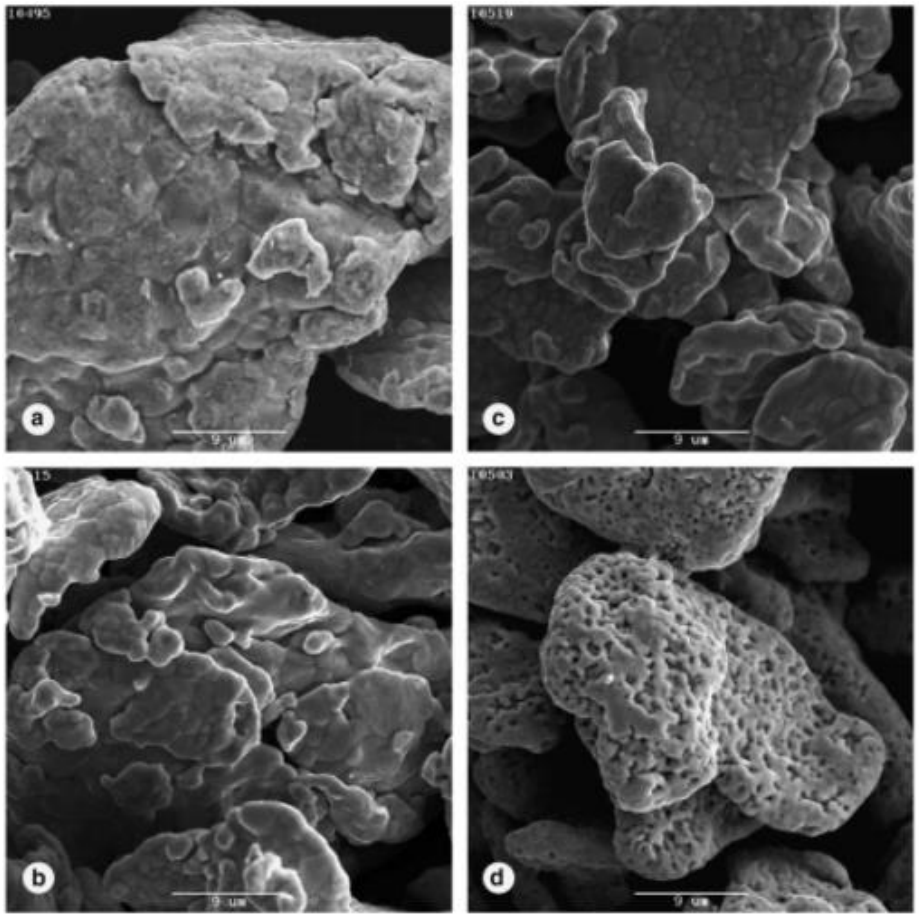

Figure 2.18 SEM photos of Fe catalysts using three bake-out methods: (a) Untreated catalyst. (b) Treated catalyst using method one. (c) Treated catalyst using method two. (d) Treated catalyst using method three. Scale bar equal to 9 µm. Figure from Hua *et al.* (2004).

2.3.5 Fe Catalyst

The choice of catalyst is a critical aspect in producing graphite from ultra-small samples, as the catalyst should be pure (contain no lithium or carbon), have a large and reactive surface area, and be the correct mesh size. Lithium should not be present as it can cause sparking in the accelerator (Smith *et al.*, 2010), and any extraneous carbon in the catalyst is considered a contaminant. The type of catalyst used can affect graphite yield, reaction time, target loading and performance in the ion source (Smith *et al.*, 2016a).

2.3.5.1 Case Study

One case study relating to the choice of Fe catalyst is presented below.

Smith *et al.* (2010) assessed four Fe catalysts using reaction pressure, reaction time, and SEM imaging as parameters. The four catalysts were as follows:

- Sigma Aldrich, mesh size -400, 99.99% purity (SA-400).
- Sigma Aldrich Fe_2O_3, mesh size unspecified, 99.999% purity (SA Fe_2O_3).
- Fe nano, mesh size 25 nm, 99.6% purity.
- Cerac, mesh size -325, 99.9% purity.

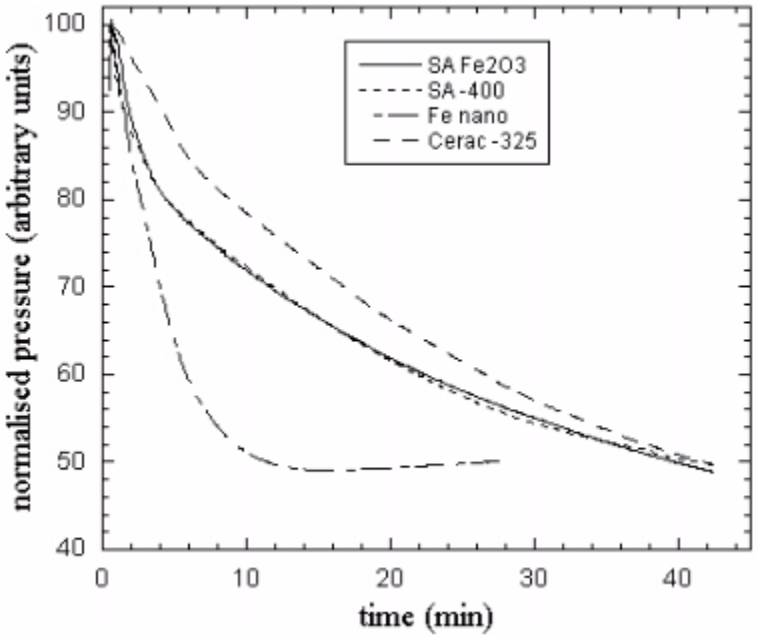

Figure 2.19 Reaction pressure curves for four Fe catalysts. Figure from Smith *et al.* (2016a).

Figure 2.19 illustrates how graphitisation times differed for each Fe catalyst under the same reaction conditions. Fe nano took the shortest time, and therefore was the favoured Fe catalyst. The difference in reaction times was thought to be due to differences in particle size (and therefore surface area) where the Fe nano had the greatest surface area.

SEM images for each of the four catalysts were taken after a H_2 bake-out, and also after graphitisation. **Figure 2.20** illustrates how the appearance of each catalyst can vary quite considerably. For example, SA-400 in **Figure 2.20b** has a coral-like appearance while Fe nano in **Figure 2.20f** is evenly covered by filamentous graphite. The appearance and ability to press produced graphite into cathode targets, using the nomenclature outlined by Santos *et al.* (2007a) (described in Chapter 4), were

also assessed. Graphite produced from SA-400, SA Fe_2O_3 and Cerac -325 was described as being “firm”, while graphite produced from Fe nano was “fluffy”. Even with these physical differences, it was stated by Smith *et al.* (2016a) that in terms of the physical characteristics of graphite produced from the four Fe catalysts, there was no preference.

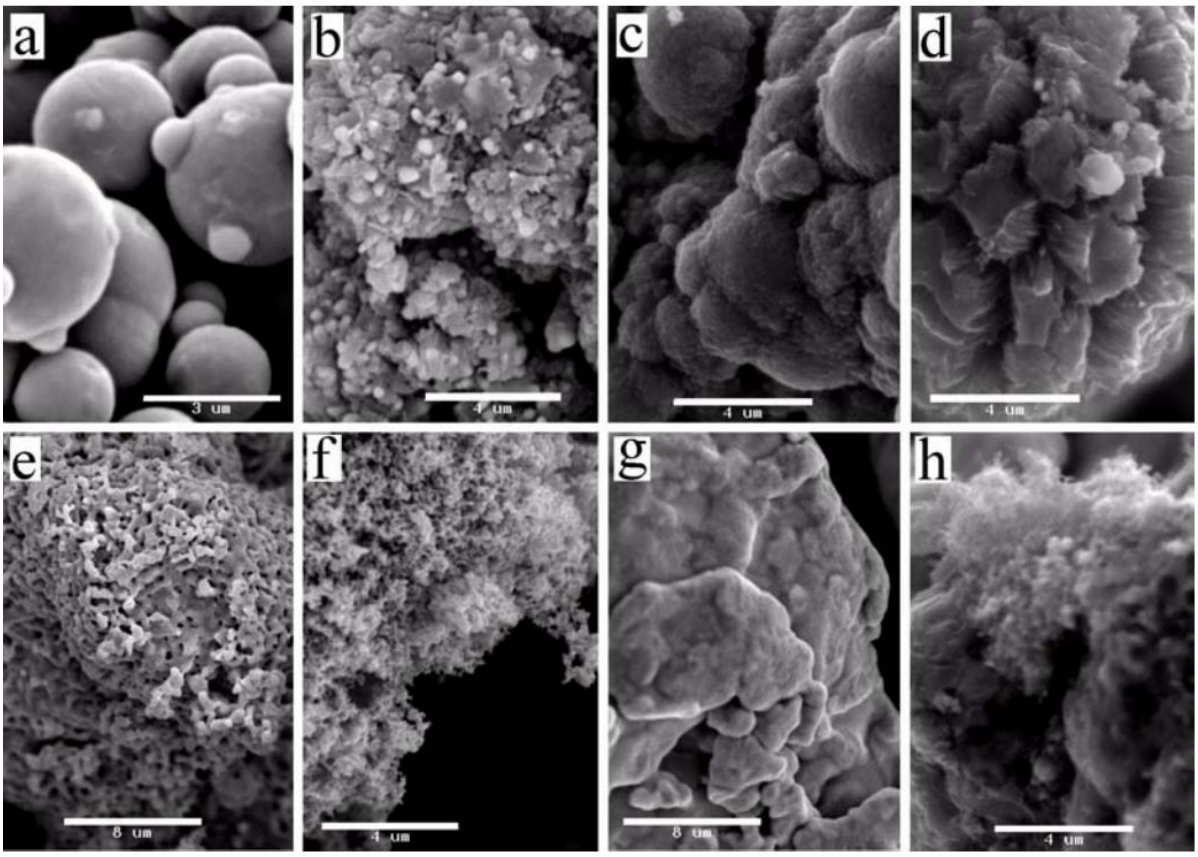

Figure 2.20 SEM images of four Fe catalysts following a H_2 bake-out, and then graphitisation at 600ºC. SA-400: (a) H_2 bake-out and (b) graphitisation. SA Fe_2O_3: (c) H_2 bake-out and (d) graphitisation. Fe nano: (e) H_2 bake-out and (f) graphitisation. Cerac -325: (g) H_2 bake-out and (h) graphitisation. Figure from Smith *et al.* (2010).

2.3.6 Graphite Pressing

Once a sample has been converted to graphite, it is pressed into a cathode target. This is undertaken to halt the absorption of atmospheric CO_2 before analysis. During the process of a sample being transferred from a tube (or similar) into a cathode target, contamination or sample loss can occur (discussed in section 2.3.7).

2.3.6.1 Case Study

One case study relating to reducing contamination during graphite pressing is presented below.

National Institute for Nuclear Physics, Florence

To reduce modern contamination (*e.g.*, dust from the natural environment) for ultra-small samples, Fedi *et al.*, 2020 investigated the use of a laminar flow box during graphite pressing. **Figure 2.21** illustrates how working in a dust free environment may improve background values for ^{14}C depleted samples.

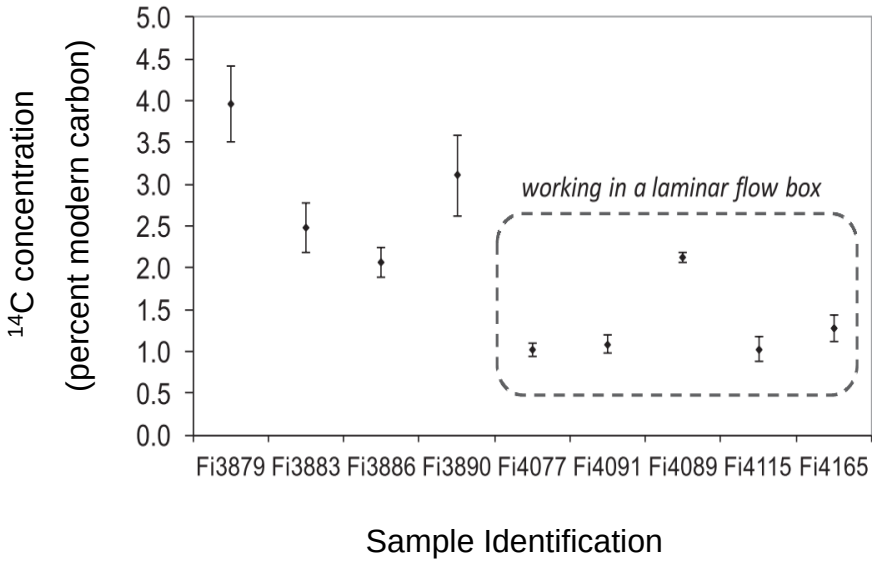

Figure 2.21 ^{14}C concentration measurements for ~0.05 mgC blank samples. Figure from Fedi *et al.* (2020).

2.3.7 Reducing Sample Loss

For samples that are already of limited size, reducing the possibility of sample loss is vital. At each stage of the radiocarbon dating process, there is potential for sample loss to occur, though some stages pose more risk than others.

2.3.7.1 Case Study

One case study aimed at reducing the possibility of sample loss is presented below.

National Institute for Nuclear Physics, Florence

Fedi *et al.* (2020) stated that sample loss can occur when CO_2 is transferred to the graphite reactor, and when graphite is pressed into the cathode target. To reduce

sample loss, Fedi *et al.* (2020) pressed Fe powder into small copper insets before graphitisation, and placed these insets into graphite reactors. Once graphitisation was complete, each inset was then placed into cathode targets that are routinely used. It was found that this method reduced sample loss, as graphite forms directly on the Fe surface in the copper insets, thereby no longer requiring graphite to be tipped from tubes into cathode targets. While it was stated that this improved radiocarbon results, several other techniques were also undertaken at the same time, and so it is not possible to evaluate if any improvement was specifically related to the use of copper insets.

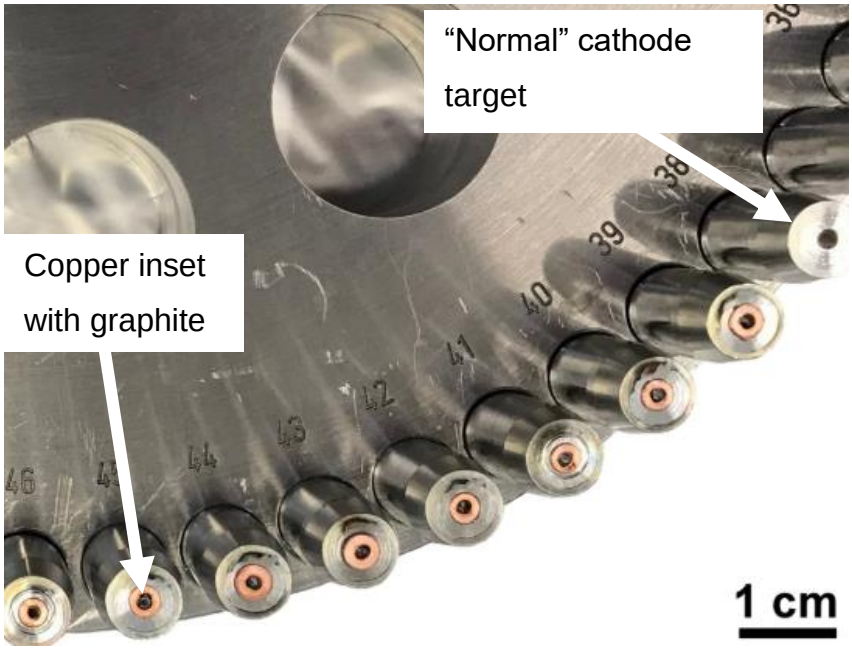

Figure 2.22 Copper insets in cathode targets. Figure from Fedi *et al.* (2020).

2.4 Summary

Successfully radiocarbon dating ultra-small samples opens up many avenues of research, but to achieve this, several issues need to be overcome. One of the main difficulties associated with samples of this size is the observation that as sample size decreases, modern and dead carbon (^{14}C-depleted) contamination increases, resulting in sample ages appearing younger or older than their true age. This observation is progressive, with smaller samples being affected by contamination more than larger samples. Increased fractionation and low graphite yield are also problems associated with radiocarbon dating ultra-small samples.

A selection of methods/modifications that have been used worldwide to improve radiocarbon dating of ultra-small samples were researched for this thesis. These included reducing the volume of the graphite reactor, reducing the reaction temperature, testing new water removal methods during graphitisation, investigating methods to “clean” the Fe catalyst before graphitisation, assessing the qualities of different Fe powders, pressing graphite in a laminar flow hood, and the use of copper insets in cathode targets. While many of the methods/modifications in the literature had promising results, several papers implemented several modifications all at once. This in turn means it was difficult to ascertain what specific modification resulted in the reported successful outcomes.

A selection of methods/modifications were tested in this thesis, as outlined in Chapter 3 and 4. Radiocarbon results using these methods are presented in Chapter 5 and 6.

Chapter 3

Experimental Methodology

3.1 Introduction

This chapter outlines volume reduction modifications to improve ultra-small radiocarbon dating at the Waikato Radiocarbon Dating Laboratory (WRDL). Radiocarbon results obtained using these volume reductions are examined in Chapter 5.

3.2 Current Laboratory Methodology

3.2.1 Shell Processing

The protocols for radiocarbon analysis at the WRDL are described in brief below. Because shell samples are the focal point of this research, the protocols mentioned predominantly relate to shell processing. For a more detailed description of these processes and the chemicals used, refer to the WRDL AMS processing technical report (Radiocarbon Dating Laboratory, 2017), and Appendix A.

1) Pre-treatment: While pre-treatment protocols vary between sample types, the common aim is to remove contaminants from the sample and isolate the carbon fraction of interest. Shell samples are given a 30 minute 0.1 M hydrochloric acid wash at 80°C to remove surface contaminants. The amount of acid added is proportional to the weight of the sample, as the acid wash is designed to remove 45% of the surface.
2) Evolution of CO_2: For shells, CO_2 is evolved by adding 85% orthophosphoric acid under vacuum at 70°C for 30 – 60 minutes (depending on sample size). The chemical reaction for the evolution of CO_2 from shell samples is as follows:

$$3CaCO_{3(s)} + 2H_3PO_{4(aq)} \rightarrow Ca_3(PO_4)_{2(aq)} + 3CO_{2(g)} + 3H_2O_{(l)}$$

3) Graphitisation: The CO_2 reaction vessel is attached to a vacuum line consisting of (in sequence) a glass cracker or needle transfer port, a water trap, one standard volume glass ampoule with an attached pressure transducer, and eight graphite reactors. Each graphite reactor has a dedicated 550°C furnace to reduce CO_2 to graphite which is monitored in real-time using a customised LabVIEW™ program. Each graphite reactor is equipped with magnesium perchlorate ($Mg[ClO_4]_2$) to remove water vapour, iron (Fe) powder which acts as a catalyst for the reaction, and an AMS 5812 pressure transducer which has a pressure range of 0 – 2068 mb (analog microelectronics, accessed 10/5/2022). Hydrogen (H_2) is introduced into the graphite reactor when needed by a valve connected to the vacuum line. **Figure 3.1** demonstrates the chemical reaction that takes place.

$$CO_{2(g)} + 2H_{2(g)} \xrightarrow[\text{Catalyst (Fe)}]{550^{\circ}C} C_{(s)}\,(\text{graphite}) + 2H_2O_{(aq)}$$

Figure 3.1 Graphitisation reaction (Beta Analytic, accessed 30/4/22)

4) Sample pressing: Graphite samples are pressed to 350 psi into a 3 mm hole of a cathode target, using a cathode press. The pressed graphite is stored in a cabinet with a 0.1 M sodium hydroxide reservoir to reduce atmospheric CO_2 absorption prior to being packaged and sent for analysis.

5) Graphite is analysed at the Keck AMS Radiocarbon Dating Laboratory, University of California, Irvine, using an NEC 0.5MV 1.5SDH-1 AMS analyser (Beverly *et al.*, 2016).

3.2.2 Quality Control

A range of standards of different ^{14}C content are routinely measured at the WRDL. These provide a constant check on the accuracy of different pre-treatment and CO_2 purification processes. Monitoring standards and blanks also quickly resolves any issues associated with pre-treatment or graphite production.

For this thesis, three standards of known age were used to assess the success of any improvements (including those outlined in Chapter 4): primary, background, and an in-

house secondary standard. The secondary and background standards are chosen to match the unknown sample type age and undergo the same chemical pre-treatment as the unknown sample to be radiocarbon dated. At the WRDL, the mean age and Gaussian standard deviation of the last ten standard results are monitored, allowing any issues to be resolved immediately. The standards that were used in this thesis are as follows:

- Primary Standard: Oxalic Acid II (Ox-II, also referred to as Ox-I) is an internationally accepted standard prepared by the US National Bureau of Standards that has a consensus value of 1.3407 $\pm$ 0.0019 $F^{14}C$ (Stenström *et al.*, 2011). $F^{14}C$ is used to report ^{14}C measurements of post-bomb (modern) samples (Reimer, Brown, & Reimer, 2016). Oxalic Acid II is used to set up and tune the AMS system and normalise $^{14}C/^{12}C$ ratios (Santos *et al.*, 2016b).
- In-house secondary standard: Tridacna is an in-house secondary shell standard with a ^{14}C age of 3028 $\pm$ 16 years.
- Background standard: Carrara Marble is a background standard with a ^{14}C activity beyond detection limits (*i.e.*, there is no ^{14}C left). It is used as a way of assessing modern contamination. The age of the Carrara Marble standard, expressed as $F^{14}C$, is 0.00172 ± 0.00047.

At the WRDL, for samples below 0.3 mgC, an additional small background standard of the same size is measured. This allows monitoring of small samples which are more prone to contamination problems. Due to ultra-small samples being classified as <0.1 mgC, modern and background standards of similar size are required to assess the levels of modern and dead contamination added at each stage of the process.

3.3 Avenues of Improvement

Chapter 2 outlined multiple methods/modifications to improve the precision and accuracy of radiocarbon results of ultra-small samples. Following this discussion, several avenues of improvement were investigated. These were chosen based on the reported effectiveness, resources available at the WRDL, and financial viability. Volume modifications are discussed in this chapter, while selected chemical modifications are outlined in Chapter 4.

It has been determined that a reduction in the volume of the vacuum line and graphite reactors can aid in reducing contamination via surface area reduction (Delqué-Koli Caffy *et al.*, 2013, Fedi *et al.*, 2020, Santos *et al.*, 2007b, Walter *et al.*, 2016). Having a glassblower onsite and the ease of making modifications to glassware meant this was considered a viable option. Modifications to metal sections of the vacuum lines were also possible using the services of Pace Engineering.

3.4 Volume Modifications

The WRDL AMS facility is equipped with dedicated glass vacuum lines connected by Swagelok® Ultra-Torr® vacuum fittings, maintained under vacuum by Pfeiffer HiCube 80 turbo drag pumps. **Figure 3.2** illustrates the vacuum line system that is currently in use (referred to as the “current vacuum line” in this thesis), consisting of a measuring manifold and graphite manifold. Modifications involved replacement of existing parts, or their elimination, with the aim of reducing volume and surface area in order to reduce contamination. Additionally, modifications were also designed to reduce “dead space”, which refers to areas where pumping efficiency is reduced. All modifications were designed to be reversible as permanent alterations to the current vacuum line would be problematic as there is a greater demand for larger samples. Therefore, it was important to design a system that could easily be reverted to the current vacuum line.

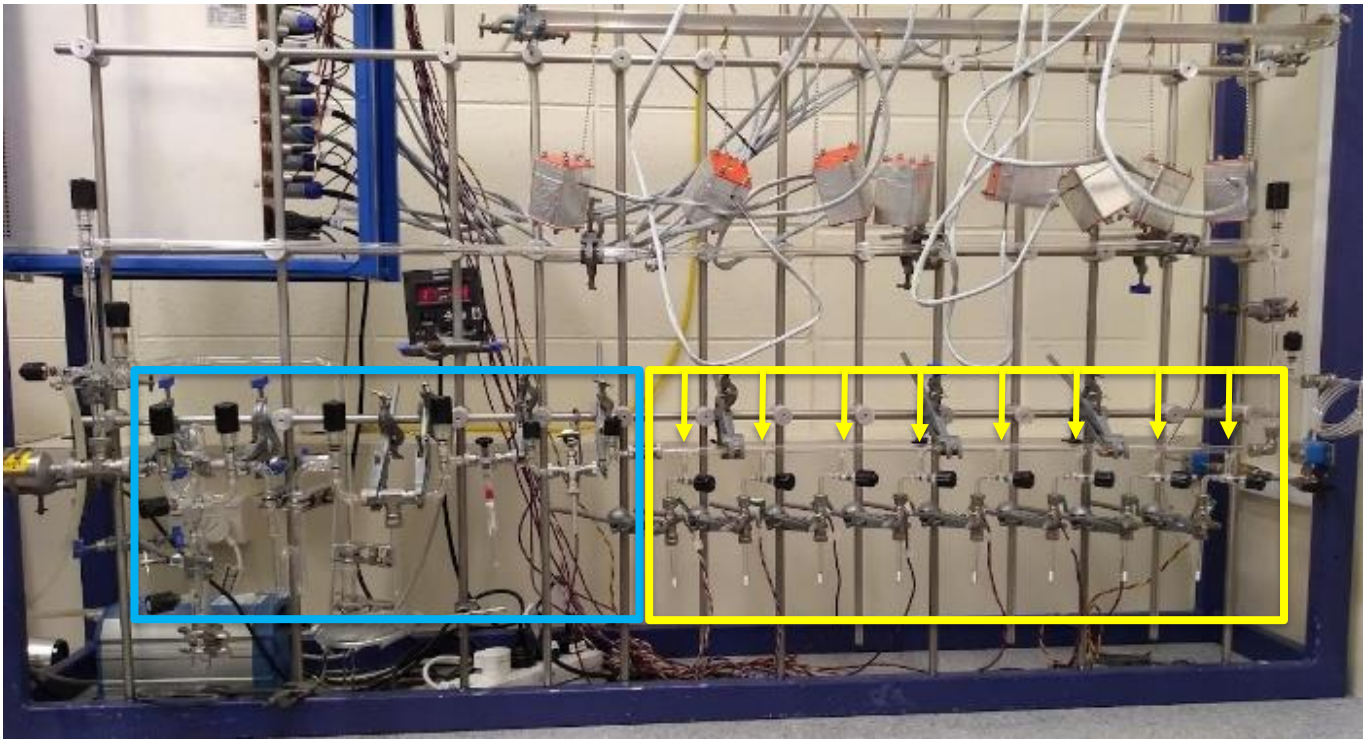

Figure 3.2 Current vacuum line used at the WRDL. Blue box: measuring manifold. Yellow box: graphite manifold with eight graphite reactors.

3.4.1 Measuring Manifold Modifications

The components that make up the current measuring manifold at the WRDL are shown in **Figure 3.3**. These include:

- Ultra-Torr® vacuum fittings (metal components). Please see Appendix B for a full description of each fitting.
- Borosilicate glass tubing from Brandon Scientific Glassblowing (BSG).
- High vacuum stopcock plugs from BSG.
- Viton® O-rings.

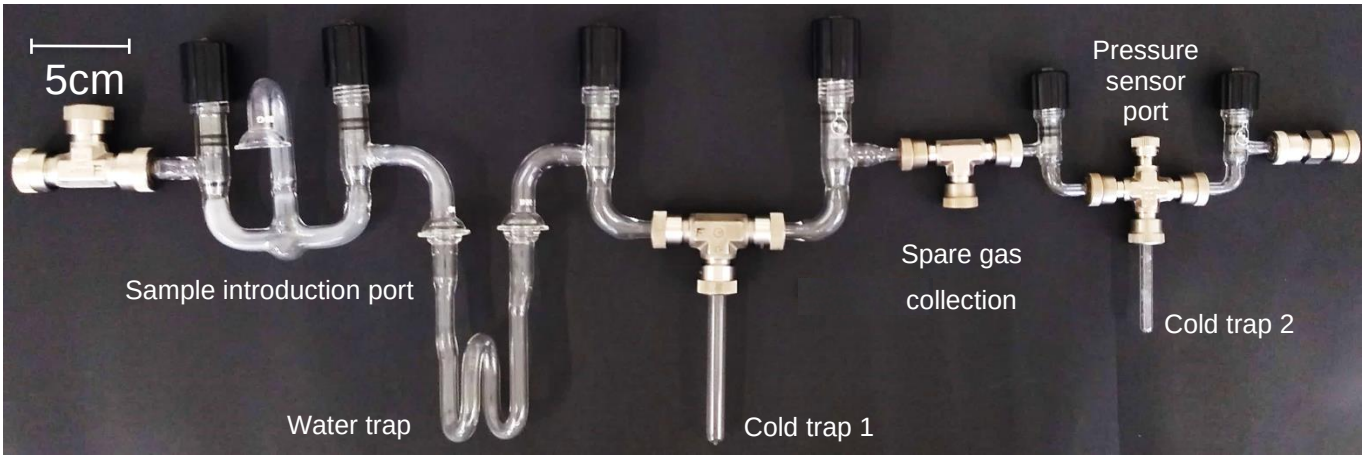

Figure 3.3 Measuring manifold of the current vacuum line used at the WRDL.

Several modifications were undertaken to reduce the volume of the current measuring manifold. These are summarised in **Figure 3.4** and discussed in detail below.

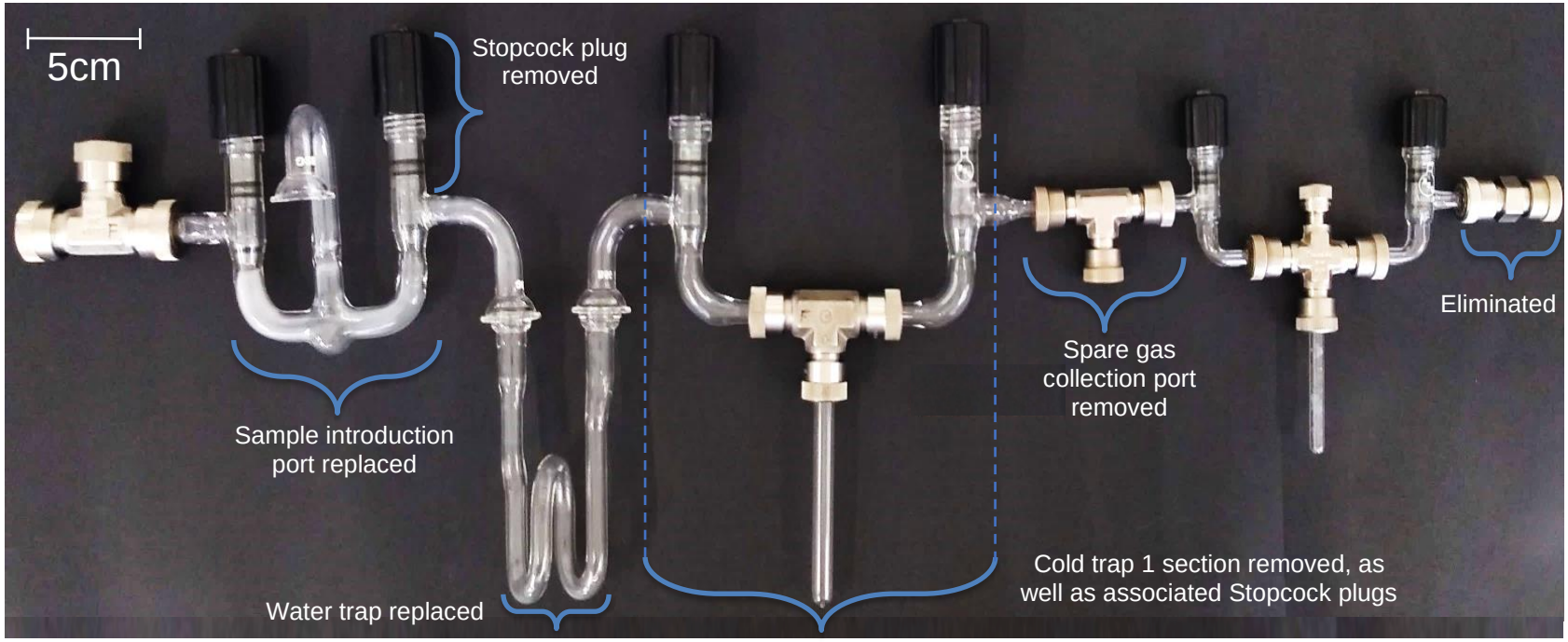

Figure 3.4 Current measuring manifold with sections that have been replaced or eliminated.

3.4.1.1 Stopcock Plug Modifications

BSG glass tubing and stopcock plugs were replaced with Swagelok® SS-4P4T-UT4 valve taps (**Figure 3.5**), which serves two purposes:

- Ultra-Torr® vacuum fittings are built into the valve taps, reducing the volume.
- The Swagelok® valve taps straighten the vacuum line, thereby minimising dead space.

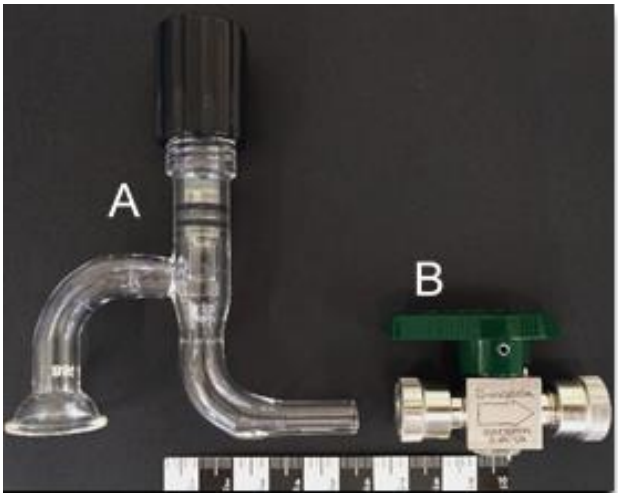

Figure 3.5 (A) Borosilicate glass tubing from BSG with a stopcock plug. (B) Swagelok® SS-4P4T-UT4 valve tap.

3.4.1.2 Water Trap

The current measuring manifold uses modified borosilicate glass tubing to form a coiled water trap. This is used in conjunction with dry ice and denatured alcohol (“slush”) to maintain the temperature of the coil at -70°C, thereby removing water produced from the dissolution of $CaCO_3$ into CO_2. Because smaller samples produce much less water, the coiled water trap was replaced with a straight 9 mm x 12.5 cm borosilicate tube with a tapered 6 mm end (**Figure 3.6**).

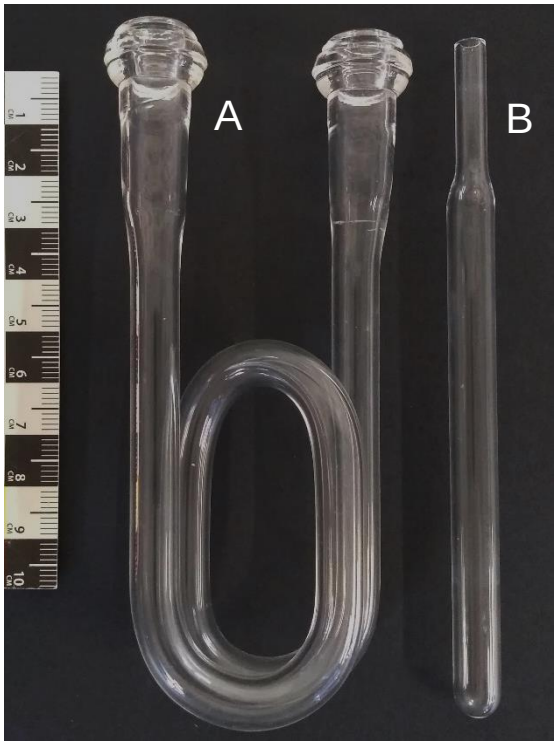

Figure 3.6 (A) Coiled water trap used on the current measuring manifold. (B) Straight water trap for the ultra-small measuring manifold.

3.4.1.3 Cold Trap

Carbon dioxide (CO_2) is initially frozen (using liquid nitrogen) in the cold trap, and any non-condensable gases (such as sulphur oxide and hydrogen sulphide [Dincer & Ezzat, 2018]) are pumped away. The current measuring manifold has two cold traps: cold trap A (9 mm x 9 cm), which serves as the main cold trap, and cold trap B (6 mm x 6 cm), which acts as a CO_2 reduction/manipulation measurement volume (**Figure 3.7**). Because the amount of CO_2 produced from ultra-small samples is so small, cold trap A was removed.

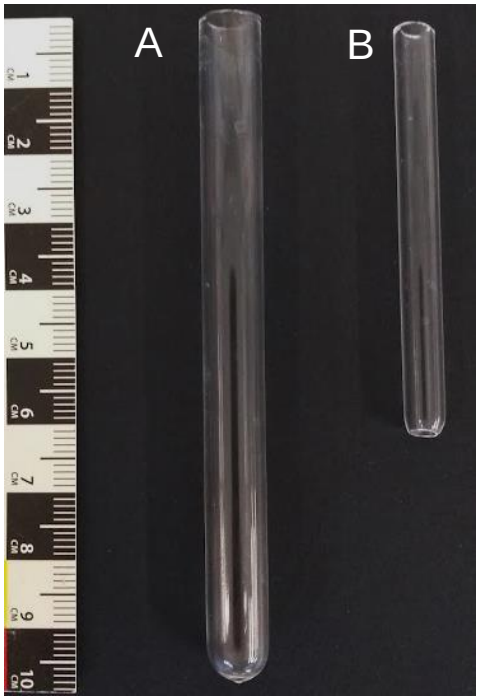

Figure 3.7 (A) Main cold trap on the current measuring manifold. (B) New cold trap for the ultra-small measuring manifold.

3.4.1.4 Sample Introduction

CO_2 produced via acid hydrolysis is introduced into the measuring manifold by a Luer-lock™ needle, which on the current measuring manifold has two attachments: an Ultra-Torr®-Union-straight and a borosilicate glass ball-joint. Because shell samples are the focus of this research project, the Luer-lock™ needle has been integrated directly into the measuring manifold, reducing volume and dead space (**Figure 3.8**). It should be noted that this method of sample introduction can be interchanged so that other sample types, such as charcoal or wood, can be processed through the ultra-small measuring manifold.

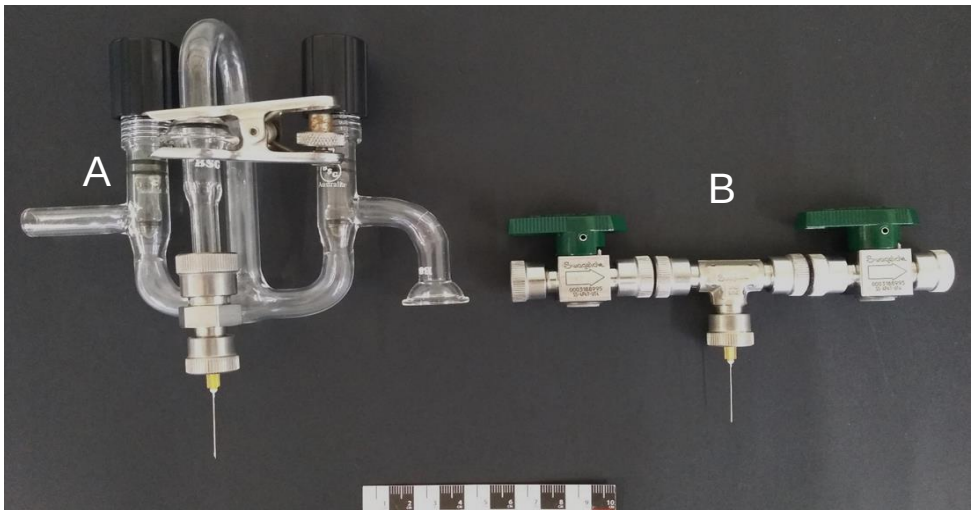

Figure 3.8 (A) Current introduction port. (B) New shell CO_2 introduction port.

3.4.1.5 Glass Connections

Due to the elimination of stopcock plugs, borosilicate glass connectors were made to link the Swagelok® valve taps and the two Ultra-Torr®-Union vacuum fittings. This included the use of five 3 cm x 6 mm connectors, and one variable diameter glass adapter of 3.5 cm length (to connect two different sized Ultra-Torr®-Union-tees of 6 mm and 9 mm diameter). **Figure 3.9** and **Figure 3.10** illustrate these connectors.

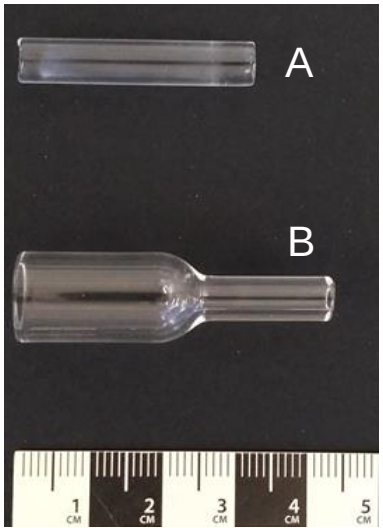

Figure 3.9 (A) 6 mm x 3 cm glass connector. (B) Variable 3.5 cm glass connector.

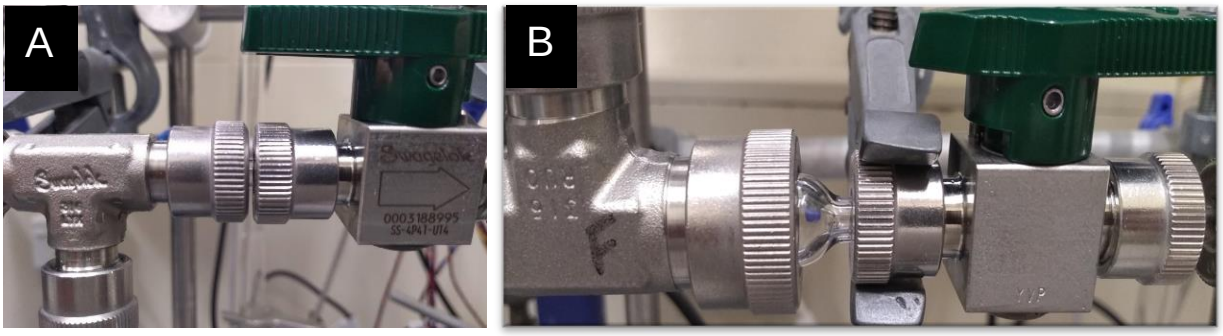

Figure 3.10 New shell sample connectors on the measuring manifold. (A) 6 mm x 3 cm glass connector. (B) Variable 3.5 cm glass connector.

3.4.1.6 Ultra-Torr® Fittings

On the current measuring manifold, an SS-6-UT-3 Ultra-Torr® vacuum fitting links the cold trap to borosilicate glass tubing on either side. This was replaced with an SS-4-UT-3 Ultra-Torr® fitting (**Figure 3.11**). The smaller Ultra-Torr® fitting also contributes to a further volume reduction.

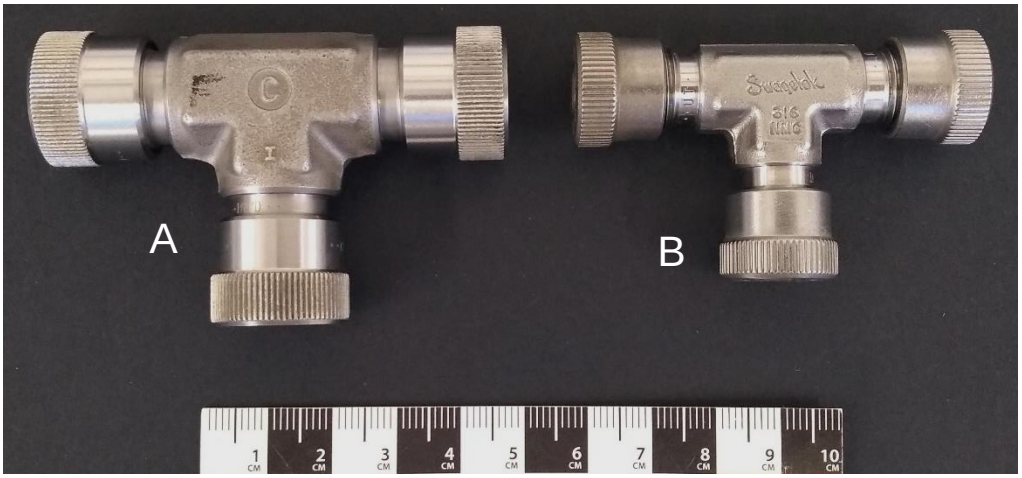

Figure 3.11 (A) Larger (SS-8-UT-3) and (B) smaller (SS-4-UT-3) Ultra-Torr® fittings for the cold trap on the current and ultra-small measuring manifold, respectively.

3.4.1.7 Ultra-Small Measuring Manifold

Figure 3.12 demonstrates the new ultra-small measuring manifold after eliminating and reducing various sections of the current measuring manifold. The schematic diagrams in **Figure 3.13** offers an additional visual aid to illustrate the differences between the current and ultra-small vacuum lines. It should be noted that while the two diagrams of each vacuum line are not drawn to scale (stopcock plugs, Ultra-Torr® fittings, Swagelok® valve taps) the length (horizontally) of both vacuum lines has been drawn so they are proportionally correct.

The ultra-small measuring manifold is reduced in both length and volume compared to the current measuring manifold. The current measuring manifold is 67 cm in length, whereas the new ultra-small line is 43 cm, equating to a 36.0% length reduction. This reduction created a gap between the measuring manifold and the start of the graphite manifold and so to remedy this, a 6 mm x 24 cm borosilicate glass tube was used to connect the two sections. A volume reduction was also calculated, equating to 82.2%. This was calculated by measuring the same quantity of gas in both measuring manifolds: on the current measuring manifold, 31 mb of CO_2 resulted in 175 mb in the ultra-small measuring manifold.

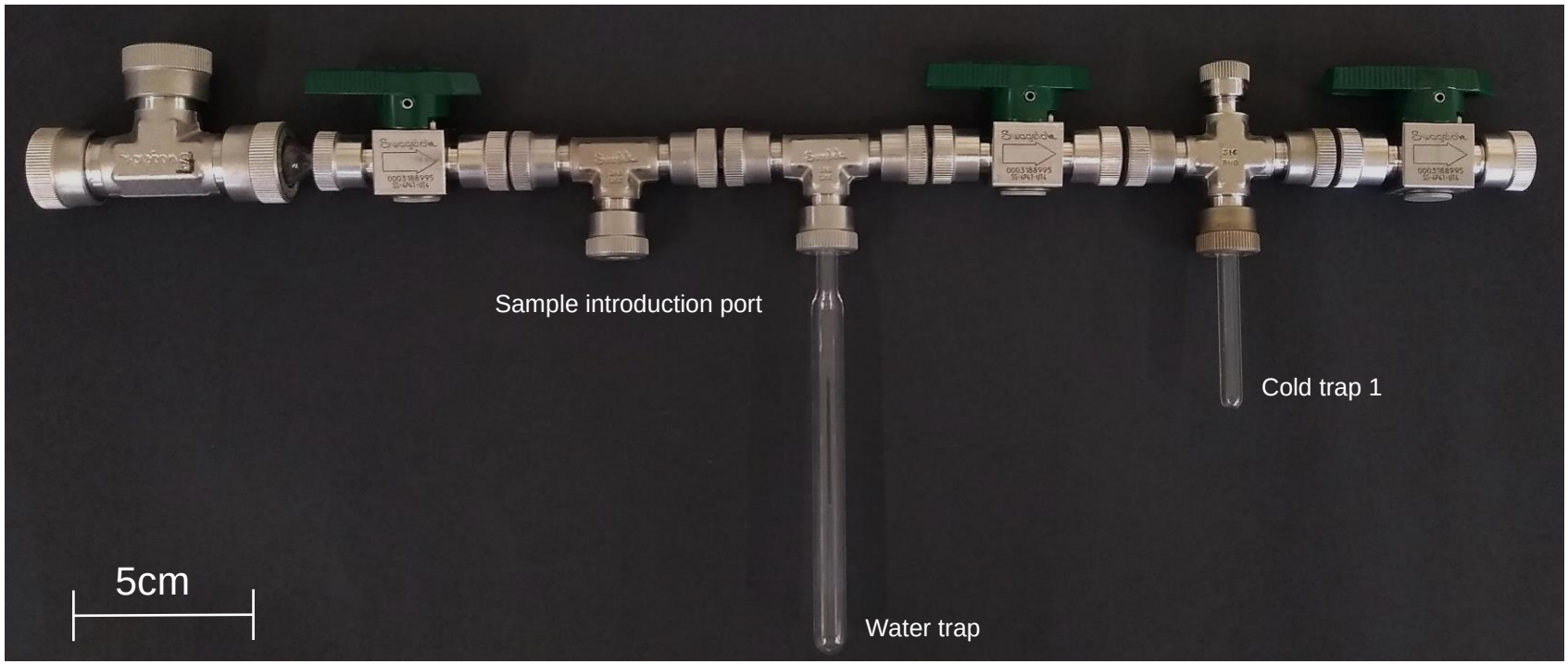

Figure 3.12 Ultra-small measuring manifold.

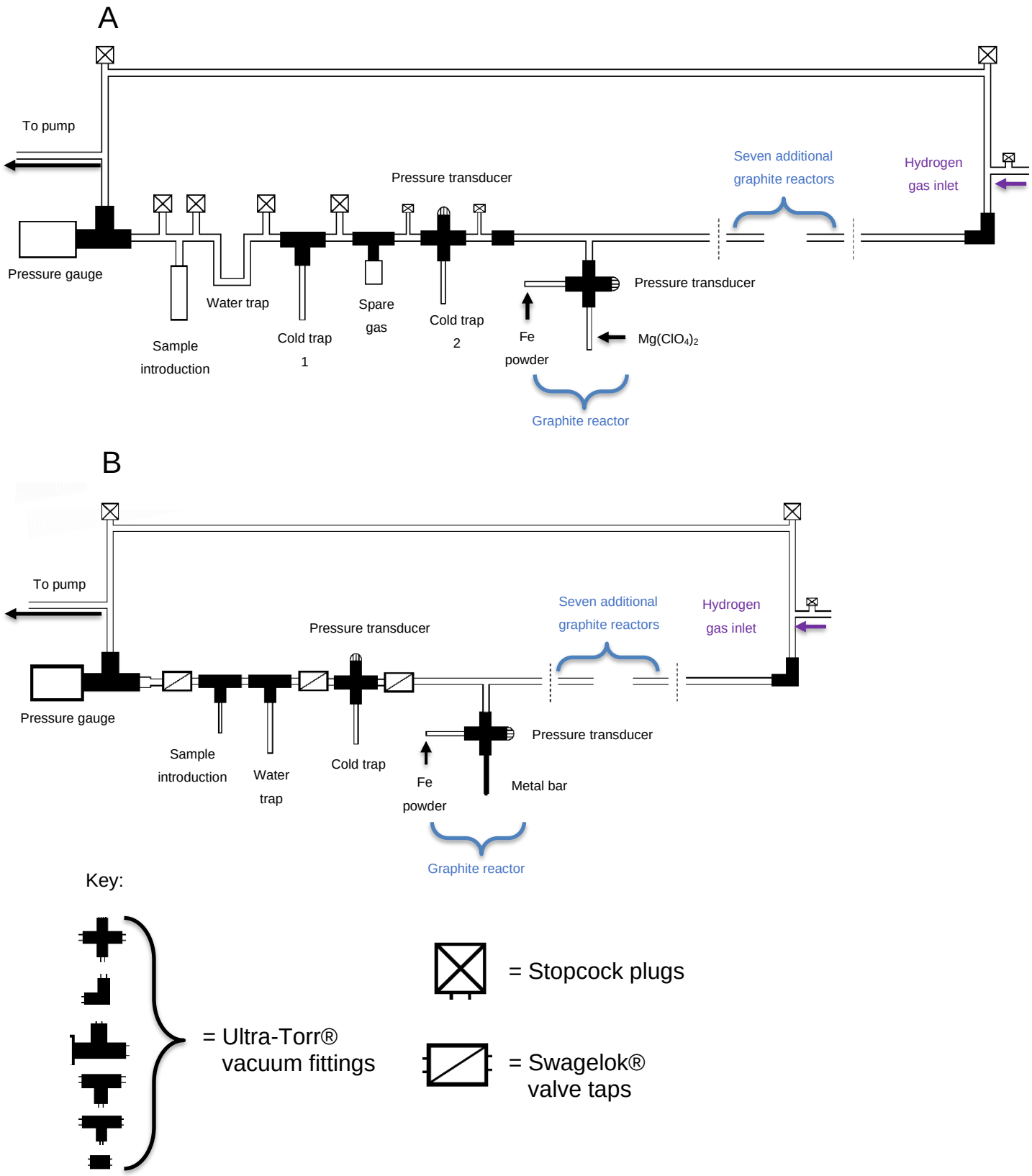

Figure 3.13 Schematic diagram of (A) Current vacuum line, and (B) ultra-small vacuum line. See Appendix B for a description of each Ultra-Torr® vacuum fitting.

3.4.2 Graphite Reactor Modifications

Volume reductions were applied to the eight graphite reactors (**Figure 3.14**) that are connected to the graphite manifold. Modifications involved reducing the volume of the Ultra-Torr®-Union-Cross as well as reducing the volume of the 6 mm x 7 cm quartz tubes that contain Fe catalyst and $Mg(ClO_4)_2$. Quartz tubes are used because this type of glass can withstand very high temperatures, whereas borosilicate glass will start to deform at temperatures close to those needed for graphitisation (550ºC) and glassware cleaning.

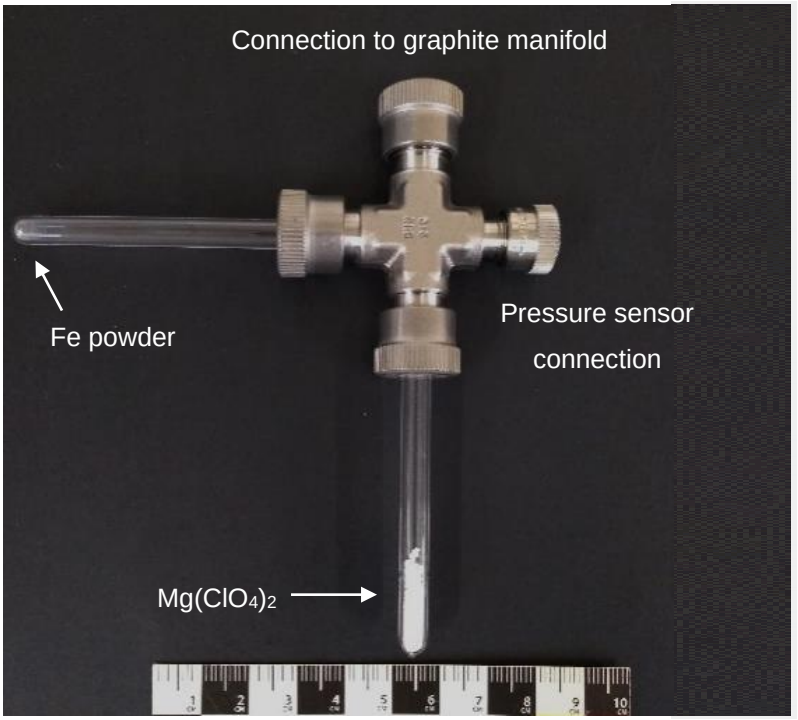

Figure 3.14 Current graphite reactor.

3.4.2.1 Ultra-Torr®-Union-Cross

The current Ultra-Torr®-Union-Cross has three ¼-inch and one $^1/_8$-inch connection ports (**Figure 3.15A**). Modifications to reduce the volume were made by Pace Engineering (**Figure 3.15B**), resulting in a small Ultra-Torr®-Union-Cross.

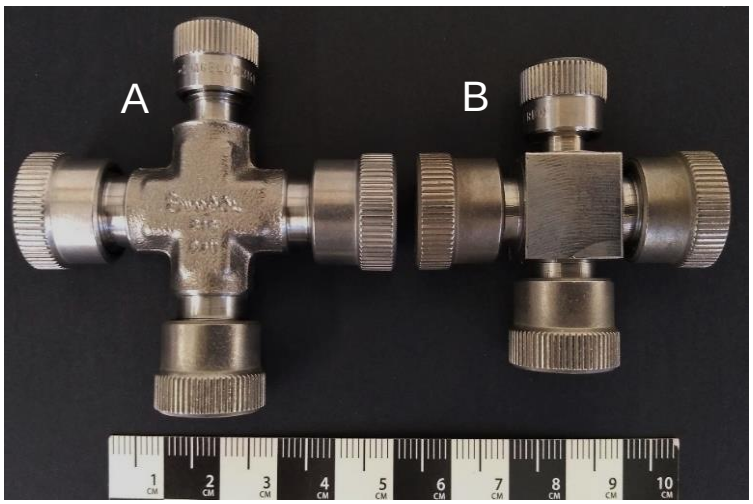

Figure 3.15 (A) Current Ultra-Torr®-Union-Cross. (B) Small Ultra-Torr®-Union-Cross.

3.4.2.2 Water Removal

At the WRDL, $Mg(ClO_4)_2$, which removes water produced during graphitisation, is placed in a 6 mm x 7 cm quartz tube. The minimum length possible for this tube to be reduced to was 4 cm as there needs to be enough space between the liquid nitrogen (used to freeze CO_2 into the graphite volume) and the Viton™ O-ring (housed in the Ultra-Torr®-Union-Cross) as to prevent the Viton™ O-ring freezing (which can lead to leaks). The dashed blue lines in **Figure 3.16** represent how far up the tube liquid nitrogen is placed, and **Figure 3.17** illustrates this.

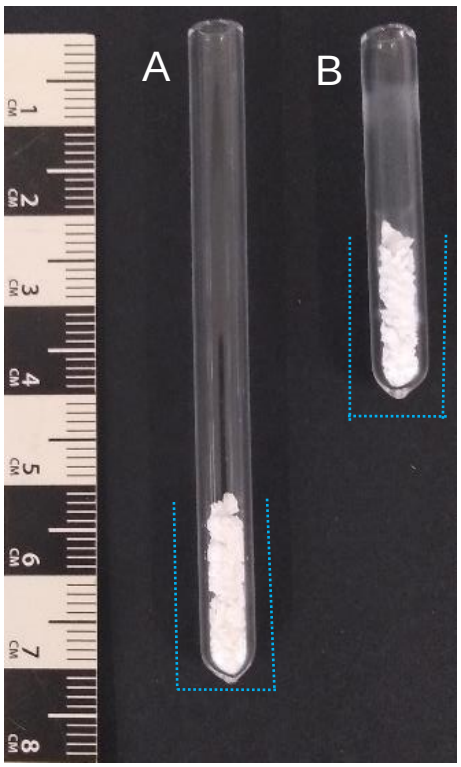

Figure 3.16 (A) Current quartz tube for $Mg(ClO_4)_2$. (B) Reduced quartz tube for $Mg(ClO_4)_2$.

Figure 3.17 Liquid nitrogen is placed around the quartz tube, containing $Mg(ClO_4)_2$, to freeze CO_2 into the graphite reactor.

3.4.2.3 Fe Catalyst

At the WRDL, Fe powder is placed inside a 6 mm x 7 cm quartz tube. Fe powder acts as a catalyst for the conversion of CO_2 to graphite (carbon) and during graphitisation, a small furnace set at 550°C is placed over the quartz tube. The length of the quartz tube was reduced to 5 cm (**Figure 3.18**). This was the minimum length that the quartz tube could be reduced to, otherwise the weight of the furnace on the tube could push down on the connection and result in leaks, or the furnace would not be able to sit securely on the tube (**Figure 3.19**).

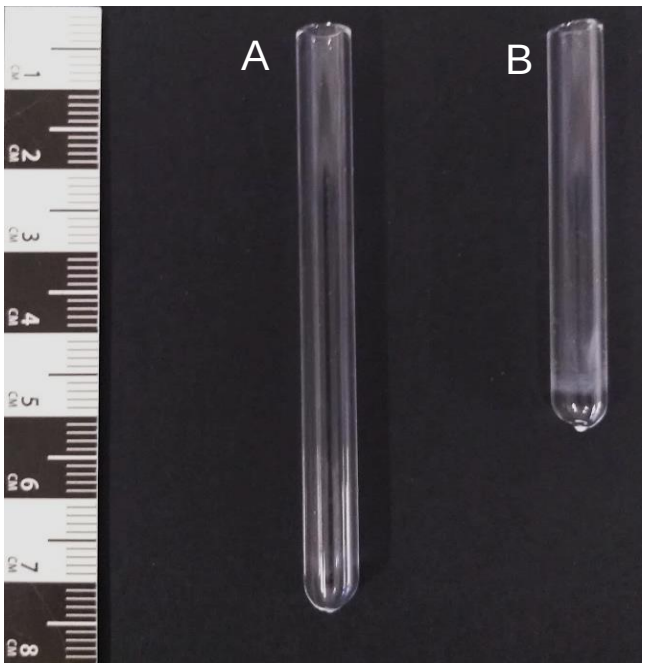

Figure 3.18 (A) Current quartz tube used for Fe powder. (B) Reduced length quartz tube for Fe powder.

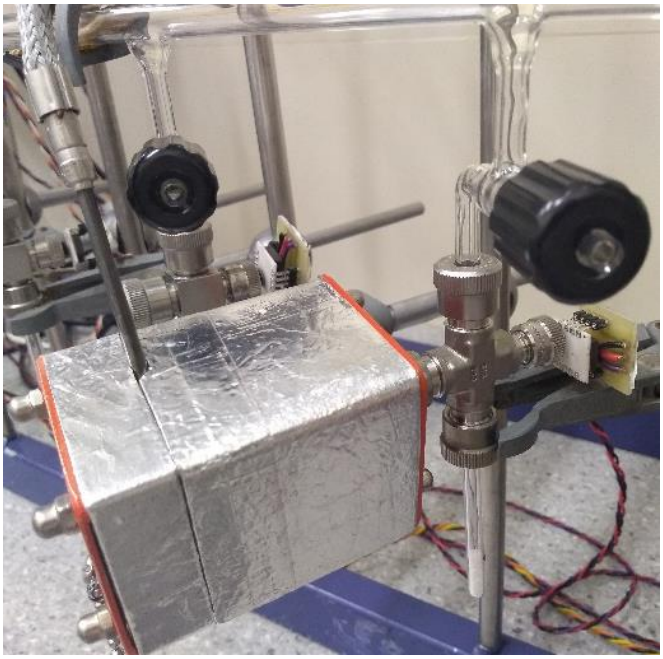

Figure 3.19 Placement of furnace on quartz tube containing Fe powder.

3.4.2.4 Final Ultra-Small Graphite Reactor

The ultra-small graphite reactor is shown in **Figure 3.20**. The percentage decrease in volume of the ultra-small graphite reactor compared to the current graphite reactor equated to 47.7%, as 1 mgC of CO_2 in the current graphite reactor resulted in 545 mb, but in the ultra-small graphite reactor this resulted in 1043 mb. Note that the use of the ultra-small measuring manifold (**Figure 3.12**) in conjunction with the ultra-small graphite reactor is referred to as the “ultra-small vacuum line” from Chapter 4 onwards.

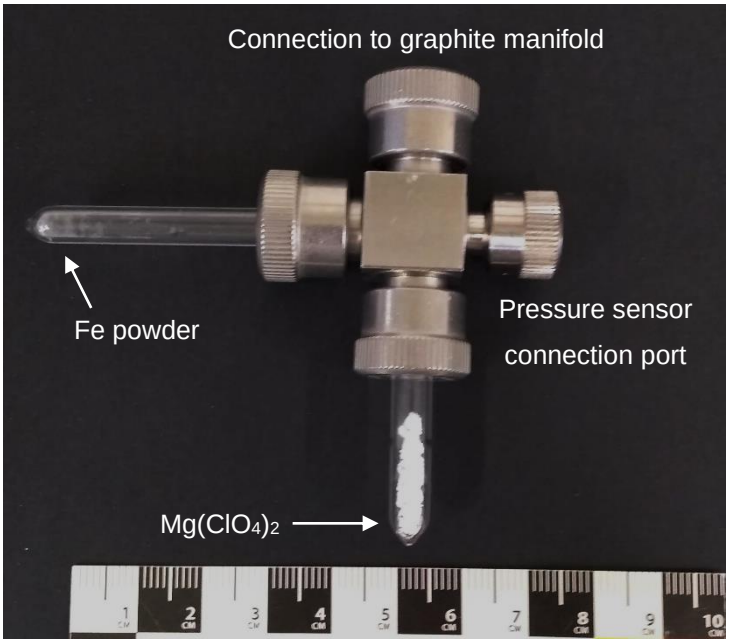

Figure 3.20 Ultra-small graphite reactor.

3.5 Discussion

The design of the ultra-small measuring manifold resulted in several operational advantages and disadvantages. Because of this, the comments below are separate from the radiocarbon results presented in Chapter 5 and 6. No operational advantages or disadvantages were observed for the ultra-small graphite reactors.

Advantages

After volume modifications, the current measuring manifold and graphite reactors were reduced in volume and length. This led to reduced areas of dead space and fewer complex glass components, thereby reducing the need for an onsite

glassblower. Furthermore, borosilicate glass connectors can be easily made by technicians at the WRDL, using readily available materials. The reduction in length of the ultra-small measuring manifold also resulted in a space saving aspect.

Disadvantages

The Swagelok® valve taps on the ultra-small measuring manifold are heavier and stiffer than the stopcock plugs, and care needs to be taken to avoid excess movement, as this can cause leaks. Movement can be alleviated by careful positioning of clamps to hold the tap securely, however, in scenarios where there is not enough space to use additional clamps, the valve body needs to be held while the valve handle is turned. This issue could be remedied by increasing the lengths of the glass connecters.

As previously discussed, samples below 0.3 mgC are required to have an additional small blank standard (Carrara Marble) that matches the size of the sample. Reducing the amount of standard CO_2 to match ultra-small sample CO_2 is no longer straightforward. The design of the current measuring manifold means that reducing or increasing the amount of CO_2 is relatively easy. However, because the ultra-small measuring manifold has fewer components, the ability to accurately adjust the amount of CO_2 has been eliminated. While CO_2 can be let into the graphite manifold (only the manifold, not the graphite reactors), anything that involves moving or splitting the sample runs the risk of fractionation. Therefore, accurate weighing of standards prior to CO_2 conversion is essential. While this may be time-consuming, weighing the correct amount of standard is critical for assessing laboratory-induced contamination.

3.6 Summary

A series of volume modifications were carried out on the current measuring manifold and graphite reactors in order to reduce contamination when processing ultra-small samples. These modifications involved either replacing or eliminating existing parts to reduce the overall volume and surface area. Modifications to the current measuring manifold resulted in a 36% decrease in length and 82.2% decrease in volume. The volume reduction to the current graphite reactor equated to 47.7%.

Compared to the current measuring manifold at the WRDL, the ultra-small measuring manifold is shorter so has the advantage of saving space. Less glassware minimises the need for an onsite glassblower and some glassware components can be easily made by radiocarbon technicians.

One disadvantage of the ultra-small measuring manifold was that due to the stiffness and weight of the Swagelok® valve taps, turning the valves means there is a tendency for the Swagelok® valve taps to move, which can lead to breaking the seal from the Viton® O-ring, causing leaks. This could however be solved using extra clamps to hold the Swagelok® valve taps in place, and care by the operator. Another disadvantage is the inability to adjust the amount of CO_2 gas from standards, requiring weighing of standards on a high precision balance prior to CO_2 conversion.

The small graphite reactors offered no obvious disadvantages or advantages from an operational perspective.

Chapter 4
Chemical Modifications and Method Optimisation

4.1 Introduction

This chapter outlines chemical modifications that have been documented to have promising results in the graphitisation process (Fedi *et al.*, 2020, Santos *et al.*, 2007a, Santos *et al.*, 2016a, Smith *et al.*, 2016a, Yang, Smith, & Hua, 2013). Chapter 2 outlined several processes where contamination can be introduced, and Chapter 3 explained the methodology for reducing the volume of the vacuum line in order to reduce contamination. Chapter 4 deals with contamination that stems from chemicals used for graphitisation, and the methods that can be used to minimise this. A possible source of sample loss is also investigated. The results of subsequent experiments undertaken to improve the methodology for processing ultra-small samples at the Waikato Radiocarbon Dating Laboratory (WRDL) are presented in the second half of the chapter.

4.2 Current Laboratory Methodology

Magnesium perchlorate ($Mg[ClO_4]_2$) and iron (Fe) powder are used for the graphitisation process at the WRDL. $Mg(ClO_4)_2$ removes water formed during graphitisation, and Fe powder acts as a catalyst for the formation of graphite. However, their use for ultra-small samples can result in the introduction of contaminant carbon (Santos *et al.*, 2007a, Santos *et al.*, 2016a). To reduce contamination stemming from these two chemicals, a literature review of other radiocarbon dating laboratory protocols and findings was conducted. These included an alternative to using $Mg(ClO_4)_2$ for water removal and using oxygen (O_2), in addition to hydrogen, as a method of cleaning Fe powder.

The 6-decimal point balance that is routinely used for weighing shell samples has been investigated as a possible source of sample loss due to the observation that samples of the same measured weight produced different CO_2 yields (unpublished data, Petchey). For normal sized shell samples (>5 mg), this discrepancy would not

be problematic but with ultra-small shell samples, sample weights need to be more precise in order to correctly weigh standards.

4.3 Experimental Methodology and Results

4.3.1 Sample Weighing and CO_2 Yield

While sample loss can occur during various stages of the radiocarbon dating process, such as sample being insufficiently acidified, or sample becoming stuck in the vial or septa lid, errors in the initial weight readings were considered a likely cause for differences in observed CO_2 produced by samples of similar measured weight.

Shell samples at the WRDL are routinely weighed using a 4-decimal point balance (Mettler Toledo, New Classic, MS204S /01) that has a readability down to 0.1 mg. This balance was designated Balance A. Ultra-small shell samples in this research have been defined as <0.10 mgC, which translates to approximately 0.80 mg of shell. As discussed in Chapter 3, small shell samples require the measurement of a Carrara Marble standard of the same size. While it is possible to manipulate CO_2 if too much shell is weighed, this is not good practice, and needing to do multiple weighings to obtain the correct amount of CO_2 is time-consuming. Therefore, initial weight readings need to be sufficiently reliable for the task. To test this, Balance A was compared to a 6-decimal point balance (Sartorius Ultra Micro Balance MSE6.6S – 000 – DM) that has a readability down to 0.001 mg. This was designated Balance B.

To assess and compare the precision of each balance, two experiments were undertaken. Firstly, twenty samples of Carrara Marble standard ranging between 0.4 – 6.0 mg were weighed into pre-baked glass vials. Each sample was weighed on Balance A three times and then weighed on Balance B three times. Results are presented in **Table 4.1**, along with mean and standard deviation values where applicable.

Secondly, the amount of CO_2 produced from ten different weights of Carrara Marble was also investigated. Sample sizes ranging from 0.5 – 5.0 mg were weighed out six times into pre-baked glass vials; three on Balance A and three on Balance B. This

was an important experiment as it allowed the impact of each balance's precision on CO_2 yield to be directly assessed and compared.

Samples were converted to CO_2 via acidification using orthophosphoric acid, and processed through the current vacuum line set up at the WRDL. Carrara Marble weights, corresponding CO_2 values, and the standard deviation values for Balance A and B are listed in **Table 4.2** and **Table 4.3**. To account for slight differences in the starting weights of each sample, the CO_2 produced from each sample was divided by its initial weight, thereby obtaining a weight to CO_2 ratio, which (in theory) should be the same no matter the amount of starting material.

Table 4.1 Table showing the recorded weights for twenty samples of Carrara Marble, weighed on Balance A and then Balance B

	Balance A					Balance B				
	Weight (mg)			Mean	Std Deviation	Weight (mg)			Mean	Std Deviation
1	0.4	0.3	0.2	0.3	0.100	0.708	0.709	0.709	0.709	0.001
2	0.6	0.6	0.8	0.7	0.115	0.879	0.878	0.879	0.879	0.001
3	0.8	0.9	1.2	1.0	0.208	1.065	1.064	1.065	1.065	0.001
4	0.8	0.6	0.5	0.6	0.153	0.776	0.771	0.775	0.774	0.003
5	1.1	1.0	1.2	1.1	0.100	1.275	1.274	1.276	1.275	0.001
6	1.2	1.0	1.2	1.1	0.115	1.248	1.245	1.246	1.246	0.002
7	1.3	1.6	1.5	1.5	0.153	1.559	1.560	1.561	1.560	0.001
8	1.6	1.4	1.6	1.5	0.115	1.536	1.453	1.457	1.482	0.047
9	2.0	2.2	2.1	2.1	0.100	2.392	2.391	2.392	2.392	0.001
10	2.3	2.5	2.4	2.4	0.100	2.521	2.523	2.751	2.598	0.132
11	2.5	2.7	2.4	2.5	0.153	2.758	2.759	2.759	2.759	0.001
12	2.7	2.8	3.0	2.8	0.153	2.840	2.842	2.839	2.840	0.002
13	2.8	2.8	3.0	2.9	0.115	2.291	2.291	2.290	2.291	0.001
14	3.2	3.3	3.4	3.3	0.100	3.353	3.414	3.412	3.393	0.035
15	3.5	3.5	3.9	3.6	0.231	3.764	3.758	3.765	3.762	0.004
16	3.8	3.8	3.9	3.8	0.058	4.070	4.066	4.072	4.069	0.003
17	4.5	4.6	4.3	4.5	0.153	4.638	4.640	4.639	4.639	0.001
18	4.9	4.8	4.6	4.8	0.153	5.089	5.089	5.088	5.089	0.001
19	5.4	5.2	5.5	5.4	0.153	5.296	5.298	5.298	5.297	0.001
20	5.7	5.4	5.5	5.5	0.153	5.669	5.668	5.669	5.669	0.001

Table 4.2 CO_2 values obtained from samples weighed on Balance A and B.

Balance A				Balance B			
Weight (mg)	CO_2 (mb)	Std deviation of CO_2	CO_2(mb)/weight(mg)	Weight (mg)	CO_2 (mb)	Std deviation of CO_2	CO_2(mb)/weight(mg)
0.5	4		8.0	0.502	5		9.960
0.4	8	2.082	20.0	0.536	8	1.538	14.925
0.4	5		12.5	0.588	6		10.204
0.7	12		17.1	0.836	10		11.962
0.8	18	5.508	22.5	0.915	9	0.587	9.836
0.7	7		10.0	0.724	10		13.812
1.0	14		14.0	1.225	13		10.612
0.9	15	6.083	16.7	0.936	9	2.319	9.615
1.1	25		22.7	0.964	9		9.336
1.3	16		12.3	1.498	15		10.013
1.4	34	11.358	24.3	1.402	14	0.587	9.986
1.4	37		26.4	1.405	15		10.676
2.1	44		21.0	2.339	27		11.543
2.1	42	7.572	20.0	2.114	26	0.587	12.299
2.2	30		13.6	2.135	26		12.178
2.9	27		9.3	2.948	32		10.855
2.8	26	1.000	9.3	2.905	29	2.082	9.983
2.8	28		10.0	2.864	33		11.522
3.2	48		15.0	3.294	34		10.322
3.3	44	6.110	13.3	3.314	33	1.538	9.958
3.3	36		10.9	3.256	31		9.521
3.7	37		10.0	3.809	40		10.501
3.8	43	3.055	11.3	3.745	38	2.527	10.147
3.7	39		10.5	3.881	43		11.080
4.8	43		9.0	4.947	54		10.916
4.9	45	5.859	9.2	4.783	51	1.538	10.663
4.9	54		11.0	4.890	52		10.634
5.1	49		9.6	5.154	56		10.865
5.2	47	3.606	9.0	5.288	57	2.082	10.779
5.2	54		10.4	5.361	60		11.192

Table 4.3 Mean and standard deviation values for Balance A and B for CO_2/weight ratio values, as listed in **Table 4.2**.

	Mean value of CO_2/weight	Std Deviation of CO_2/weight
Balance A	14.0	5.331
Balance B	10.863	1.224

4.3.2 Fe Catalyst Assessment

The hydrogen (H_2) reduction method is used at the WRDL to convert sample CO_2 to graphite, where Fe powder is used as a catalyst. As per the reaction equation in Chapter 3 (**Figure 3.1**), when H_2 and heat are applied to CO_2, this results in graphitisation and the formation of graphite, which precipitates on the surface of the Fe catalyst (Christensen, 2022). Santos *et al.* (2007b) describe the optimal catalyst as resulting in rapid graphitisation, and producing graphite characterised by homogeneity, lack of sintering, and minimal amounts of modern and dead carbon. In addition to these qualities, three physical characteristics of the graphite were determined to play a role (Santos *et al.*, 2007a). These are given in order of preference:

- Fluffy: Graphite falls easily into a target holder, and no material sticks to the graphitisation tube.
- Firm: Only some of the graphite falls easily into the target holder. Most of the mixture is in the form of a pellet, but it can be easily broken up with a pin.
- Solid: Most graphite is sintered into a hard pellet, which is difficult to break apart into the target holder. A spatula is required to remove the hard pellet from the graphitisation tube.

The WRDL tested Prolabo® and BDH® Fe powders in 2009 during the initial development of the H_2/Fe graphitisation system. The parameters tested included current generated during analysis by the accelerator mass spectrometer (measured in nanoamps [nA]) and $F^{14}C$ values (the higher the $F^{14}C$ value, the higher the ^{14}C content). Additional tests were undertaken in 2011 where Alfa Aesar® Fe powder was also analysed. The results for the 2009 and 2011 tests are presented in **Table 4.4**. For comparison, Alfa Aesar® Fe powder results reported by Southon, J.

(University of California Irvine [UCI], Keck Carbon Cycle Accelerator Mass Spectrometer Facility, *pers comm,* 2009 and 2011) are also included.

Table 4.4 $^{12}C+$ current and $F^{14}C$ values for BDH®, Prolabo® and Alfa Aesar® Fe powders from tests undertaken in 2009 and 2011 at the WRDL. For reference, UCI results for their Alfa Aesar® Fe powder are also given.

	Fe powder	$^{12}C+$ current (nA)	$F^{14}C$
2009	BDH® Fe powder	1540	0.84
	BDH® Fe powder	1870	0.88
	BDH® Fe powder	1160	0.72
	BDH® Fe powder	1210	0.68
	Prolabo® Fe powder	290	0.22
	Prolabo® Fe powder	300	0.16
	Prolabo® Fe powder	730	0.10
	Prolabo® Fe powder	810	0.16
2011	BDH® Fe powder	290	0.30
	BDH® Fe powder	330	0.30
	Prolabo® Fe powder	980	0.50
	Prolabo® Fe powder	405	0.17
	WRDL Alfa Aesar®	920	0.60
	WRDL Alfa Aesar®	915	0.60
	UCI Alfa Aesar® -325	395	0.75
	UCI Alfa Aesar® -325	325	0.90

A combination of low current and low carbon contamination is favoured for analysis, with Prolabo® and BDH® Fe powders producing better results than Alfa Aesar®. The high current value for one aliquot of the Prolabo® Fe powder (980 nA) may have been caused by dirt on the surface of the pressed sample (*pers comm* Southon, J [2011]). Because the Prolabo® Fe powder had been used for several years, the decision was made to continue with this brand even though BDH® produced better currents (*pers comm* Petchey, F [2011]).

For this thesis, the visible qualities of the Fe powders were investigated using a Hitachi Regulus 8230 FEG-SEM Scanning Electron Microscope, housed in The University of Waikato, School of Engineering. Scanning electron microscopy (SEM) images are presented in **Figure 4.1** and **Figure 4.2**. For reference, SEM images by Santos *et al.*, 2007a are also reported.

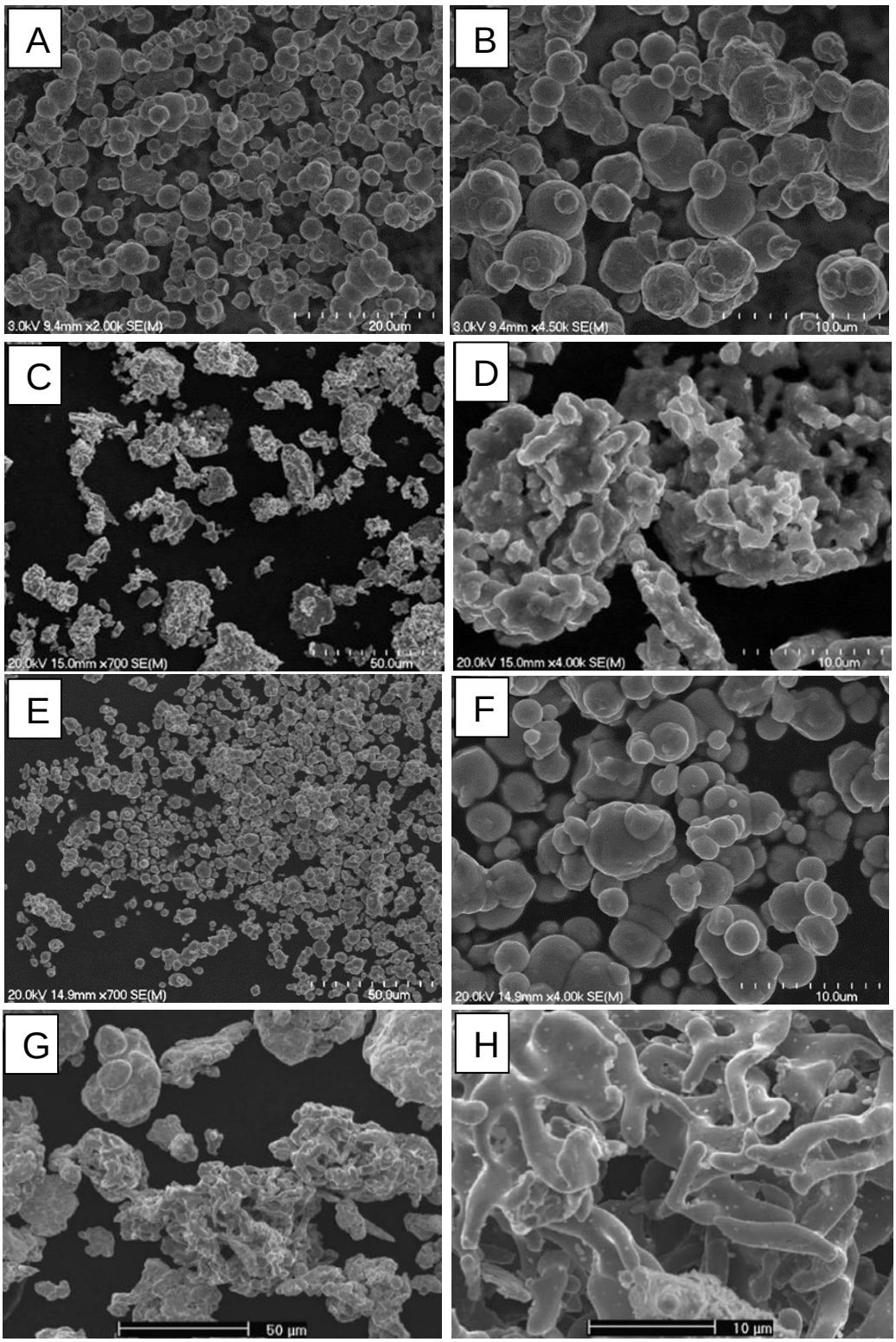

Figure 4.1 SEM pictures of four types of Fe powder. (A) and (B) Prolabo®, 20 µm and 10 µm. (C) and (D) Alfa Aesar®, 50 µm and 10 µm. (E) and (F) BDH®, 50 µm and 10 µm. (G) and (H) Alfa Aesar® -325, 50 µm and 10 µm, reproduced from Santos *et al.* (2007a).

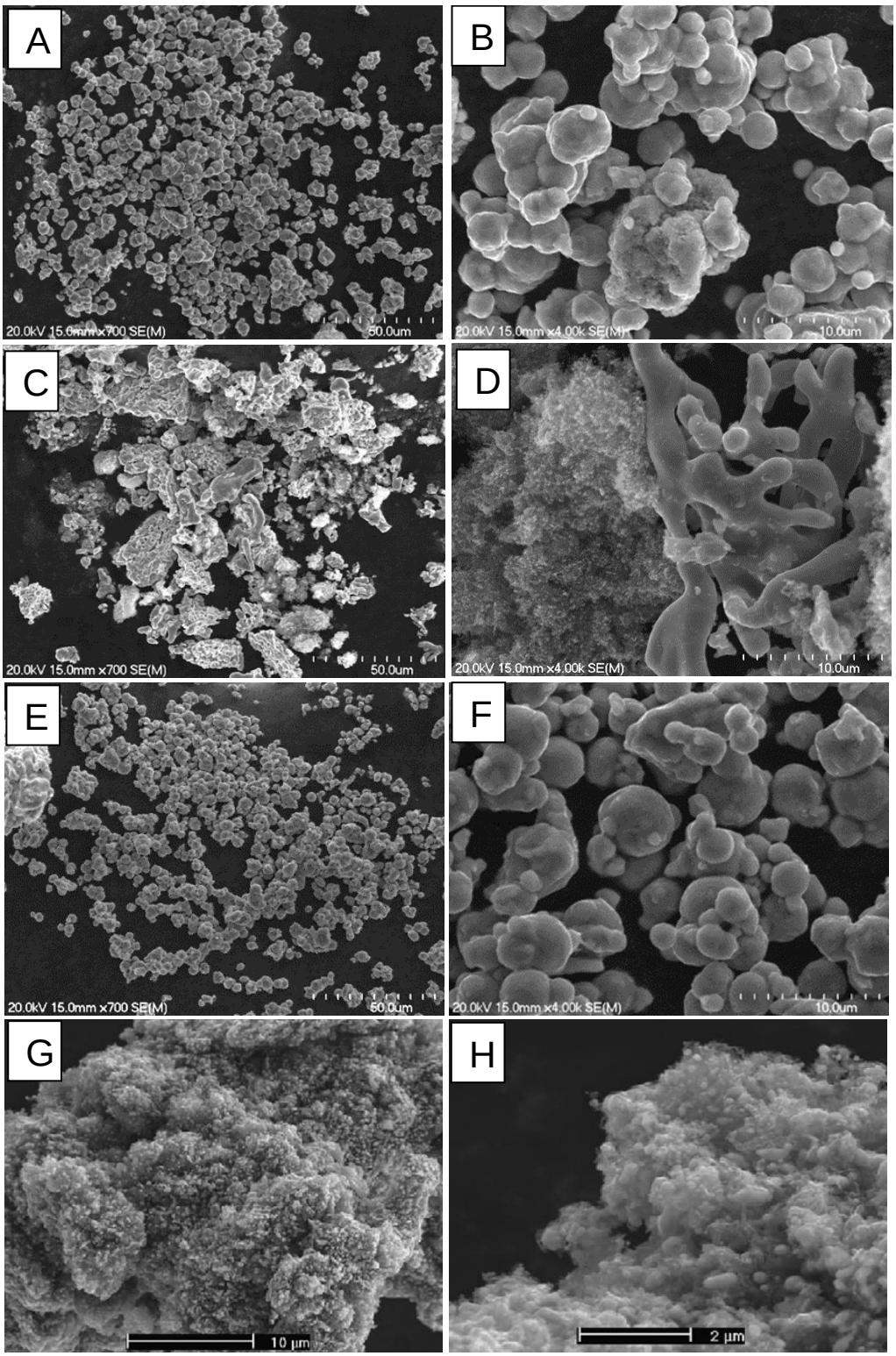

Figure 4.2 SEM pictures of graphitised (H_2 bake-out) alpha-cellulose pre-treated Ancient Wood standard using three different Fe catalysts. (A) and (B) Prolabo®, 20 µm and 10 µm. (C) and (D) Alfa Aesar®, 50 µm and 10 µm. (E) and (F) BDH®, 50 µm and 10 µm. (G) and (H) Alfa Aesar® -325, 50 µm and 10 µm, reproduced from Santos *et al.* (2007a).

4.3.3 Oxygen

The current protocol at the WRDL to remove impurities from Fe powder is to fill the vacuum line with 1000 mb of H_2 and heat the Fe powder at 400˚C for one hour under vacuum. This is termed a H_2 bake-out. Hua *et al.* (2004) reported favourable results, in terms of short graphitisation times and high graphite yield, from the use of a O_2 bake-out before a H_2 bake-out. Specfic parameters for these bake-outs, as outlined by Hua *et al.* (2004), are as follows: 500 mb O_2 at 450˚C for 30 minutes, followed by 750 mb H_2 at 600˚C for one hour. Both bake-outs were run under vacuum. While Hua *et al.* (2004) stated that the O_2 bake-out oxidises the Fe catalyst, and the H_2 bake-out reduces iron oxide back to Fe, the chemistry behind why this method is thought to improve graphitisation time and yield was not mentioned.

Following the protocol outlined by Hua *et al.* (2004), two experiments using O_2 were undertaken. Initially, the Fe powder underwent a 500 mb O_2 bake-out for 30 minutes at 400°C. In a subsequent separate experiment, the quantity of O_2 was increased to 1000 mb. The H_2 bake-out protocol used at the WRDL was kept the same (1000 mb H_2, one hour, 400˚C) for both of these experiments. **Figure 4.3** illustrates the change in pressure observed during the 500 mb O_2 and 1000 mb H_2 bake-out. SEM imaging was carried out on the three Fe powders (Prolabo®, BDH®, and Alfa Aesar®) to assess whether the O_2 bake-out at 500 mb and 1000 mb affected graphite morphology. These images are shown in **Figure 4.4** and **Figure 4.5**.

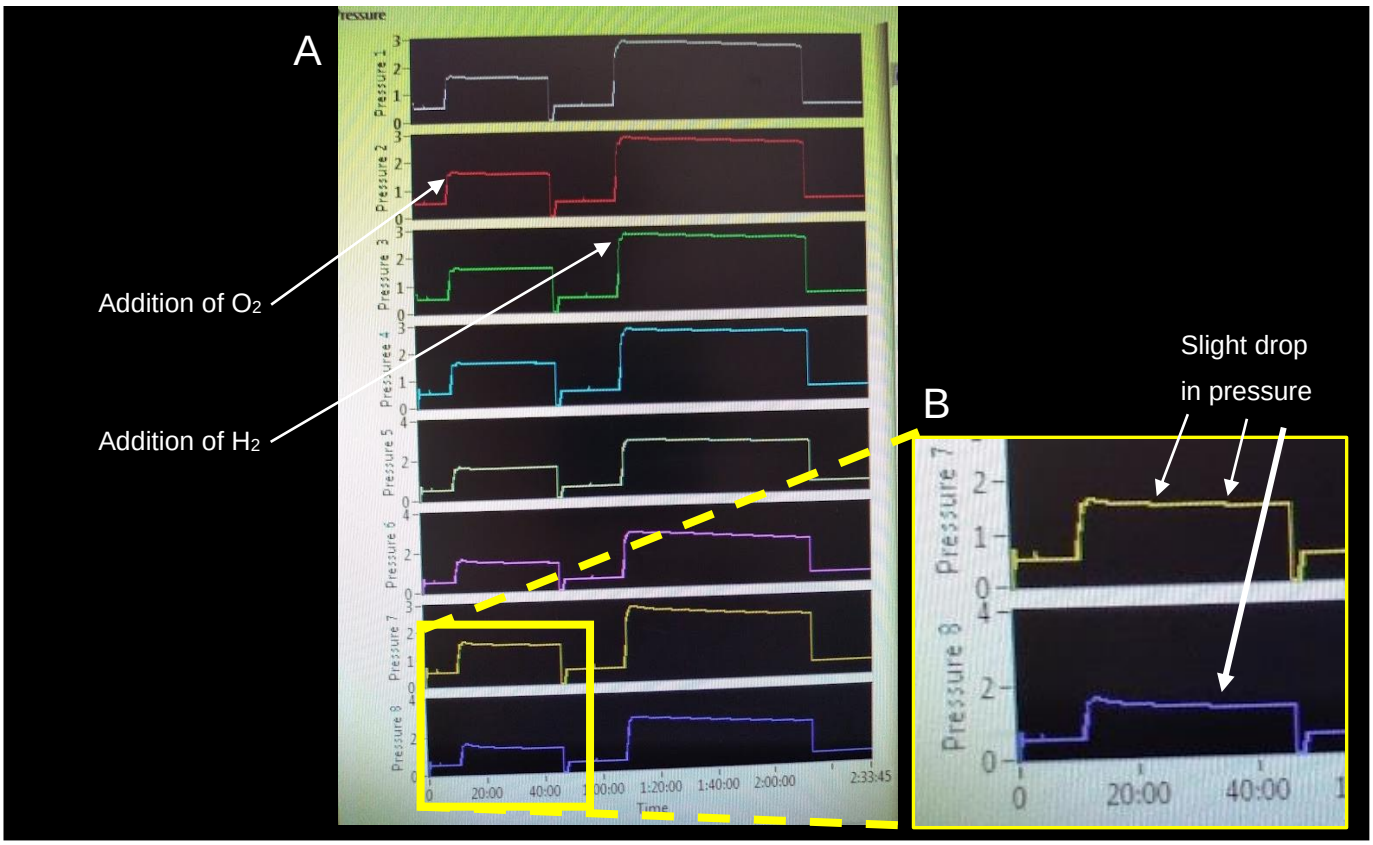

Figure 4.3 (A) LabVIEW™ plot showing the change in pressure during the 500 mb O_2 and 1000 mb H_2 bake-out. (B) Close up of pressure drop during the O_2 bake-out phase.

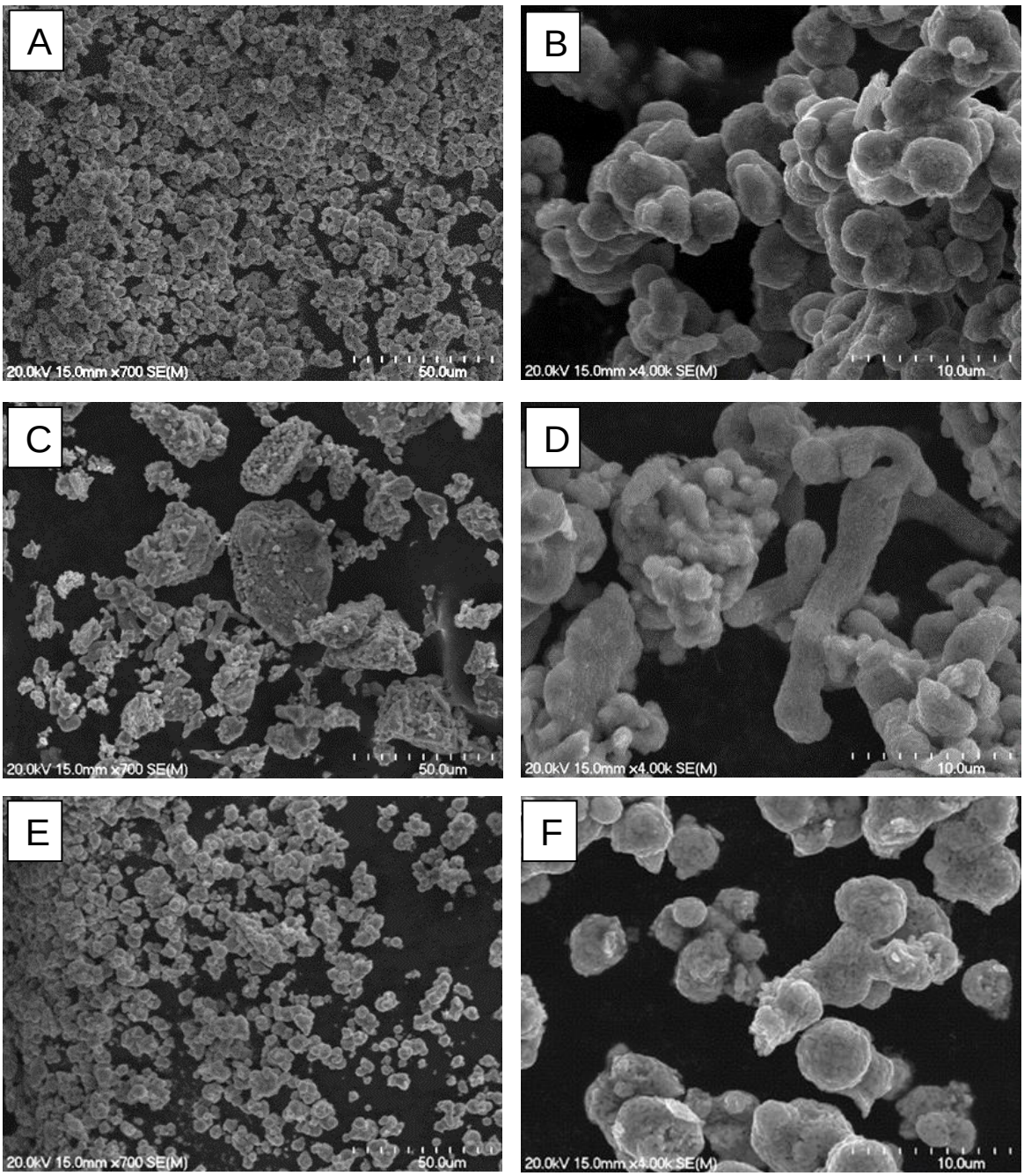

Figure 4.4 SEM pictures of graphite samples produced from an alpha-cellulose pre-treated Ancient Wood standard. Each Fe catalyst underwent a 500 mb O_2 bake-out, followed by a 1000 mb H_2 bake-out. (A) and (B) Prolabo®, 20 µm and 10 µm. (C) and (D) Alfa Aesar®, 50 µm and 10 µm. (E) and (F) BDH®, 50 µm and 10 µm.

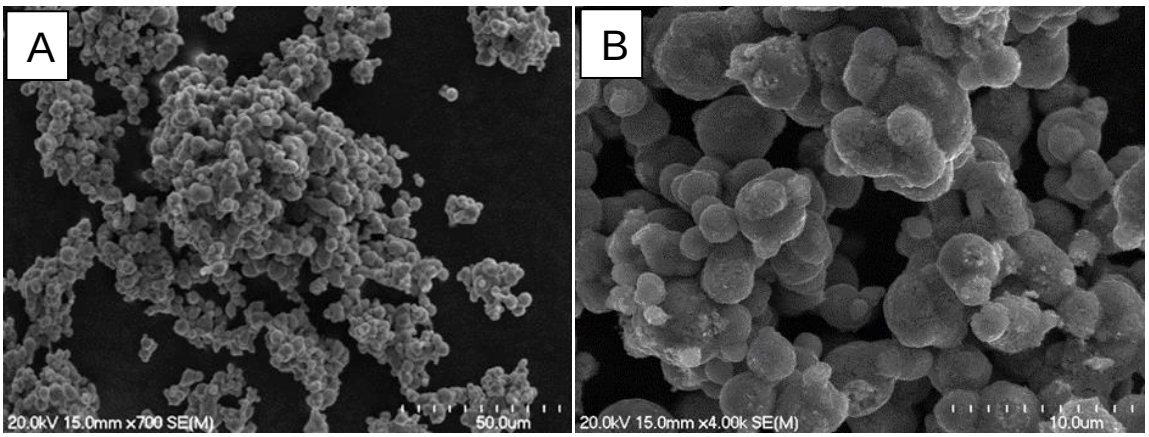

Figure 4.5 SEM pictures of graphite samples produced from an alpha-cellulose pre-treated Ancient Wood standard. The Fe catalysts were baked-out using 1000 mb O_2 and 1000 mb H_2. (A) and (B) Prolabo, 50 µm and 10 µm.

4.3.4 Water Removal

At the WRDL, $Mg(ClO_4)_2$ is used to remove water produced during graphitisation. It is added to a 6 mm x 7 cm quartz tube and replaced after three uses to minimise memory effects and cross-contamination, following the recommendations of Santos *et al.* (2016a). Fedi *et al.* (2020) eliminated $Mg(ClO_4)_2$ as a means of water removal and instead used a silver bar cooled to -25˚C by two small Peltier modules thermally coupled in series. Walter *et al.* (2016) also chose not to use $Mg(ClO_4)_2$, instead using a Pyrex® tube cooled with slush.

Following the experiments of Fedi *et al.* (2020) and Walter *et al.* (2016), $Mg(ClO_4)_2$ was replaced with a 5 mm x 6 cm metal bar with a 2 mm hole drilled down the middle (**Figure 4.6**). The metal bar was immersed in a metal walled thermos flask containing -70°C slush. In keeping with the aim of reducing the volume where possible, as outlined in Chapter 3, the reduced length and small canal also reduced the overall volume of the graphite reactor. Because insufficient water removal can lead to longer graphitisation times and leaks (Smith *et al.*, 2016b) tests were undertaken to compare graphitisation times using a metal bar with slush, and the current method of water removal ($Mg[ClO_4]_2$). Both water removal methods used current Ultra-Torr®-Union-Cross components (“Current UTUC”) and 6mm x 7 cm quartz tubes for Fe powder. The only difference was the use of 6mm x 7cm quartz tubes for $Mg(ClO_4)_2$, and the metal bar with slush.

For this experiment, eight Carrara Marble samples ranging in size (0.5, 0.4, 0.3, 0.2, 0.1, 0.05, 0.03 and 0.02 mgC) were graphitised using $Mg(ClO_4)_2$, and another eight of the same size range were graphitised using the metal bar and slush. A range of sizes were chosen to assess whether sample size would be a factor: 0.4 mgC and 0.5 mgC CO_2 samples are routinely run at the WRDL, and samples below 0.2 mg and 0.05 mgC are classified as small and ultra-small, respectively, and so are representative of the sizes that are of interest for this research.

Initial tests showed extended graphitisation times (Section 4.4.4), and so a further experiment was carried out to assess whether this was caused by the use of the metal bar, due to it being inadequately cooled, or due to the use of slush. The metal bar was replaced in subsequent experiments with a 6 mm x 7 cm quartz tube (as used for $Mg[ClO_4]_2$), thereby allowing the use of the metal bar to be assessed. All other experimental conditions, such as the sample type and size, were kept the same. The three water removal methods were also rerun using the small Ultra-Torr®-Union-Cross components ("small UTUC") (**Figure 3.11**). Results are presented in **Figure 4.7**. In order to obtain additional data, a final experiment where the six different water removal methods were run on the same day was also undertaken (**Figure 4.8**).

Figure 4.6 (A) 6 mm x 7 cm quartz tube used for $Mg(ClO_4)_2$. (B) 5 mm x 6 cm metal bar with a 2 mm hole drilled through the middle.

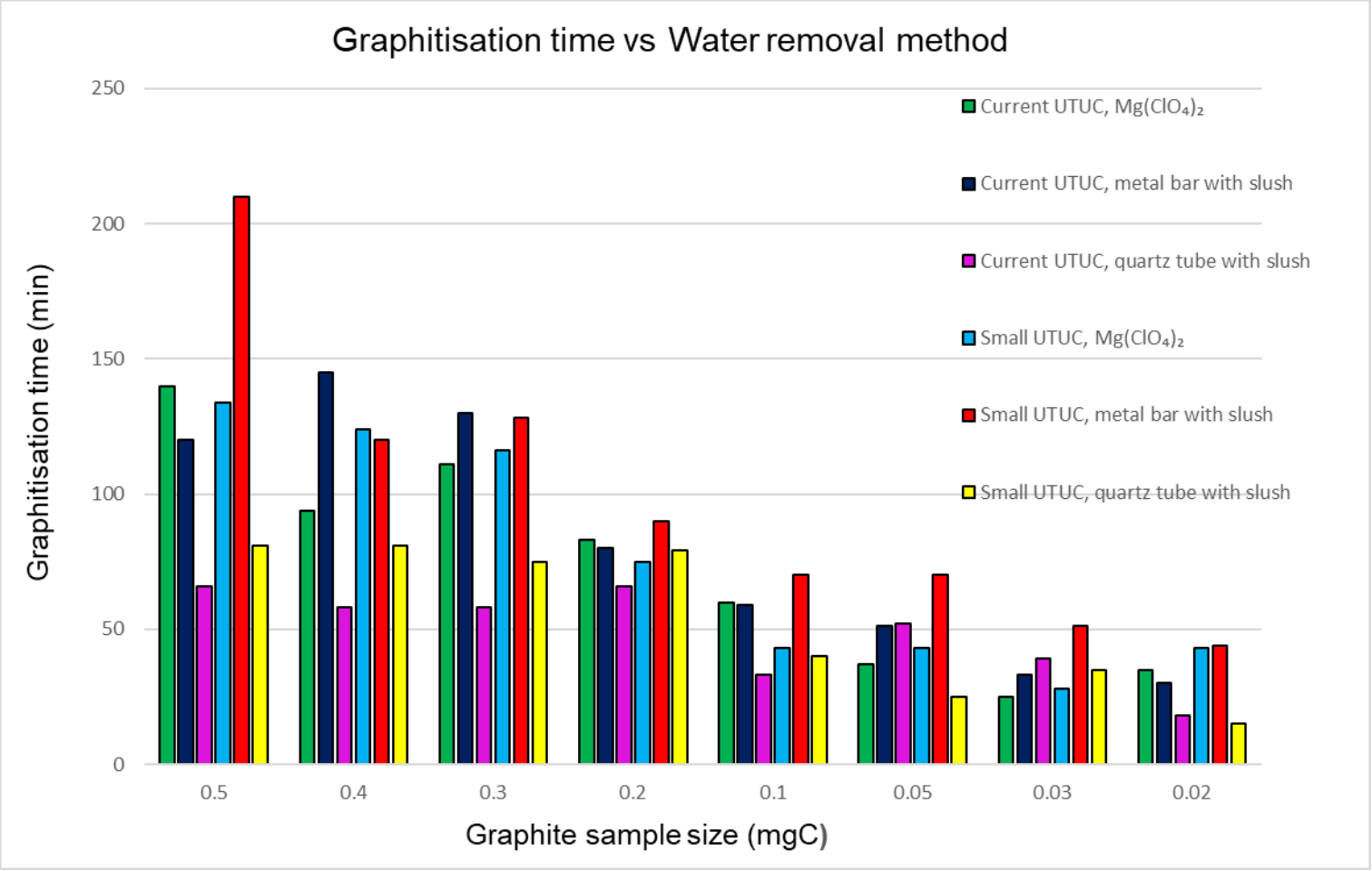

Figure 4.7 Bar graph showing graphitisation times for three water removal methods. $Mg(ClO_4)_2$, a metal bar with slush, and a quartz tube with slush were tested using current and small Ultra-Torr®-Union-Cross (UTUC) components. CO_2 was produced from Carrara Marble.

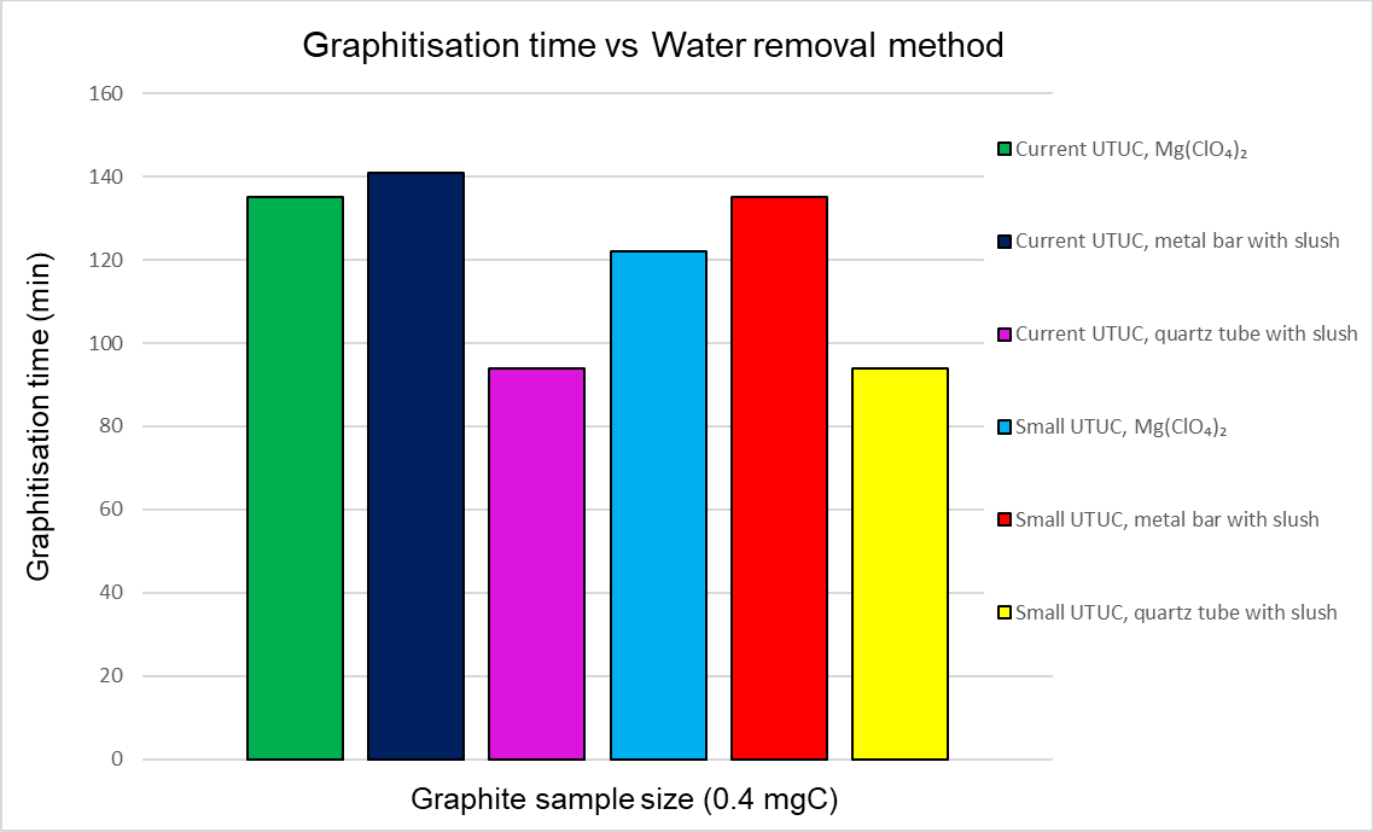

Figure 4.8 Graphitisation times for 0.4 mgC samples. $Mg(ClO_4)_2$, a metal bar with slush, and a quartz tube with slush were tested using current and small Ultra-Torr®-Union-Cross (UTUC) components. CO_2 was produced from Carrara Marble.

4.3.5 Graphite Yield Calculation

Graphite yield refers to the percentage of CO_2 that is graphitised/converted to graphite (carbon). This is calculated using the equation outlined by Hua *et al.* (2001), where initial and final pressure refer to the combined pressure of H_2 and CO_2 at the start and end of graphitisation, and CO_2 refers to the pressure of sample CO_2 in the graphite reactor (before graphitisation). Graphite yield was calculated to assess if different water removal methods, and the volume reduction of the graphite reactors, had any effect on graphite yield. In addition to calculating the graphite yield for the samples using different water removal methods, graphite yield calculations for the eleven standards and the three shell samples that were graphitised using the ultra-small graphite reactor (**Figure 3.20**), as outlined in Chapter 6, were also calculated. **Figure 4.9** illustrates all the calculated graphite yields. Error bars were calculated using the percentage error associated with the pressure transducers (analog microelectronics, accessed 10/5/2022). For the solid red data points, reduced Fe and $Mg(ClO_4)_2$ quartz tubes were used. Every other data point and water removal method used the current Fe powder (Prolabo® Fe) and $Mg(ClO_4)_2$ quartz tubes.

$$Graphite\ yield\ (\%) = \frac{Initial\ pressure - Final\ pressure}{3 \times CO_2} \times 100$$

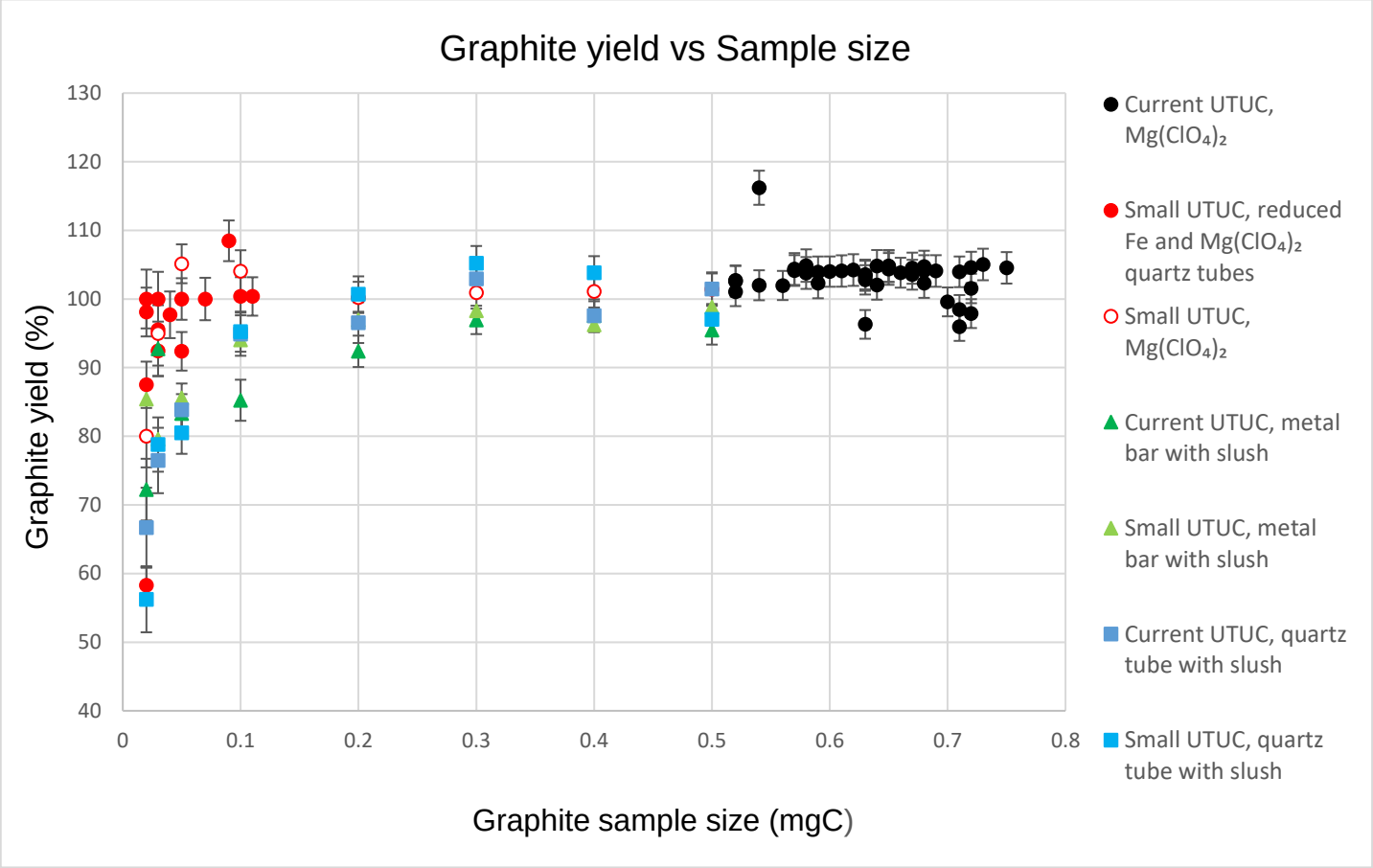

Figure 4.9 Calculated graphite yield for varying methods of water removal during graphitisation.

4.4 Discussion

4.4.1 Sample Weighing and CO_2 Yield

The initial comparison between weight readings (**Table 4.1**) shows that the precision of the 6-decimal point balance is higher than the 4-decimal point balance. While this is not unexpected, the impact of using a more precise balance is higlighted in the subsequent CO_2 yield experiment. The shell sample weight, corresponding CO_2 generated, and the standard deviation values for each of the ten weights for Balance A and B are listed in **Table 4.2** and **Table 4.3**. The CO_2/weight ratio values are not the same for either balance, even though in theory, they should be. However, the standard deviation is much lower for Balance B compared to Balance A; 1.224 compared to 5.331 (**Table 4.3**). This leads to the conclusion that ultra-small samples, including standards, should be weighed on the 6-decimal point balance (Balance B)

as the 4-decimal point balance (Balance A) contributes to errors in the weight measurements.

4.4.2 Fe Catalyst

SEM images of the three Fe powders, before and after graphitisation, are shown in **Figure 4.1** and **Figure 4.2**. Each figure contains the three Fe catalysts examined in this thesis as well as an example of “fluffy” Fe powder (Alfa Aesar® -325), produced from Santos *et al.* (2007a) at UCI. Because this Fe powder is the same type tested at the WRDL (Alfa Aesar®), it has been designated as Alfa Aesar®UCI, whereas the Alfa Aesar® Fe powder analysed for this thesis has been designated as Alfa Aesar®WRDL.

Figure 4.1 shows the morphology of the two Alfa Aesar® Fe powders is quite different from Prolabo® and BDH® Fe powders, as they are rounded and ball-shaped while the Alfa Aesar® Fe powders are clumped with irregular shapes. **Figure 4.2** shows that after a H_2 bake-out/graphitisation, Prolabo®, BDH®, and Alfa Aesar®UCI are homogenous, where Prolabo® and BDH® retain their round ball-shaped morphology and Alfa Aesar®UCI is quite “fluffy”. In contrast, Alfa Aesar®WRDL is heterogenous after graphitisation. One interesting observation is that the Alfa Aesar®UCI Fe powder is quite different before and after graphtisation. Before graphitisation (**Figure 4.1**), it is smooth but after graphitisation (**Figure 4.2**), it has a “fluffy” appearance. In contrast, the morphologies of the other three Fe powders do not appear to be that different before and after graphitisation.

The observation of different Fe powder morphologies is to be expected, as this has been reported by other researchers (Santos *et al.*, 2007a, Smith *et al.*, 2010). SEM imaging can be used to explain why observations in other experiments occur, *e.g.*, greater surface area of Fe powder contributes to faster graphitisation times (Hua *et al.*, 2004). Because no experiments were undertaken to observe if graphitisation speed or ^{14}C measurements differed between the use of different Fe powders, a conclusion as to how the morphologies of the assessed Fe powders affect these parameters is unable to be reached.

4.4.3 Oxygen

Figure 4.3 shows the pressure reading for eight graphite reactors over time during a 500 mb O_2 and 1000 mb H_2 bake-out. It is evident that a slight drop in pressure

occured during the O_2 bake-out phase, indicating that oxygen is being consumed during the formation of iron oxide. Pressure readings were not reported by Hua *et al.* (2004) during their experimentation with oxygen.

SEM images of each Fe powder following a O_2 and H_2 bake-out are illustrated in **Figure 4.4** (500 mb) and **Figure 4.5** (1000 mb O_2). While there are no significant differences between SEM images for the H_2 bake-out (**Figure 4.2**) and O_2/H_2 bake-out (**Figure 4.4**), the morphology of each Fe catalyst when the O_2 bake-out is implemented appears to be slightly fluffy. This observation is more pronounced in the graphite produced from Prolabo® and BDH® Fe powders. This slight change in morphology somewhat reflects the findings of Hua *et al.* (2004), who report that the O_2 bake-out resulted in a sponge-like appearance with significantly increased surface area (**Figure 2.18**), compared to catalysts treated without the O_2 bake-out. Hua *et al.* (2004) hypothesised that increased surface area was the reason for the faster reaction rate. A significant difference with regards to graphite morphology between the use of a H_2 bake-out and O_2/H_2 bake-out was not observed in this thesis. Differences in the type of Fe catalyst used and reaction temperature are possible reasons, especially with regards to the type of catalyst used (the brand was not stated by Hua *et al.*, 2004). As evident from **Figure 4.1**, before the Fe catalyst is baked out, untreated catalysts display quite different morphologies, and so this could affect how each catalyst responds to a O_2 bake-out.

Increasing the O_2 pressure from 500 mb to 1000 mb (**Figure 4.5**) didn't appear to have any significant effect on the morphology of the Prolabo® Fe powder compared to using 500 mb O_2.

Because of temporary lab closures during parts of 2020 and 2021 in response to Covid-19 restrictions, further experimentation to assess the effect that an O_2 bake-out has on graphitisation time was unable to be assessed. As mentioned earlier, Hua *et al.* (2004) reported shorter graphitisation times and increased graphite yield when an O_2 bake-out was implemented, and so further experimentation is recommended on the influence that a O_2 bake-out has on graphitisation time at the WRDL.

4.4.4 Water Removal

Using the current Ultra-Torr®-Union-Cross, the initial experiment comparing the use of $Mg(ClO_4)_2$ to the metal bar with slush showed that for five of the eight samples, the graphitisation time took longer when the metal bar and slush were used. This is especially prominent for 0.4 mgC samples, where the metal bar resulted in an additional 51 minutes for graphitisation to be completed. In contrast, the graphitisation times were halved when the metal bar was replaced with a quartz tube, except for 0.05 mgC and 0.03 mgC samples, which took either the same time or slightly longer compared to the metal bar with slush. Graphitisation times using the small Ultra-Torr®-Union-Cross are similar to using the current Ultra-Torr®-Union-Cross.

These results suggest that the method of water removal has an impact on graphitisation time. The observed graphitisation time, from longest to shortest is as follows; metal bar with slush, quartz tube with $Mg(ClO_4)_2$, quartz tube with slush. Reasons why the metal bar results in slower graphitisation times is unclear at this stage. It is possible that the metal bar did not reach the appropriate temperature for efficient water removal, or perhaps the 2 mm hole was too small, leading to water blocking the tube. The observed faster graphitisation times using a quartz tube with slush are significant and therefore, further investigation of this is recommended as faster graphitisation times reduce the likelihood of contamination (Smith *et al.*, 2016b).

It was noted that the use of slush required a higher amount of operator input compared to the use of $Mg(ClO_4)_2$. This was due to the time required to arrange the slush-filled thermoses for the quartz tube. Moreover, only four samples could be graphitised at a time when using slush-filled thermoses, as the size of the thermoses meant there was limited space. To solve this issue, the use of smaller thermoses is recommended.

Because of temporary lab closures during parts of 2020 and 2021 in response to Covid-19 restrictions, further experimentation using different methods of water removal and their potential impact on radiocarbon dates was suspended. However, this area of investigation is highly recommended for future work and is necessary to assess the effects of longer or shorter graphitisation times on radiocarbon results.

4.4.5 Graphite Yield

Figure 4.9 illustrates that regardless of the water removal method, or the use of current or small Ultra-Torr®-Union-Cross components, graphite yield starts to progressively drop for samples ≤0.10 mgC, an observation that is also reported by Delqué-Koli Caffy *et al.* (2013). Limited data however means it is not possible to attribute any statistical significance to the results, and a larger dataset is therefore required to properly assess how graphite yield is affected by the method of water removal. Moreover, not all the water removal methods cover the range of sample sizes that were tested, *e.g.*, data points for the use of current Ultra-Torr®-Union-Cross with $Mg(ClO_4)_2$ are only reported for samples above 0.5 mgC. To directly compare how different water removal methods, and graphite reactor volume, impacts graphite yield, each variable needs to be tested on similar size samples.

An interesting observation was that most samples above 0.5 mgC were calculated to have graphite yields over 100%, which suggests either the pressure transducers are measuring some pressure readings inaccurately, or there is methane (CH_4) present in the residual pressure. Yang, Smith, & Hua (2013) reported that the latter could contribute to an over-estimation in conversion efficiency calculations.

There is insufficient data to establish a statistical relationship between graphite yield and the reliability of radiocarbon measurements. This relationship is recommended for future research as Walter *et al.* (2016) noted that incomplete graphitisation, as indicated by a low graphite yield, can lead to incorrect blank corrections with the smallest samples being affected the most.

4.5 Summary

The results from the sample weighing and CO_2 yield experiments revealed that the 4-decimal point balance is not suitable for weighing ultra-small samples, due to poor precision as shown from the obtained CO_2 yield results. Therefore, ultra-small samples should only be weighed on a 6-decimal point balance.

The reported results of current and inherent carbon content of Prolabo® and BDH® and Alfa Aesar® Fe powders, from experiments in 2009 and 2011 highlight how different Fe powders possess different qualities. To assess the visible qualities of each Fe powder, SEM imaging was undertaken. The impact of an additional pre-

cleaning step for each Fe powder (O_2 bake-out) was assessed via SEM imaging. SEM images showed that different brands of Fe powder can have markedly different morphologies, as both Alfa Aesar® Fe powders had distinctively different morphologies compared to Prolabo® and BDH®. While Hua *et al.* (2004) noted differences in morphology when a O_2 bake-out was implemented, this was not observed in this thesis except for a slightly "fluffy" appearance. The pressure readings for the 500 mb O_2 / 1000 mb H_2 bake-out showed a slight drop in pressure during the O_2 bake-out phase, indicating oxygen was being consumed during the formation of iron oxide.

The water removal experiments showed how different methods can have a significant impact on graphitisation time. It was observed that a quartz tube with slush significantly reduced graphitisation time compared to using a metal bar with slush. While radiocarbon measurements were unable to be carried out using the different water removal methods, this is recommended for further investigation. A higher amount of operator input is required when using slush, and therefore, this would need to be remedied if it were to be implemented.

The pressure values from the various water removal methods were used to calculate graphite yield, with results showing that regardless of the method, graphite yield progressively decreased for samples ≤0.10 mgC. This observation, however, is based on limited data and therefore, a bigger data set is required to enable any statistically significant conclusion.

Chapter 5
Standard Radiocarbon Results using the Ultra-Small Vacuum Line

5.1 Introduction

This chapter outlines radiocarbon results for three standards using the ultra-small vacuum line, as outlined in Chapter 3. Radiocarbon results for the *Gafrarium* sp. shellfish, which were run alongside the standards, are presented in Chapter 6.

5.2 Experiment Methodology

The ultra-small vacuum line was used to process eleven standards of varying sizes; four Carrara Marble (one 0.1 mgC, three <0.03 mgC), four Tridacna (one 0.1 mgC, three <0.03 mgC) and three Oxalic Acid II (three <0.03 mgC).

The vials that are used for shell samples exceeded the weight of the 6-decimal point balance (Sartorius Ultra Micro Balance MSE6.6S – 000 – DM). Instead, shell samples were weighed onto a piece of pre-weighed tinfoil and then transferred to a glass vial before being opened to a vacuum. Following this, CO_2 was evolved under vacuum with orthophosphoric acid. From a previously combusted tube, Oxalic Acid II was split on the current vacuum line system and then transferred to the ultra-small vacuum line.

To recap, the age of each standard is as follows:

- Oxalic Acid II: 1.3407 $\pm$ 0.0019 $F^{14}C$ (international consensus value) (Stenström *et al.*, 2011).
- Carrara Marble: >50,000 years (based on the mean age for ten duplicates)
- Tridacna: 3028 $\pm$ 16 ^{14}C years (based on the mean age for ten duplicates)

All radiocarbon results were prepared using the ultra-small vacuum line, which consisted of the ultra-small measuring manifold (**Figure 3.12**) and ultra-small graphite reactors (**Figure 3.20**).

5.3 Shell Standard Results

Figure 5.1, **Figure 5.2**, and **Figure 5.3** illustrate ^{14}C measurements obtained for Oxalic Acid II, Tridacna, and Carrara Marble. The use of the ultra-small vacuum line is represented by green diamond data points, and oxygen bake-out tests are indicated by yellow and red square data points. Black circular data points represent samples processed using the current vacuum line at the WRDL.

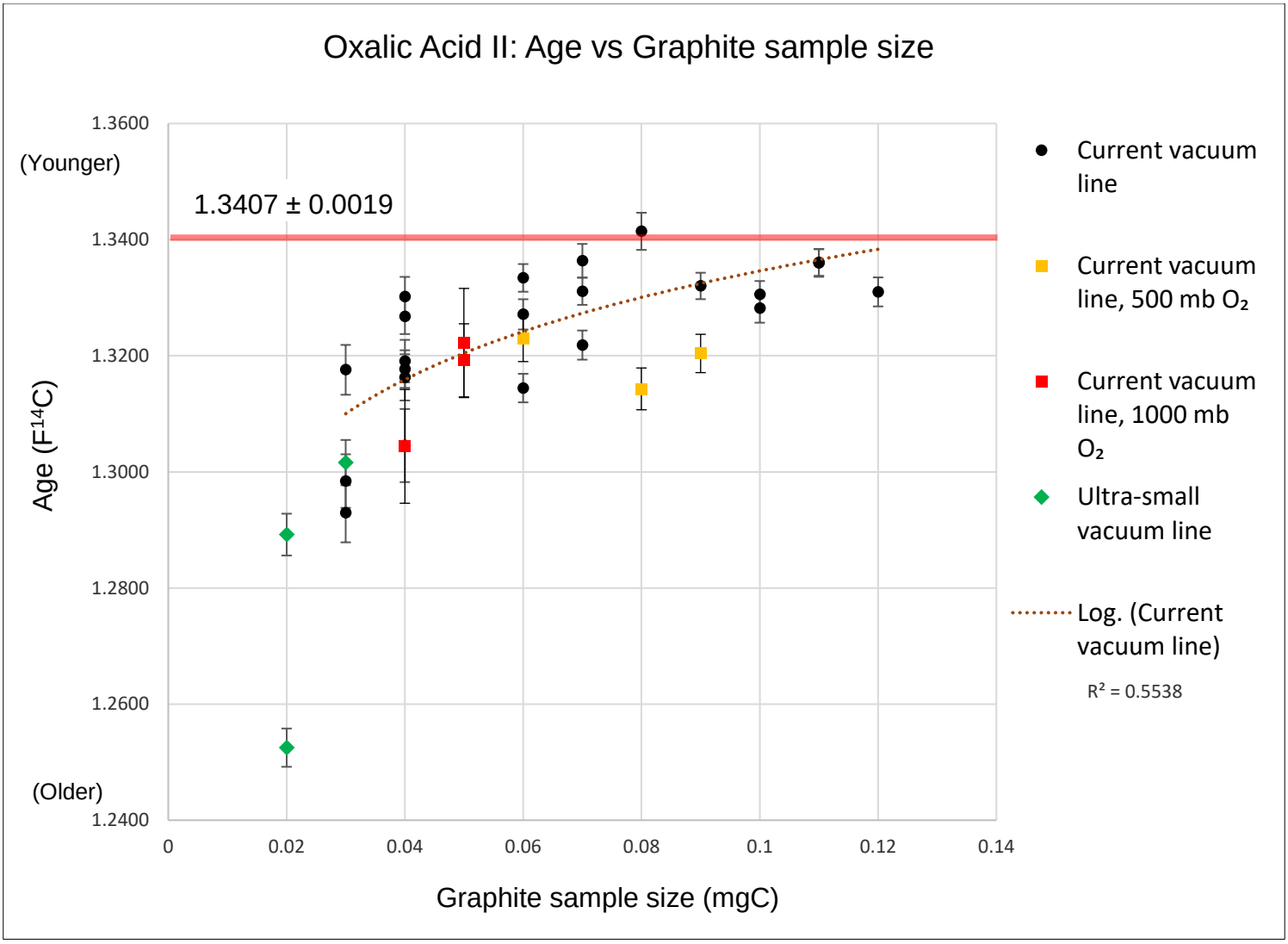

Figure 5.1 $F^{14}C$ results for Oxalic Acid II. The horizonal red bar represents the international consensus value for this standard. The yellow, red, and green data points represent different experimental processes undertaken for this thesis. Black data points represent samples processed using current operating procedures at the WRDL.

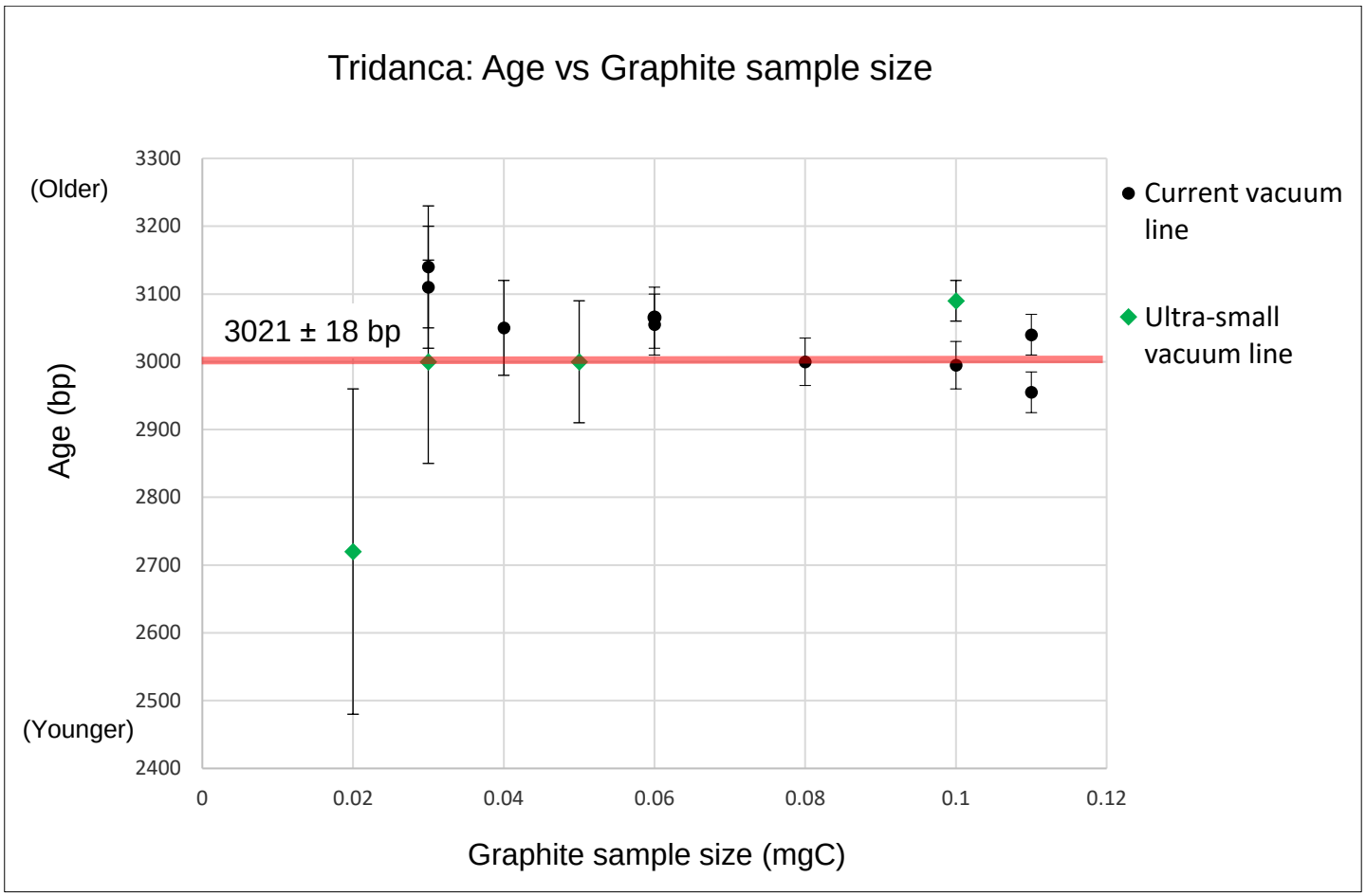

Figure 5.2 ^{14}C results for Tridacna, expressed as age bp. The horizonal red bar represents the consensus value for this standard. The green data points represent the use of the ultra-small vacuum line to process CO_2 from Tridacna for this thesis. Black data points represent samples processed using current operating procedures at the WRDL.

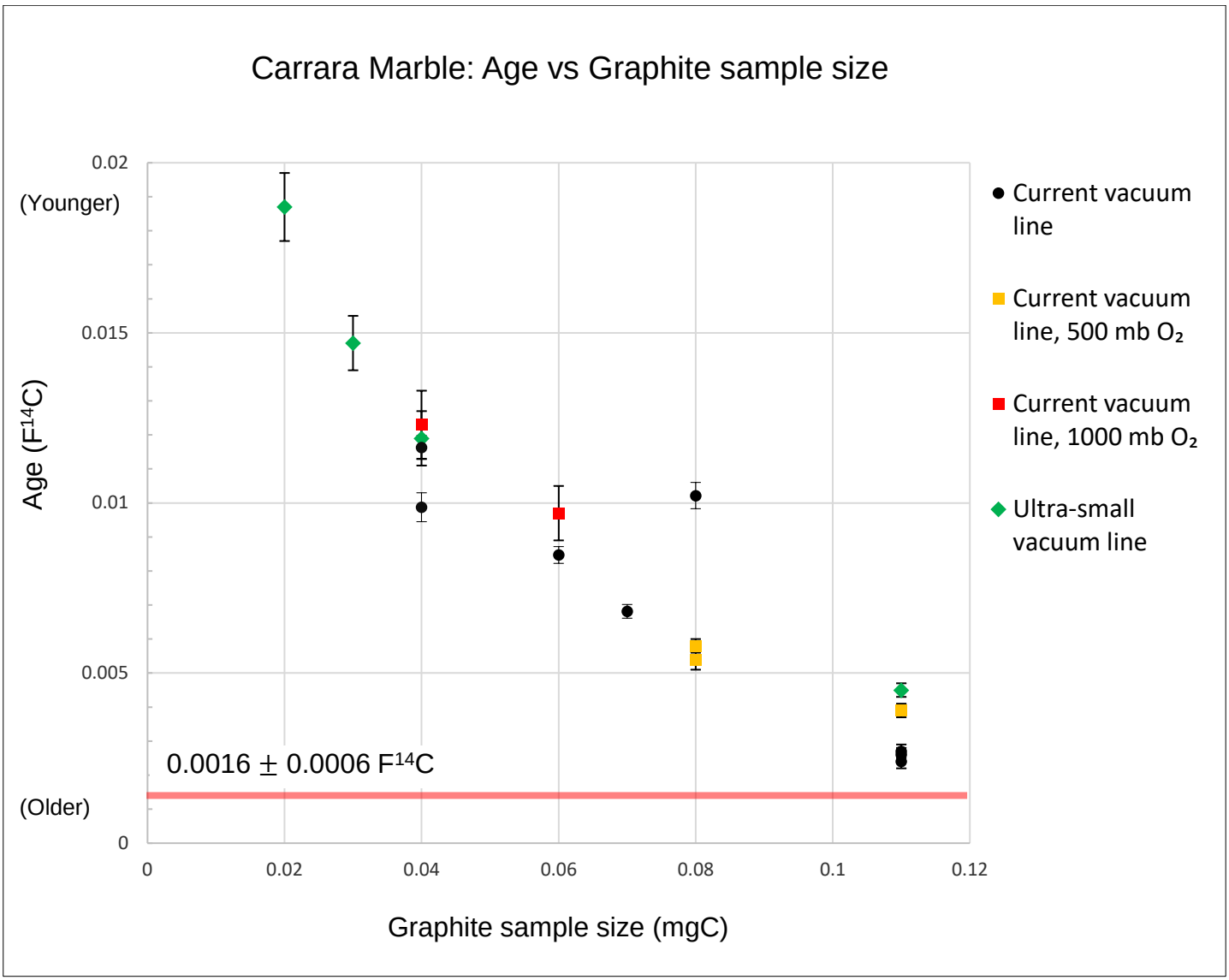

Figure 5.3 $F^{14}C$ results for Carrara Marble. The horizonal red bar represents the consensus value for this standard. The yellow, red, and green data points represent different experimental processes undertaken for this thesis. Black symbols represent samples processed using current operating procedures at the WRDL.

5.4 Discussion

Several conclusions can be drawn from **Figure 5.1**, **Figure 5.2**, and **Figure 5.3**.

Figure 5.1 illustrates that Oxalic Acid II is affected by dead carbon contamination for samples <0.10 mgC, *i.e.*, as the sample size decreases, the apparent age becomes progressively older.

Figure 5.2 shows that for Tridacna, the majority of the data points for samples >0.03 mgC agree with the consensus value. At 0.02 mgC, however, the radiocarbon date is

younger by ~300 years compared to the consensus value, indicating modern carbon contamination. The error associated with each radiocarbon date is larger for samples <0.05 mgC, especially for 0.02 mgC. This reflects the radiocarbon result for Wk 45920-2, a 0.03 mgC sample with an error of 169 ^{14}C years (Section 6.2.1). **Figure 5.2** illustrates that for samples that are approximately 3000 years old, a sample size of ≥0.03mgC is required to obtain a reliable radiocarbon date. In scenarios where a simple determination of "young" or "old" is required (*i.e.,* 3000 or 30,000 years), sample sizes of <0.03 mgC are sufficient. Because the radiocarbon ages from the *Gafrarium* sp. shell, presented in Chapter 6, are ~200 years apart (Section 6.2.1), a large error will result in statistically indistinguishable results.

Figure 5.3 shows Carrara Marble is affected by modern carbon contamination for samples <0.10 mgC, and the error associated with each radiocarbon date is larger for samples <0.06 mgC. **Figure 5.2** and **Figure 5.3** illustrate that Carrara Marble is affected by modern contamination to a greater extent than Tridacna. Tridacna is impacted by modern carbon contamination at 0.02 mgC whereas Carrara Marble is impacted at 0.10 mgC. Based on these results, ancient samples, *i.e*., > 50,000 years, should only be radiocarbon dated if samples are >0.10 mgC.

The trend observed for the modern age Oxalic Acid II standard and ^{14}C depleted Carrara Marble standard, of increasing contamination as sample size decreases, reflects the results of Walter *et al.*, 2016 (NOSAMS Facility), who reported that a consistent amount of "process" blank was identified for both modern and ^{14}C depleted samples.

While the volume modifications and implementation of an oxygen bake-out do not appear to have resulted in any significant improvements, insufficient data means it is difficult to make a definitive conclusion and therefore, it is recommended that a bigger data set be collected for future work.

5.5 Summary

Radiocarbon results showed that at 0.10 mgC, Oxalic Acid II was affected by dead carbon contamination, whereas Carrara Marble was affected by modern carbon contamination. Based on the Carrara Marble results, a sample size ≥0.10 mgC is required for radiocarbon dating ancient samples (*i.e.,* >50,000 years). Radiocarbon

results from Tridacna showed that it was impacted by modern carbon contamination at 0.03 mgC, and for samples 0.05 mgC or below, the error associated with the radiocarbon date was larger than for samples >0.05 mgC. This large error reflects the error observed for Wk 45920-2, a 0.03 mgC sample with an error of 169 ^{14}C years. Based on these results, a sample size ≥0.03 mgC is required for radiocarbon dating samples that are approximately 3000 years old.

While the results from the standards showed no significant improvements between the current protocols that are used at the WRDL, and the volume and chemical modifications implemented in this thesis, a lack of data means it is difficult to say that the modifications have no impact and therefore, a bigger data set is needed to make a definitive conclusion.

Chapter 6
Radiocarbon Results for a Subsampled *Gafrarium* sp. Shellfish using the Ultra-Small Vacuum Line

6.1 Introduction

This chapter outlines the hypothesis put forward by Petchey *et al.* (2018) for using ^{13}C to identify shell growth bands impacted by hard water; sampling methods used for ^{14}C measurements of a *Gafrarium* sp. shellfish from the Mariana Islands; and the radiocarbon results from the subsampled *Gafrarium* sp. shellfish using the ultra-small vacuum line as outlined in Chapter 3.

6.2 Hypothesis

The hypothesis put forward by Petchey *et al.* (2018) differentiated estuarine and marine shells based on ^{13}C. However, because some shell taxa have a tolerance for marine and estuarine environments, a mix of estuarine and marine $\delta^{13}C$ signals poses a problem for obtaining reliable radiocarbon dates unless a shell growth band deposited during periods of growth in a marine environment can be sampled and identified. This necessitates the ability to measure ^{14}C of individual growth bands, which in turn necessitates the ability to date very small samples of shell material.

6.2.1 Previous Research

Figure 6.1, **Figure 6.2** and **Figure 6.3** illustrate the basis behind the hypothesis put forward by Petchey *et al.* (2018). **Figure 6.1** and **Figure 6.2** represent two *Tegillarca granosa*[2] shellfish from the same archaeological context, but with radiocarbon dates that are ~250 years apart (data supplied by Petchey). **Figure 6.1** represents the *Tegillarca granosa* shellfish with the younger radiocarbon date, where the majority of the ^{13}C data points (green circles) fall within the average ocean ^{13}C signal for the Mariana Islands. In

[2]This research uses *Tegillarca granosa* shellfish. *Tegillarca granosa* are filter-feeding bivalves that are highly adaptive as they occupy different niches, from fully marine to estuarine environments (Petchey *et al.*, 2017, Broom, 1985).

contrast, all associated ^{13}C values for the older *Tegillarca granosa* shellfish (**Figure 6.2**) fall well below the average ocean ^{13}C signal, indicating this shellfish lived in an estuarine environment and may have been affected by hard water. As discussed in Chapter 1, the hard water effect results in old ^{14}C being introduced into the shell, which in this scenario may explain the observed ~250-year difference.

Figure 6.3 illustrates a *Gafrarium* sp.[3] shellfish from the same context. Eleven points were subsampled for ^{13}C analysis by Petchey, where sample point #1 (first green data point on the left) correlates as being closest to the ventral margin (**Figure 6.4**). $\delta^{13}C$ values sit within and just below the average ocean ^{13}C signal, reflecting a tolerance for changing water conditions. The areas encompassing two of the eleven $\delta^{13}C$ points (#1 and #3) were radiocarbon dated using the current vacuum line at the Waikato Radiocarbon Dating Laboratory (WRDL). Radiocarbon results from these two sampling points support the hypothesis of Petchey *et al.* (2018) as the older date (3520 ± 60 bp) had a $\delta^{13}C$ lower than 1.3‰ ($\delta^{13}C$ = 0.2‰) indicating an estuarine environment. The younger date (3382 ± 169 bp) however, had a $\delta^{13}C$ value within the average ocean range ($\delta^{13}C$ = 1.5‰), indicating a marine environment. These radiocarbon dates were obtained on samples of different sizes, 0.10 mgC for sample point #1 (3520 ± 60 bp) and 0.03 mgC for sample point #3 (3382 ± 169 bp). While these results support the hypothesis put forward by Petchey *et al.* (2018), there was uncertainty surrounding the reliability of the results due to their small size.

[3]This research uses *Gafrarium* sp. shellfish. *Gafrarium* sp. are estuarine filter-feeding shellfish that prefer inner-lagoon habitats (Petchey *et al.*, 2017).

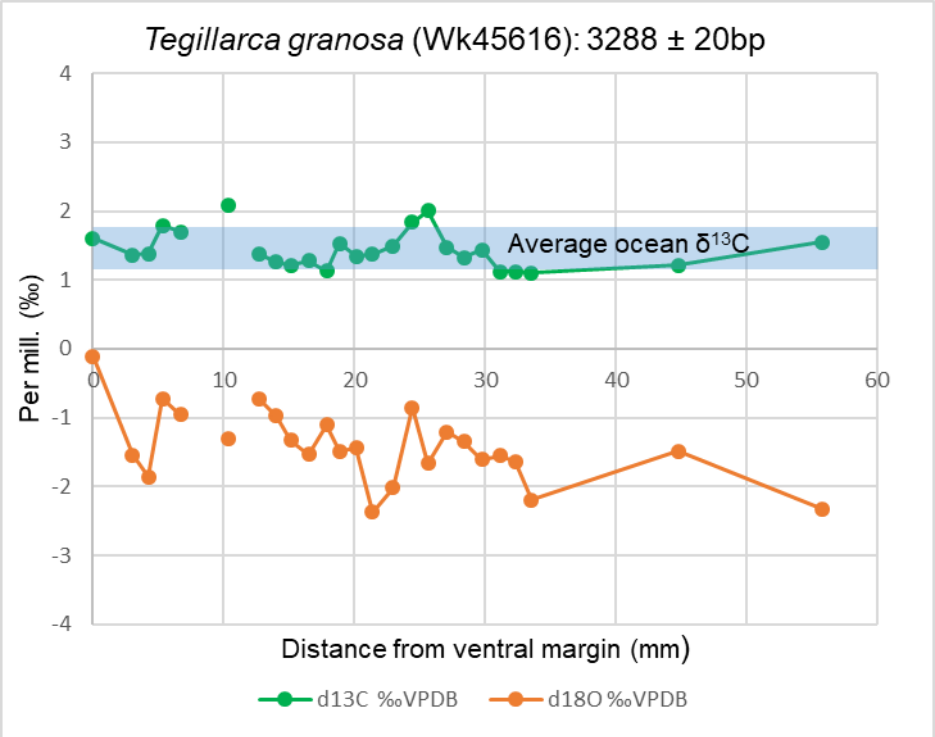

Figure 6.1 $\delta^{13}C$ and $\delta^{18}O$ values for a *Tegillarca granosa* shell indicative of a marine environment. The average overage $\delta^{13}C$ signal is represented by the light blue horizontal bar (Tagliabue & Bopp, 2008). Figure supplied by Petchey.

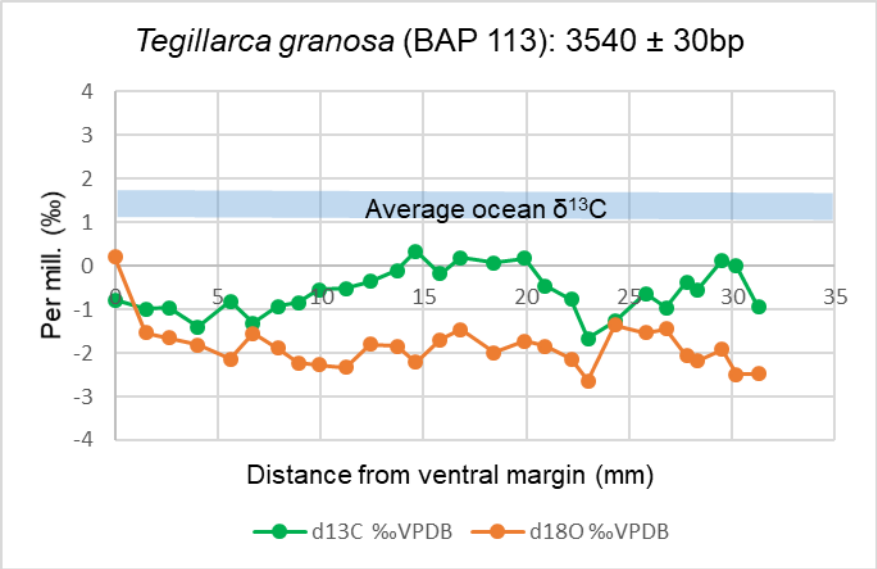

Figure 6.2 $\delta^{13}C$ and $\delta^{18}O$ values for a *Tegillarca granosa* shell indicative of an estuarine environment. The average overage $\delta^{13}C$ value is represented by the light blue horizontal bar (Tagliabue & Bopp, 2008). Figure supplied by Petchey.

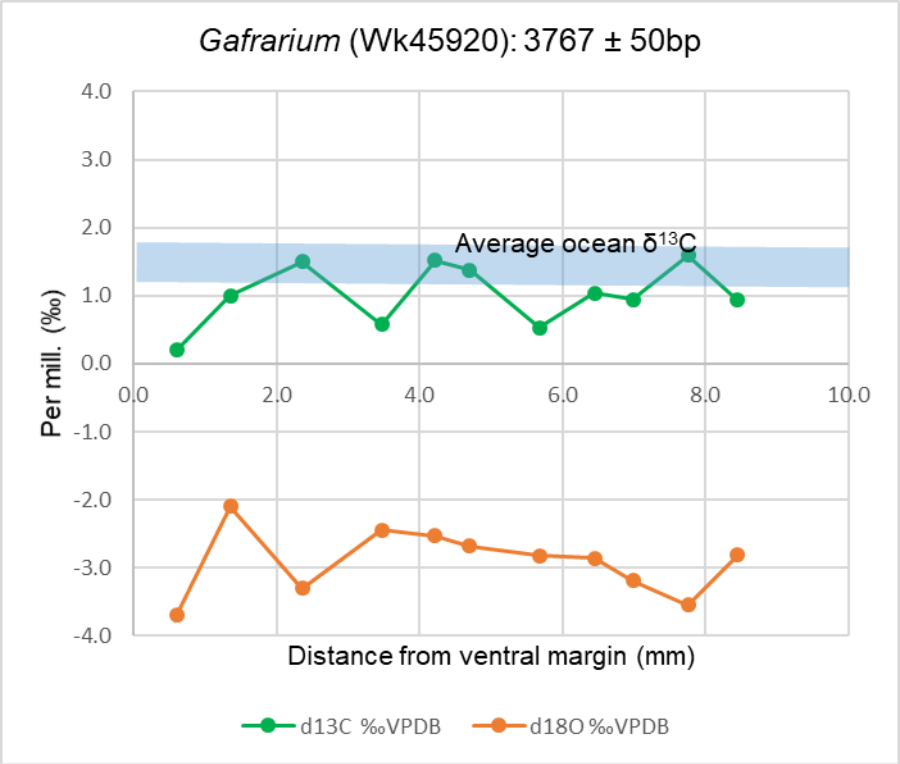

Figure 6.3 $\delta^{13}C$ and $\delta^{18}O$ data points vs distance from the ventral margin for a *Gafrarium* sp. shellfish. The average overage $\delta^{13}C$ value is represented by the light blue horizontal bar (Tagliabue & Bopp, 2008). Figure supplied by Petchey.

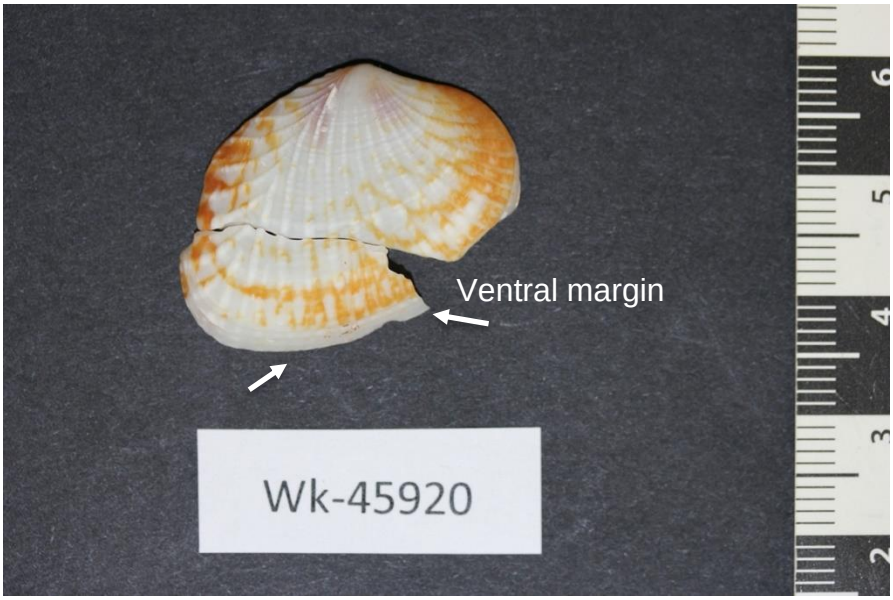

Figure 6.4 *Gafrarium* sp. shell showing the ventral margin. Photo supplied by Petchey.

6.3 Experimental Methodology

Obtaining a radiocarbon sample from the same area where subsampling for ^{13}C has occurred is not straightforward because a lot more sample is required. To sample growth bands and reliably identify marine and estuarine signals, decreasing the minimum sample size for radiocarbon analysis is vital.

All radiocarbon results were prepared using the ultra-small vacuum line, which consisted of the ultra-small measuring manifold (**Figure 3.12**) and ultra-small graphite reactors (**Figure 3.20**).

6.3.1 Subsampling for ^{14}C Measurement

The subsampling of the *Gafrarium* sp. shell (**Figure 6.3**) was challenging. As discussed in Chapter 1, the aim was to radiocarbon date individual shell growth bands to establish a relationship between ^{13}C, ^{14}C, and hard water exposure. Therefore, obtaining the correct amount of sample for radiocarbon analysis was critical. If the sample size is too big, there is a risk that more than one growth band will be subsampled. If too small, the precision of the date would be low, and it would not be possible to confirm the hypothesis as statistically significant.

A Dremel drill (model 8200) with a 0.5 mm Dremel bit (tungsten carbide round ball bur) was used to drill into the surface of the shell following the growth band. Subsampling was restricted to the surface due to shells being composed of two main layers: an outer and inner layer (**Figure 6.5**). Because growth bands are deposited differently for each layer, only the outer layer could be subsampled (Scientific American, 2006). Locations of ^{13}C and ^{14}C sampling have been indicated in **Figure 6.6**. Initially, the sample was loaded into glass vials for shell radiocarbon analysis. However, this proved problematic because the vials exceeded the maximum weight capacity of the 6-decimal point balance (Sartorius Ultra Micro Balance MSE6.6S – 000 – DM). Instead, shell samples were weighed onto a piece of pre-weighed tinfoil and then transferred to the glass vial. Following this, CO_2 was evolved under vacuum with orthophosphoric acid.

Three samples for radiocarbon dating were obtained from separate growth bands on a *Gafrarium* sp.[4] shell. Sampling points #3, #5, and #7 (**Figure 6.3**) were radiocarbon dated and assigned laboratory numbers Wk45920-3, Wk45920-4, and Wk45920-5, respectively. Sample point #3 was re-sampled due to the large error for the previous radiocarbon date by Petchey (± 169). Sample points #5 and #7 were chosen due to their estuarine and marine ^{13}C signals. Combined with the two radiocarbon dates by Petchey, a total of five radiocarbon dates have been obtained for the *Gafrarium* sp. shell: two duplicates for sampling point #3 and three single dates for sampling points #1, #5 and #7. Together, these five growth bands represent two “estuarine” and three “marine”. **Figure 6.7** illustrates an updated version of **Figure 6.3**, where sampling points by Petchey, alongside sampling points for this thesis have been indicated.

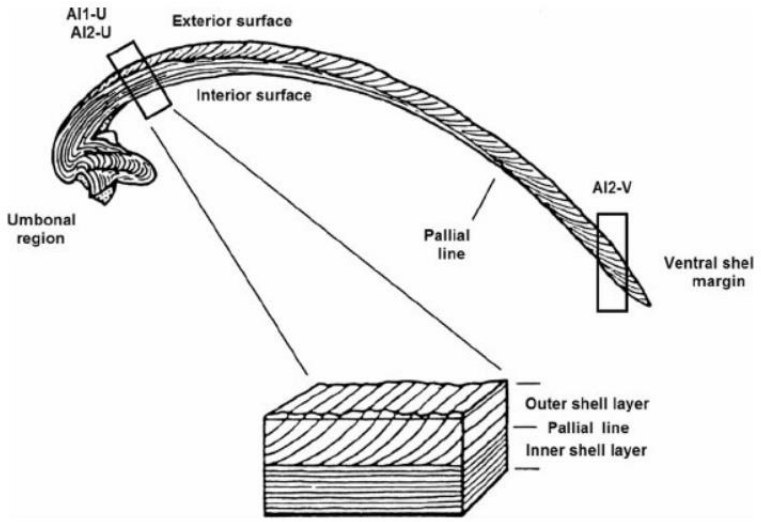

Figure 6.5 Diagram showing the inner and outer layers of shell. Figure from Carilli *et al.* (2015).

[4]Assigned laboratory number Wk45920 at the Waikato Radiocarbon Dating Laboratory

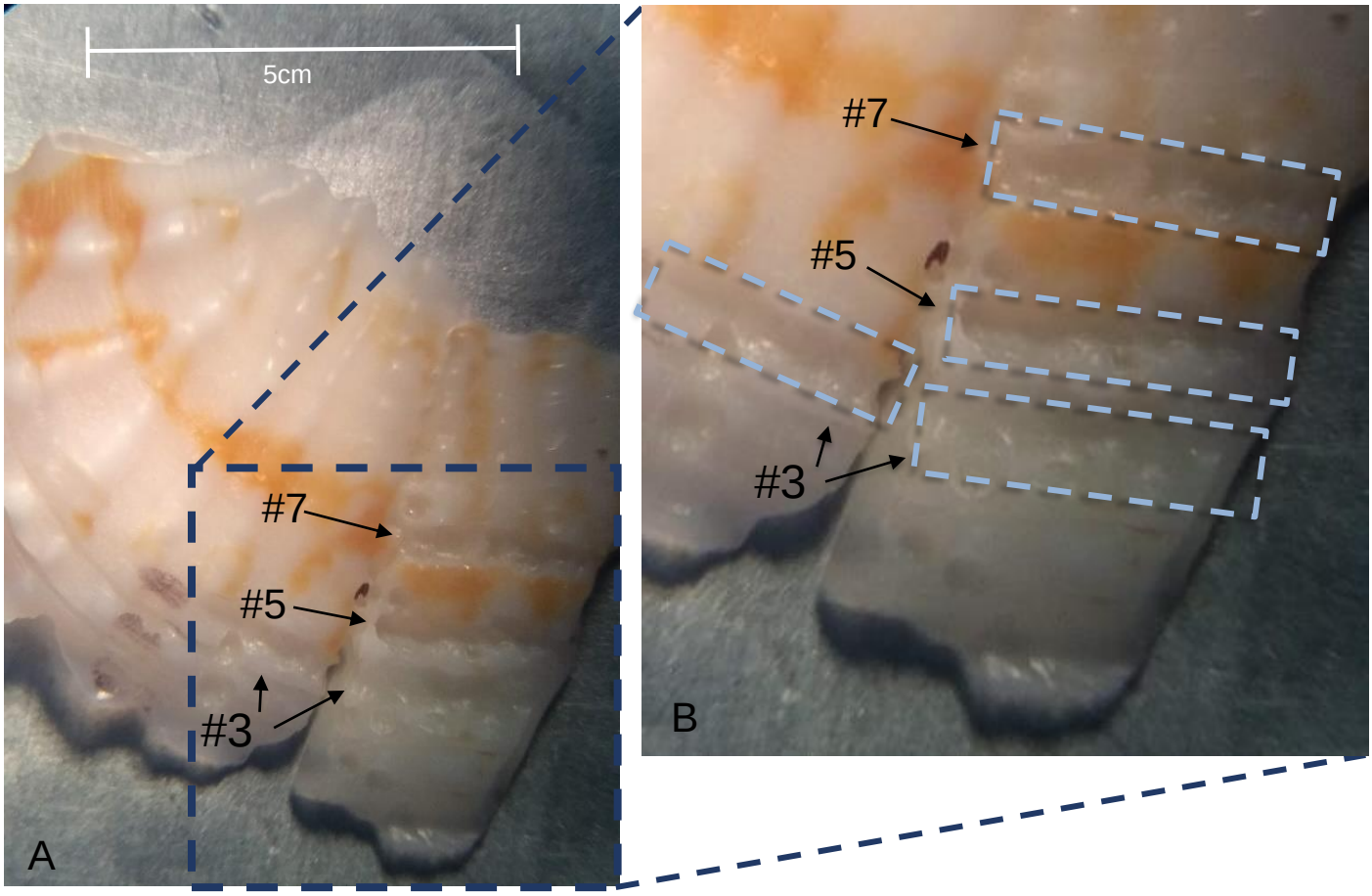

Figure 6.6 (A) Sampling points #3, #5, #7 from a *Gafrarium* sp. shell. (B) Enlarged area from image (A) (dark blue dashed square). The light blue rectangles show areas of ^{14}C sampling.

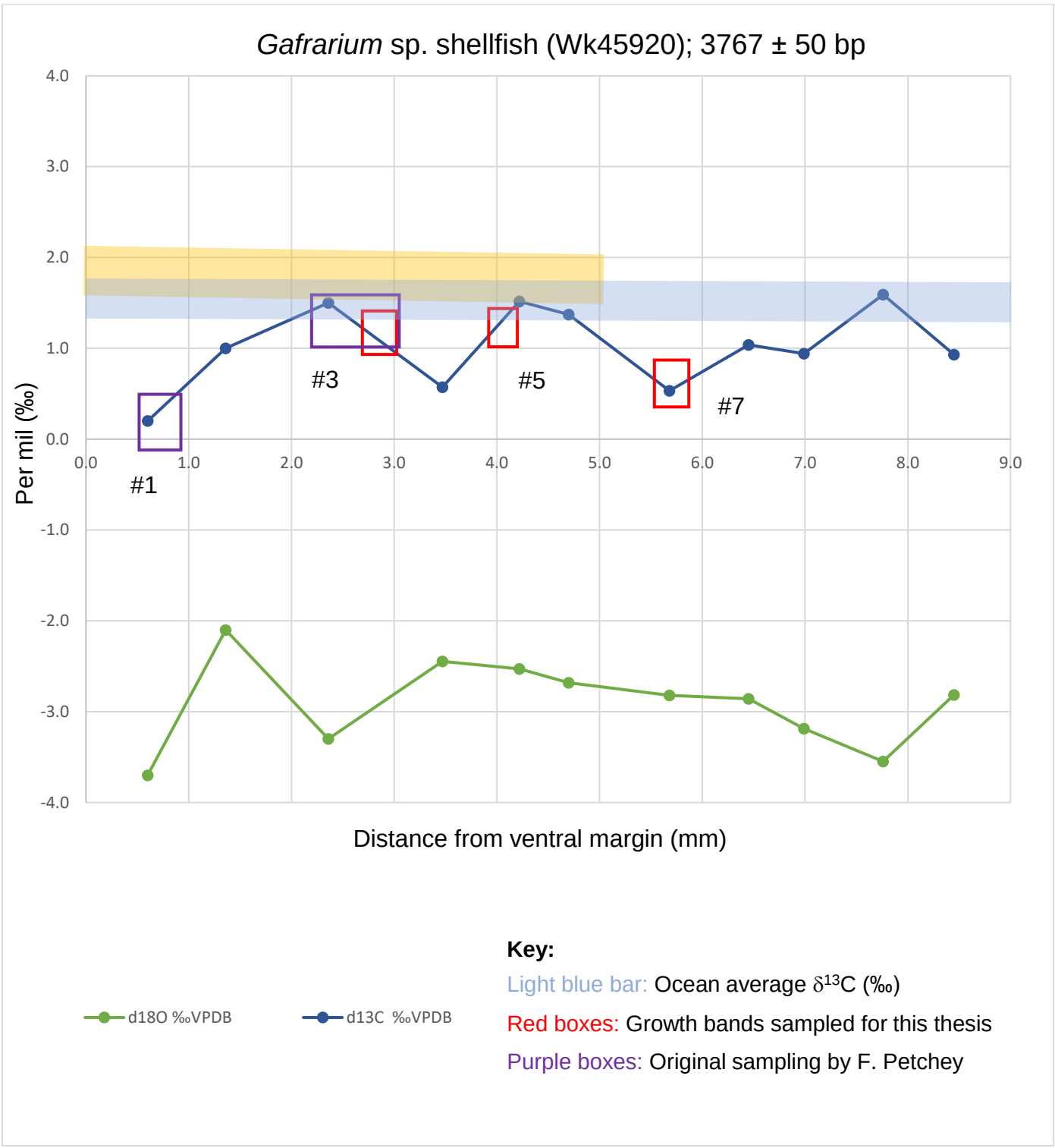

Figure 6.7 $^{13}C‰$ and $^{18}O‰$ results for eleven sampling points from a *Gafrarium* sp. shellfish from the Mariana Islands (Wk-45920). The red (*pers comm.* Petchey) and purple (this thesis) boxes represent where sampling occurred in relation to the distance from the ventral margin.

6.4 Results

Radiocarbon results, shell weights, corresponding mgC values, associated $\delta^{13}C$ values and ΔR values for the five sampling points are listed in **Table 6.1**. ΔR values were calculated using the online ΔR calculator: http://calib.org/deltar13/. A short-lived nut sample (2985 ± 30 BP [SANU-11619]) from the same context was used as the "paired" terrestrial sample, and because the Mariana Islands are in the Northern Hemisphere, the IntCal calibration curve (Reimer *et al.* 2020) was selected. Each ΔR calculation represents a 68% confidence range. Appendix C lists the corresponding calculations and graphs for each ΔR calculation.

Chi-square statistics, used to determine if radiocarbon results are statistically the same or not, are listed in **Table 6.2**. Different groupings of radiocarbon dates were analysed with Chi-square statistics, which are as follows:

- All five results: to assess if the radiocarbon dates were statistically the same, or if they were statistically distinguishable.
- Three transitional marine samples, as indicated by $\delta^{13}C$ (#3A, #3B, and #5).
- Pooled mean of #3A, #3B, #5, with #1, and also #7: because the "marine" samples #3A, #3B, #5 were statistically the same, the pooled mean of their radiocarbon dates was compared to the two "estuarine" radiocarbon dates.

Table 6.1 Radiocarbon and $\delta^{13}C$ results for five sampling points from a *Gafrarium* sp. shellfish (Wk45920) from the Mariana Islands.

Note	Waikato Lab Number	Radiocarbon Age (bp) (uncorrected)	Mean age and Chi-Square statistics	Approximate Sampling locations	$\delta^{13}C$ (‰)	Weight (mg)	mgC	ΔR_{13}[1]	Environment
Petchey (*unpublished data*)	Wk 45920-1	3767 ± 50	3596 ± 32 bp t=22.46 5(9.49), gSD=162	#1	0.2	1.3	0.10	447 ± 63	Estuarine
Petchey (*unpublished data*)	Wk 45920-2	3382 ± 169		#3A	1.5	1.3	0.03	61 ± 173	Transitional marine
Sampled by C. Milson	Wk 45920-3	3520 ± 60		#3B	1.5	0.70	0.09	200 ± 72	Transitional marine
Sampled by C. Milson	Wk 45920-4	3360 ± 90		#5/6	1.4-1.5	0.85	0.05	39 ± 98	Transitional marine
Sampled by C. Milson	Wk 45920-5	3530 ± 80		#7	0.5	0.72	0.07	209 ± 89	Estuarine

[1]ΔR calculation using short-lived nut sample dating to 2985 ± 30 BP (SANU-11619).

Table 6.2 Pooled mean radiocarbon age and error, along with Chi-Square statistic results for different groupings of radiocarbon dates from a *Gafrarium* sp. shellfish from the Mariana Islands.

Pooled groupings	Mean radiocarbon age and error (bp)	Chi-square statistics	Statistically the same?
All 5 (#1, #3A, #3B, #5, #7)	3596 ± 32	$\chi^2_{4:0.05} = 22.46 > 9.49$, GSD = 162	No
Marine samples (#3A, #3B, and #5)	3463 ± 48	$\chi^2_{2:0.05} = 2.44 < 5.99$	Yes
Pooled mean (#3A, #3B, #5) and #1	3608 ± 35	$\chi^2_{1:0.05} = 19.24 > 3.84$ GSD=214.96	No
Pooled mean (#3A, #3B, #5) and #7	3481 ± 42	$\chi^2_{1:0.05} = 0.52 < 3.84$	Yes

6.5 Discussion

The five radiocarbon results from the *Gafrarium* sp. shell displayed just over a 400-year difference (3360 ± 90 bp to 3767 ± 50 bp). Chi-square results show they are statistically distinguishable, a significant result considering each sample was from the same shell.

Sampling points #3A, #3B, and #5 have the same $\delta^{13}C$ signal, 1.5‰, indicating a transitional marine signal. In contrast, sampling points #1 and #7 have $\delta^{13}C$ signals that reflect a clear estuarine signal, 0.2‰ and 0.5‰, respectively. Therefore, it is logical to expect sampling points #3A, #3B, and #5 to be younger than sampling points #1 and #7.

Chi-square statistics show #3A, #3B, and #5 are statistically the same and, moreover, the pooled mean of #3A, #3B and #5 is significantly younger than sampling area #1, with an observed difference of 304 ^{14}C years (3463 ± 48 bp compared to 3767 ± 50 bp). Chi-square statistics confirm they are statistically distinguishable. Because the $\delta^{13}C$ value of sampling area #1 indicates an estuarine signal, hard water exposure is hypothesised to the cause of this large difference in radiocarbon ages.

The pooled mean of #3A, #3B and #5 (marine) is also younger than the radiocarbon age of #7 (estuarine), but this time only by 67 ^{14}C years. Chi-square statistics show they are statistically the same. One potential cause of this observation is variability in hard water exposure. As discussed in Chapter 1, old ^{14}C water is discharged at Laulau Bay, where Bapot-1 is located. The tide, along with wind and storms, results in variable concentrations of marine and freshwater held close to the shoreline by onshore currents (Petchey *et al.*, 2017). These variable conditions result in variability of the concentration of old ^{14}C in the water. Therefore, it is possible that sampling points #1 and #7 may both have been affected by hard water, but to varying degrees. Another possibility that should be noted is imprecision in sampling. This can be in the form of imprecision in subsampling the same area for both ^{14}C and ^{13}C, and also imprecision in subsampling the correct growth band. Because the sample sizes are so small, it is possible for other growth bands to be subsampled.

The results tentatively support a correlation between ^{13}C, ^{14}C, and hard water exposure. It must be stressed however that these results are preliminary, and additional tests on these and other shells from a range of locations are needed before any decisive conclusions can be drawn. To first establish reliable “marine” and “estuarine” samples, ^{13}C measurements need to be more precisely measured. Results also need to be repeatable. Therefore, $^{13}C/^{14}C$ analysis needs to be undertaken at different sites, and on different taxa in areas where there is a known hard water impact in order to prove repeatability.

6.6 Summary

Five different growth bands from a *Gafrarium* sp. shellfish from the Mariana Islands were radiocarbon dated. Sampling points #3A, #3B and #5 represented “marine” growth bands, and sampling points #1 and #7 represented “estuarine” growth bands, as indicated by $\delta^{13}C$.

The five radiocarbon dates displayed a 400-year difference, and using Chi-square statistics, they were calculated to be statistically distinguishable. Radiocarbon dates from the “marine” samples were calculated to be statistically the same, and when their pooled radiocarbon age was compared to sample point #1, a difference of 304 ^{14}C years was observed. Chi-square statistics showed they were statistically distinguishable. Conversely, when the pooled radiocarbon age of the marine samples was compared to sampling point #7, they were statistically the same. This result was hypothesised to be caused by variability in the concentration of old ^{14}C.

While the results lend some support to a correlation between ^{13}C, ^{14}C, and hard water exposure, further testing from the investigated *Gafrarium* sp. shellfish in this thesis, and other shells from a range of locations is needed before any decisive conclusions can be drawn.

Chapter 7
Conclusions and Future Work

The objectives of this thesis were to:

1) Improve the precision of ultra-small radiocarbon dating by experimenting with a selection of volume and chemical modifications to Waikato Radiocarbon AMS protocols.
2) Using these new ultra-small methodologies, radiocarbon date growth bands deposited at different times, as indicated by $\delta^{13}C$, from a *Gafrarium* sp. shellfish to investigate the relationship between ^{13}C, ^{14}C, and hard water exposure.

Overall, the findings from this research project were positive and while not all the objectives were met, several experiments produced results that warrant further investigation.

7.1 Overview

Due to contamination being problematic for ultra-small samples, the aim of this thesis was to reduce contamination so that shell samples <0.1 mgC could be reliably radiocarbon dated.

Chapter 2 discussed various techniques used worldwide to improve the reliability of radiocarbon dating ultra-small samples. These included reducing the volume of the graphite reactor, lowering the temperature during graphitisation, testing different water removal methods during graphitisation, experimenting with oxygen as an additional Fe catalyst cleaning method, pressing graphite in a laminar flow hood, and the use of copper insets in cathode targets. Several authors reported promising results and following this, a selection of volume and chemical modifications were chosen for this thesis, based on their reported effectiveness, resources available at the Waikato Radiocarbon Dating Laboratory (WRDL), and financial viability.

Chapter 3 outlined modifications that were undertaken on the current vacuum line used at the WRDL, which involved reducing the volume of the measuring manifold

and graphite reactors to minimise contamination when radiocarbon dating ultra-small samples. Components were either reduced in length and volume or eliminated. Advantages of the ultra-small vacuum line included reduced areas of dead space and fewer complex glass components, and while there were some disadvantages associated with the measuring manifold, from an operational point of view, these were concluded to not inhibit its performance.

Chapter 4 outlined chemical modifications and method optimisation experiments. The suitability of using a 4-decimal point balance for weighing small shell samples was assessed by comparison to a 6-decimal point balance. Specifically, the impact on corresponding CO_2 that is generated from measured shell samples was investigated. The results showed that CO_2 yield was more precise for shell weights that were measured using the 6-decimal point balance. Because ultra-small samples require a small standard that matches the size of the sample, and due to the design of the ultra-small measuring manifold preventing manipulation of CO_2, it was concluded that ultra-small samples should only be weighed on the 6-decimal point balance.

Several chemical modifications were undertaken to test the possibility of contamination occurring at different stages of processing. Due to initial tests of Prolabo®, BDH®, and Alfa Aesar® Fe powders undertaken in 2009 and 2011, the visible qualities of each Fe powder, before and after graphitisation, were assessed via scanning electron microscopy (SEM). SEM imaging revealed that the two Alfa Aesar® Fe powders had distinctively different morphologies compared to the Prolabo® and BDH® Fe powders, as Prolabo® and BDH® Fe were rounded and ball-shaped while the Alfa Aesar® Fe powders were clumped with irregular shapes. After graphitisation, Prolabo®, BDH® and Alfa Aesar®UCI retained their morphology whereas the Alfa Aesar®WRDL Fe powder was heterogenous. The use of oxygen as an additional method of cleaning each Fe powder before graphitisation was also assessed via SEM. No significant difference in morphology from the use of a O_2/H_2 bake-out compared to only implementing a H_2 bake-out was observed.

Due to the possibility that longer graphitisation times can result in leaks from the graphite reactor, and therefore contamination, two alternative water removal methods to using magnesium perchlorate were investigated. The results showed that the use

of a metal bar with slush resulted in the longest graphitisation times. Conversely, the quartz tube with slush resulted in the shortest graphitisation times.

Chapter 5 outlined the radiocarbon results of three standards using selected volume and chemical modifications. No significant improvements from the ultra-small vacuum line, or O_2/H_2 bake-out were observed when compared to current protocols in use at the WRDL. The results however did reveal the minimum sample sizes that can be used to obtain reliable radiocarbon dates. Oxalic Acid II (modern) and Carrara Marble (>50,000 years, beyond the limits of ^{14}C) were affected by modern and dead carbon contamination at 0.10 mgC, respectively. While Tridacna was also affected by modern carbon contamination, this was for samples <0.03 mgC. Based on these results, it was concluded that a sample size ≥0.10 mgC is required for radiocarbon dating ancient samples (*i.e.,* >50,000 years). Conversely, a sample size ≥0.03 mgC is required for radiocarbon dating samples that are approximately 3000 years old. If, however, a simple determination of "young" or "old" is required for a sample (*i.e.,* 3000 or 30,000 years) sample sizes <0.03 mgC are sufficient.

Five radiocarbon dates from a *Gafrarium* sp. shellfish from the Mariana Islands were presented in Chapter 6. These five radiocarbon dates, as indicated by $\delta^{13}C$, represented two "estuarine" and three "marine" growth bands. Using Chi-square statistics, the five radiocarbon results were calculated to be statistically distinguishable, a significant observation considering each sample was from the same shell. Furthermore, one "estuarine" sample was 304 ^{14}C years older than the pooled mean of the "marine" samples. Conversely, the radiocarbon result of the other "estuarine" sample was statistically the same as the pooled radiocarbon age of the "marine" samples. An explanation as to this observation was hypothesised to be a result of variability in the concentration of old ^{14}C (hard water exposure). The results from this investigation presented preliminary evidence that supports a relationship between ^{13}C, ^{14}C, and hard water exposure. A more extensive dataset on the investigated *Gafrarium* sp. shellfish, and other shells from a range of locations is needed, however, to provide statistically significant results.

7.2 Future Work

The results of this research suggest avenues that could be further explored. By replacing the magnesium perchlorate with a quartz tube and slush, graphitisation times are reduced. This could provide an alternative water removal method to minimise contamination and speed up the reaction, a technique that warrants further investigation. However, if this method was to be routinely used, the issue of high operator input would need to be resolved. The use of smaller thermoses for slush would help remedy this.

While the volume reductions and oxygen bake-out did not result in any significant differences, insufficient data means that it is difficult to say that these methods do not have potential. In terms of the use of oxygen to further clean and condition the Fe catalyst before graphitisation, different quantities (mb) and varying bake-out times could be tested. Further exploration of Fe powders to reduce background contamination is also recommended, as different Fe powders have been found to possess varying morphological characteristics, which could potentially impact their performance to act as a suitable catalyst for the formation of graphite.

While the radiocarbon results from the *Gafrarium* sp. shellfish from the Mariana Islands provided promising preliminary results, further data is necessary to establish a statistically significant relationship between ^{13}C, ^{14}C, and hard water exposure. Additional shellfish displaying estuarine and marine ^{13}C signals, from different environments, need to be radiocarbon dated with a minimum of three radiocarbon dates from each environment. To first establish reliable “marine” and “estuarine” samples though, ^{13}C measurements need to be precisely measured, and for a statistically conclusive relationship to be established between ^{13}C, ^{14}C, and hard water exposure, results need to be repeatable, leading to the necessity to carry out $^{13}C/^{14}C$ analysis at different sites, and on different taxa in areas where there is a known hard water impact.

7.3 Conclusion

The results from this thesis have resulted in these conclusions:

1) The current methodology used at the WRDL is suitable for dating shell material down to 0.1 mgC. However, because contamination is age-dependent, size recommendations will vary depending on sample age.
2) Enhanced precision in initial sample weighing will help reduce labour and improve precision of results.
3) The use of a quartz tube and slush to remove water formed during graphitisation will improve graphitisation times and therefore minimise potential contamination during the graphitisation reaction.
4) Reliable dating of shellfish that occupy both marine and estuarine environments requires careful sample selection and evaluation of ^{13}C before ^{14}C dating is undertaken.

References

ACS Chemistry for Life. (2016). *Willard Libby and radiocarbon dating*. Retrieved 30th April, 2022, from https://www.acs.org/content/acs/en/education/whatischemistry/landmarks/radiocarbon-dating.html.

Alves, E. Q., Macario, K., Ascough, P., & Bronk Ramsey, C. (2018). The worldwide marine radiocarbon reservoir effect: Definitions, mechanisms, and prospects. *Reviews of Geophysics, 56*(1), 278-305. doi: 10.1002/2017rg000588.

Alves, E. Q., Macario, K. D., Urrutia, F. P., Cardoso, R. P., & Bronk Ramsey, C. (2019). Accounting for the marine reservoir effect in radiocarbon calibration. *Quaternary Science Reviews, 209*, 129-138. doi: 10.1016/j.quascirev.2019.02.013.

analog microelectronics. (accessed 10/5/2022). *AMS 5812 : Pressure Sensor with Analog and Digital Output (I2C)*. Retrieved 10th May, 2022, from https://www.analog-micro.com/en/products/pressure-sensors/board-mount-pressure-sensors/ams5812/.

Anderson, A., Higham, T., & Wallace, R. (2001). The radiocarbon chronology of the Norfolk Island archaeological sites. *Australian Museum*, 33-42.

Beta Analytic. (accessed 30/4/22). *Introduction to Radiocarbon Determination by the Accelerator Mass Spectrometry Method*. Retrieved 30th April, 2022, from https://www.radiocarbon.com/PDF/AMS-Methodology.pdf.

Beverly, R. K., Beaumont, W., Tauz, D., Ormsby, K. M., von Reden, K. F., Santos, G. M., & Southon, J. R. (2016). The Keck Carbon Cycle AMS Laboratory, University of California, Irvine: Status report. *Radiocarbon, 52*(2), 301-309. doi: 10.1017/s0033822200045343.

Bezerra, F. H. R., Vita-Finzi, C., & Lima Filho, F. P. (2000). The use of marine shells for radiocarbon dating of coastal deposits. *Revista Brasileira de Geociências, 30*(1), 211-213. doi: 10.25249/0375-7536.2000301211213.

Broom, M. J. (1985). *The Biology and Culture of Marine Bivalve Molluscs of the Genus Anadara*. (Vol. 12). ICLARM Studies and Reviews.

Butler, P. G., Scourse, J. D., Richardson, C. A., Wanamaker Jr, A. D., Bryant, C. L., & Bennell, J. D. (2009). Continuous marine radiocarbon reservoir calibration and the ^{13}C Suess effect in the Irish Sea: Results from the first multi-centennial shell-based marine master chronology. *Earth and Planetary Science Letters, 279*(3-4), 230-241. doi: 10.1016/j.epsl.2008.12.043.

Carilli, J., Williams, B., Schöne, B. R., Krause, R. A., & Fallon, S. J. (2015). Historical Contaminant Records from Sclerochronological Archives. In *Environmental Contaminants* (Chapter 13, pp. 355-391). doi: 10.1007/978-94-017-9541-8_13.

Carson, M. (2014). *First Settlement of Remote Oceania: Earliest Sites in the Mariana Islands.* Heidelberg: Springer.

Christensen, K. (2022). *Radiocarbon Dating*. Retrieved 8th March, 2022, from https://www.mtu.edu/unscripted/2019/01/radiocarbon-dating.html.

Chute, A. S., Wainright, S. C., & Hart, D. R. (2012). Timing of shell ring formation and patterns of shell growth in the sea scallop *Placopecten Magellanicus* based on stable oxygen isotopes. *Journal of Shellfish Research, 31*(3), 649-662, 14. doi: 10.2983/035.031.0308.

Clark, G., Petchey, F., Winter, O., Carson, M., & Patrick., O. D. (2010). New radiocarbon dates from the bapot-1 site in Saipan and neolithic dispersal by stratified diffusion. *Journal of Pacific Archaeology, 1*(1).

Currie, L. (2004). The remarkable metrological history of radiocarbon dating. *National Institute of Standards and Technology, 109*(2), 185-217.

Delqué-Koli Caffy, I., Comby-Zerbino, C., Dumoulin, J. P., Hain, S., Massault, M., Moreau, C., Quiles, A., Setti, V., Souprayen, C., Tannau, J. F., Thellier, B., & Vincent, J. (2013). Advances in handling small radiocarbon samples at the laboratoire de mesure du carbone 14 in Saclay, France. *Radiocarbon, University of Arizona, 55*(2), 648-656. doi: 10.1017/S0033822200057805.

Dincer, I., & Ezzat, M. (2018). Geothermal energy production. *Elsevier, 3*, 252-303. doi: 10.1016/B978-0-12-809597-3.00313-8.

Douka, K., Higham, T., & Hedges, R. (2010). Radiocarbon dating of shell carbonates: old problems and new solutions. *Munibe Antropologia-Arkeologia, 31*, 18-27.

Dye, T. (1994). Apparent ages of marine shells: Implications for archaeological dating in Hawai'i. *Radiocarbon, 36*(1), 51-57.

Fedi, M., Barone, S., Barile, F., Liccioli, L., Manetti, M., & Schiavulli, L. (2020). Towards micro-samples radiocarbon dating at INFN-LABEC, Florence. *Nuclear Instruments and Methods in Physics Research Section B: Beam Interactions with Materials and Atoms, 465*, 19-23. doi: 10.1016/j.nimb.2019.12.020.

Gaspar, M. B. (2004). Age and growth of *chamelea gallina* from the algarve coast (southern Portugal): Influence of seawater temperature and gametogenic

cycle on growth rate. *Journal of Molluscan Studies, 70*(4), 371-377. doi: 10.1093/mollus/70.4.371.

Global Monitoring Laboratory. (accessed 2/4/2022). *The Technical Details: Radioactive Decay Beta Decay*. Retrieved 2nd April, 2022, from https://gml.noaa.gov/outreach/isotopes/decay.html.

Gómez, E. A., Borel, C. M., Aguirre, M. L., & Martínez, D. E. (2016). Radiocarbon reservoir ages and hardwater effect for the Northeastern coastal waters of Argentina. *Radiocarbon, 50*(1), 119-129. doi: 10.1017/s003382220004340x.

Heaton, T. J., Köhler, P., Butzin, M., Bard, E., Reimer, R. W., Austin, W. E. N., Bronk Ramsey, C., Grootes, P. M., Hughen, K. A., Kromer, B., Reimer, P. J., Adkins, J., Burke, A., Cook, M. S., Olsen, J., & Skinner, L. C. (2020). Marine20 - the marine radiocarbon age calibration curve (0–55,000 cal BP). *Radiocarbon, 62*(4), 779-820. doi: 10.1017/rdc.2020.68.

Hua, Q., Jacobsen, G., Zoppi, U., Lawson, E., Williams, A., Smith, A. M., & McGann, M. (2001). Progress in radiocarbon target preparation at the ANTARES AMS Centre. *Radiocarbon, 43*, 275-282. doi: doi:10.1017/S003382220003811X.

Hua, Q., Zoppi, U., Williams, A. A., & Smith, A. M. (2004). Small-mass AMS radiocarbon analysis at ANTARES. *Nuclear Instruments and Methods in Physics Research Section B: Beam Interactions with Materials and Atoms, 223-224*, 284-292. doi: 10.1016/j.nimb.2004.04.057.

Jones, D. (1989). *Growth Rings and Longevity in Bivalves*. Retrieved 3rd April, 2022, from https://conchologistsofamerica.org/growth-rings-and-longevity-in-bivalves/.

Jull, A. J. T. (2013). Some interesting and exotic applications of carbon-14 dating by accelerator mass spectrometry. *Journal of Physics: Conference Series, 436*. doi: 10.1088/1742-6596/436/1/012083.

Keaveney, E. M., & Reimer, P. J. (2012). Understanding the variability in freshwater radiocarbon reservoir offsets: a cautionary tale. *Journal of Archaeological Science, 39*(5), 1306-1316. doi: 10.1016/j.jas.2011.12.025.

Leavitt, S. W., & Bannister, B. (2016). Dendrochronology and radiocarbon dating: The laboratory of tree-ring research connection. *Radiocarbon, 51*(1), 373-384. doi: 10.1017/s0033822200033889.

Liebl, J., Ortiz, R. A., Golser, R., Handle, F., Kutschera, W., Steier, P., & Wild, E. M. (2010). Studies on the preparation of small ^{14}C samples with an RGA and ^{13}C-enriched material. *Radiocarbon, 52*(3), 1394-1404. doi: 10.1017/S0033822200046476.

Lonsberry, K. (2022). *Quaternary dating techniques: Basics advantages and limitations age* Retrieved 3rd March, 2022, from https://slideplayer.com/slide/1587726/.

Missiaen, L., Wacker, L., Lougheed, B. C., Skinner, L., Hajdas, I., Nouet, J., Pichat, S., & Waelbroeck, C. (2020). Radiocarbon dating of small-sized foraminifer samples: Insights into marine sediment mixing. *Radiocarbon, 62*(2), 313-333. doi: 10.1017/rdc.2020.13.

Nadeau, M. J., Schleicher, M., Grootes, P. M., Erlenkeuser, H., Gottdang, A., Mous, D. J. W., Sarnthein, J., & Willkomm, H. (1997). The Leibniz-Labor AMS facility at the Christian-Albrechts University, Kiel, Germany. *Nuclear Instruments and Methods in Physics Research B, 123*, 22-30. doi: 10.1016/s0168-583x(96)00730-6.

O'Neil, D. (1998). *Chronometric techniques - Part II*. Retrieved 2nd April, 2022, from https://www2.palomar.edu/anthro/time/time_5.htm.

Peck, L. S., & Brey, T. (1996). Bomb signals in old Antarctic brachiopods. *Nature, 380*(6571), 207-208. doi: 10.1038/380207b0.

Petchey, F., & Clark, G. (2011). Tongatapu hardwater: Investigation into the ^{14}C marine reservoir offset in lagoon, reef and open ocean environments of a limestone island. *Quaternary Geochronology, 6*(6), 539-549. doi: 10.1016/j.quageo.2011.08.001.

Petchey, F., Ulm, S., David, B., McNiven, I. J., Asmussen, B., Tomkins, H., Dolby, N., Aplin, K., Richards, T., Rowe, C., Leavesley, M., & Mandui, H. (2012). High-resolution radiocarbon dating of marine materials in archaeological contexts: radiocarbon marine reservoir variability between *Anadara*, *Gafrarium*, *Batissa*, *Polymesoda* spp. and Echinoidea at Caution Bay, Southern Coastal Papua New Guinea. *Archaeological and Anthropological Sciences, 5*(1), 69-80. doi: 10.1007/s12520-012-0108-1.

Petchey, F., Phelan, M., & White, P. (2016). New ΔR values for the Southwest Pacific Ocean. *Radiocarbon, 46*(2), 1005-1014. doi: 10.1017/s0033822200036079.

Petchey, F., Ulm, S., David, B., McNiven, I. J., Asmussen, B., Tomkins, H., Richards, T., Rowe, C., Leavesley, M., Mandui, H., & Stanisic, J. (2016). ^{14}C marine reservoir variability in herbivores and deposit-feeding Gastropods from an Open Coastline, Papua New Guinea. *Radiocarbon, 54*(3-4), 967-978. doi: 10.1017/s0033822200047603.

Petchey, F., Clark, G., Winter, O., O'Day, P., & Litster, M. (2017). Colonisation of Remote Oceania: New dates for the bapot-1 site in the Mariana Islands. *Archaeology in Oceania, 52*(2), 108-126. doi: 10.1002/arco.5108.

Petchey, F., Clark, G., Lindeman, I., O'Day, P., Southon, J. R., Dabell, K., & Winter, O. (2018). Forgotten news: Shellfish isotopic insight into changing sea-level and associated impact on the first settlers of the Mariana Archipelago. *Quaternary Geochronology, 48*, 180-194. doi: 10.1016/j.quageo.2018.10.002.

Petchey, F., & Schmid, M. M. E. (2020). Vital evidence: Change in the marine ^{14}C reservoir around New Zealand (Aotearoa) and implications for the timing of Polynesian settlement. *Nature, 10*(1), 14266. doi: 10.1038/s41598-020-70227-3.

Petchey, F., & Clark, G. (2021). Clarifying the age of initial settlement horizon in the Mariana Islands and the impact of hard water: A response to Carson (2020). *Radiocarbon, 63*(3), 905-913. doi: 10.1017/rdc.2021.27.

Philippsen, B. (2013). The freshwater reservoir effect in radiocarbon dating. *Heritage Science, 1*(1). doi: 10.1186/2050-7445-1-24.

Philippsen, B. (2015). Hard water and old food. The freshwater reservoir effect in radiocarbon dating of food residues on pottery. *Documenta Praehistorica, 42*. doi: 10.4312/dp.42.10.

Quarta, G., Maruccio, L., D'Elia, M., & Calcagnile, L. (2021). Radiocarbon dating of marine samples: Methodological aspects, applications and case studies. *Water, 13*(7), 986. doi: 10.3390/w13070986.

Radiocarbon. (2021). *Radiocarbon Laboratories*. Retrieved 15th February, 2021, from https://radiocarbon.webhost.uits.arizona.edu/sites/default/files/Labs-2021_09_03.pdf.

Radiocarbon Dating Laboratory. (2017). *Waikato Radiocarbon Dating Laboratory: AMS Processing Technical Report*. Retrieved 1st May, 2022, from https://radiocarbondating.com/__data/assets/pdf_file/0010/387712/Waikato-Radiocarbon-Dating-Laboratory-AMS-Processing-Technical-Report-2017.pdf.

Reimer, P., Brown, T., & Reimer, R. (2016). Discussion: Reporting and calibration of post-bomb ^{14}C data. *Radiocarbon, 46*(3), 1299-1304. doi: 10.1017/s0033822200033154.

Santos, G. M., Mazon, M., Southon, J. R., & Rifai, S. (2007a). Evaluation of iron and cobalt powders as catalysts for ^{14}C AMS target preparation. *Nuclear Instruments and Methods in Physics Research Section B: Beam Interactions with Materials and Atoms, 259*(1), 308-315. doi: 10.1016/j.nimb.2007.01.220.

Santos, G. M., Southon, J. R., Griffin, S., Beaupre, S. R., & Druffel, E. R. M. (2007b). Ultra small-mass AMS ^{14}C sample preparation and analyses at KCCAMS/UCI Facility. *Nuclear Instruments and Methods in Physics Research Section B: Beam Interactions with Materials and Atoms, 259*(1), 293-302. doi: 10.1016/j.nimb.2007.01.172.

Santos, G. M., Southon, J. R., Druffel-Rodriguez, K. C., Griffin, S., & Mazon, M. (2016a). Magnesium perchlorate as an alternative water trap in AMS graphite sample preparation: A report on sample preparation at KCCAMS at the University of California, Irvine. *Radiocarbon, 46*(1), 165-173. doi: 10.1017/s0033822200039485.

Santos, G. M., Moore, R. B., Southon, J. R., Griffin, S., Hinger, E., & Zhang, D. (2016b). AMS ^{14}C Sample Preparation at the KCCAMS/UCI Facility: Status report and performance of small samples. *Radiocarbon, 49*(2), 255-269. doi: 10.1017/s0033822200042181.

Scientific American. (2006). *How are seashells created? Or any other shell, such as a snail's or a turtle's?* Retrieved 14th May, 2022, from https://www.scientificamerican.com/article/how-are-seashells-created/.

Smith, A. M., Hua, Q., Williams, A., Levchenko, V., & Yang, B. (2010). Developments in micro-sample ^{14}C AMS at the ANTARES AMS facility. *Nuclear Instruments and Methods in Physics Research Section B: Beam Interactions with Materials and Atoms, 268*(7-8), 919-923. doi: 10.1016/j.nimb.2009.10.064.

Smith, A. M., Yang, B., Hua, Q., & Mann, M. (2016a). Laser-heated microfurnace: gas analysis and graphite morphology. *Radiocarbon, 52*(2), 769-782. doi: 10.1017/s0033822200045781.

Smith, A. M., Petrenko, V. V., Hua, Q., Southon, J. R., & Brailsford, G. (2016b). The effect of N_2O, catalyst, and means of water vapor removal on the graphitization of small CO_2 samples. *Radiocarbon, 49*(2), 245-254. doi: 10.1017/s003382220004217x.

Stenström, K., Skog, G., Georgiadou, E., Genberg, J., & Johansson, A. (Compiler) (2011). *A guide to radiocarbon units and calculations*: Lund University.

Tagliabue, A., & Bopp, L. (2008). Towards understanding global variability in ocean carbon-13. *Global Biogeochemical Cycles, 22*(1). doi: 10.1029/2007gb003037.

Tanaka, N., Monaghan, M. C., & Rye, D. M. (1986). Contribution of metabolic carbon to mollusc and barnacle shell carbonate. *Nature, 320*(6062), 520-523. doi: 10.1038/320520a0.

Taylor, R. E., & Bar-Yosef, O. (2014). *Radiocarbon Dating: An Archaeological Perspective*. Left Coast Press, Walnut Creek WA.

Tornqvist, T., Rosenheim, B., Hu, P., Fernandez, A. (2015). *Radiocarbon dating and calibration*. John Wiley & Sons.

Walter, S. R. S., Gagnon, A. R., Roberts, M. L., McNichol, A. P., Gaylord, M. C. L., & Klein, E. (2016). Ultra-small graphitization reactors for ultra-microscale ^{14}C analysis at the national ocean sciences accelerator mass spectrometry (NOSAMS) facility. *Radiocarbon, 57*(1), 109-122. doi: 10.2458/azu_rc.57.18118.

Yang, B., Smith, A. M., & Hua, Q. (2013). A cold finger cooling system for the efficient graphitisation of microgram-sized carbon samples. *Nuclear Instruments and Methods in Physics Research Section B: Beam Interactions with Materials and Atoms, 294*, 262-265. doi: 10.1016/j.nimb.2012.08.031.

Yokoyama, Y., Koizumi, M., Matsuzaki, H., Miyairi, Y., & Ohkouchi, N. (2016). Developing ultra small-scale radiocarbon sample measurement at the University of Tokyo. *Radiocarbon, 52*(2), 310-318. doi: 10.1017/s0033822200045355.

Appendices

Appendix A

Chemicals

- EMSURE® Orthophosphoric acid, 85%.
- EMSURE® Hydrochloric acid fuming, 37%.
- BOC Ultra high purity oxygen, compressed. UN 1072. Gas code 224.
- BOC Ultra high purity hydrogen, compressed. UN 1049. Gas code 240.
- Fiegl Solution:
  - Type 1 water.
  - EMSURE® Hydrated manganese sulphate ($MnSO_4*4H_2O$). CAS-No: 10101-68-5.
  - Merck Silver sulphate (Ag_2SO_4). CAS-No: 10294-26-5.
  - LabServ™ Sodium hydroxide pellets. BSPSL740.500.
- Alfa Aesar® Magnesium perchlorate [$Mg(ClO_4)_2$]. Lot#W09G001.
- Iron powder:
  - Prolabo®, 99.5%, mesh size not mentioned. Lot# 219 GC.
  - Alfa Aesar®, 98%, -325 mesh. Lot# L26R048, Stock #39813.
  - BDH®, mesh size not mentioned. Batch 10G060007.
- Standards
  - Oxalic Acid, 1.3407 $\pm$ 0.0019 $F^{14}C$.
  - Carrara Marble, 0.00172 ± 0.00047 $F^{14}C$.
  - Tridacna, ^{14}C age of 3028 $\pm$ 16 years.

Appendix B

Ultra-Torr® vacuum fittings that were eliminated or replaced from the current measuring manifold

Part name and number	Photo	Schematic diagram representation, as described in Figure 3.13
Union Tee SS-8-UT-3		
Union Tee SS-6-UT-3		
Union Tee SS-4-UT-3		
¼-inch Union Tee with adapted $^{1}/_{8}$-inch OD input SS-4-UT-3 (¼-inch) SS-2-UT-3 ($^{1}/_{8}$-inch)		
Union 1-inch Tube SS-16-UT-6		
Union Elbow, ¼-inch Tube OD SS-4-UT-9		

Appendix C

Δ*R* graphs

Δ*R* values were calculated using the online Δ*R* calculator http://calib.org/deltar13/.

Marine ^{14}C age: 3767 ± 50 bp
Terrestrial age BP: 2985 ± 30
68% confidence range: [384:510] 447 ± 63
95% confidence range: [317:573] 445 ± 128

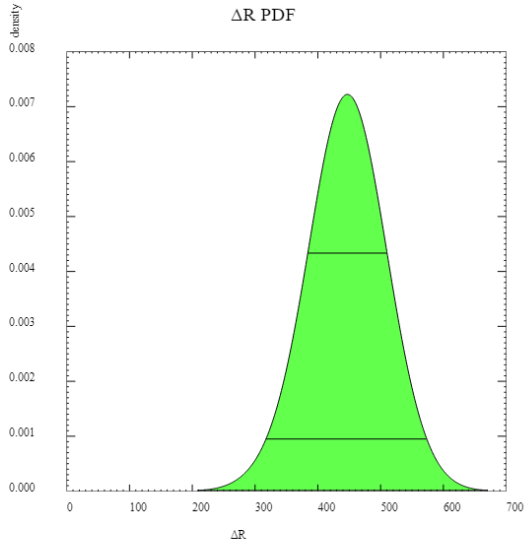

Marine ^{14}C age: 3382 ± 169 bp
Terrestrial age BP: 2985 ± 30
68% confidence range: [-112 : 234] 61 ± 173
95% confidence range: [-284 : 404] 60 ± 344

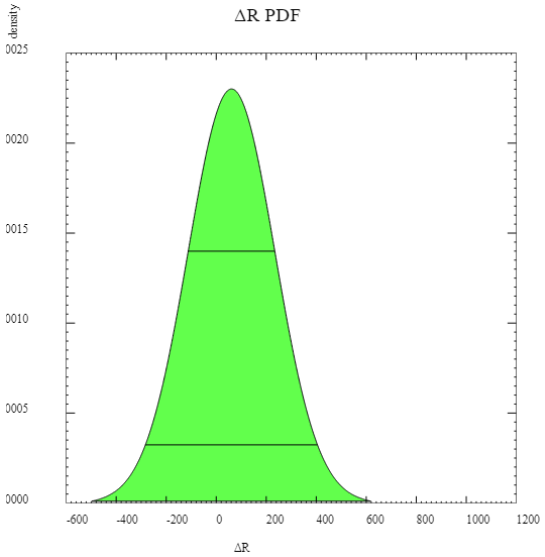

Marine ^{14}C age: 3520 ± 60 bp
Terrestrial age BP: 2985 ± 30
68% confidence range: [128 : 271] 200 ± 72
95% confidence range: [54 : 342] 198 ± 144

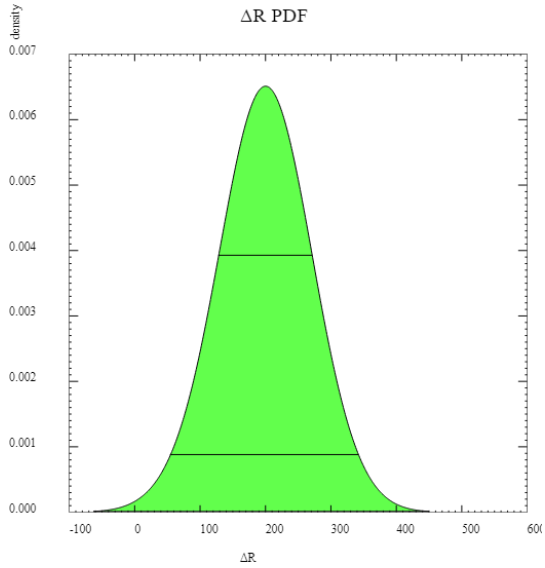

Marine ^{14}C age: 3360 ± 90 bp
Terrestrial age BP: 2985 ± 30
68% confidence range: [-59 : 137] 39 ± 98
95% confidence range: [-157 : 234] 38 ± 196

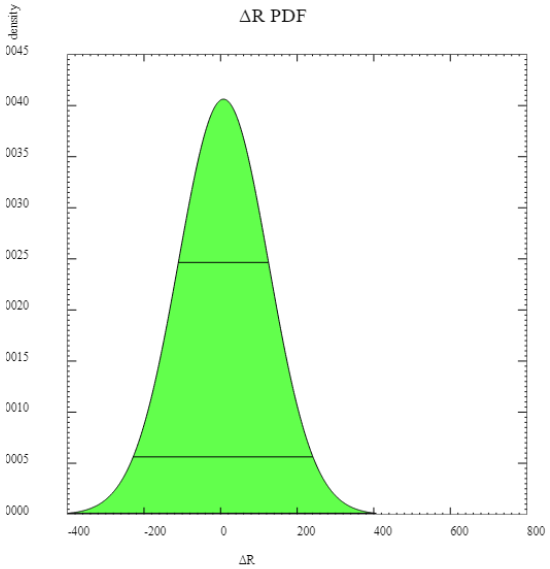

Marine ^{14}C age: 3530 ± 80 bp
Terrestrial age BP: 2985 ± 30
68% confidence range: [120 : 298] 209 ± 89
95% confidence range: [30 : 386] 208 ± 178